

AD-A103 931

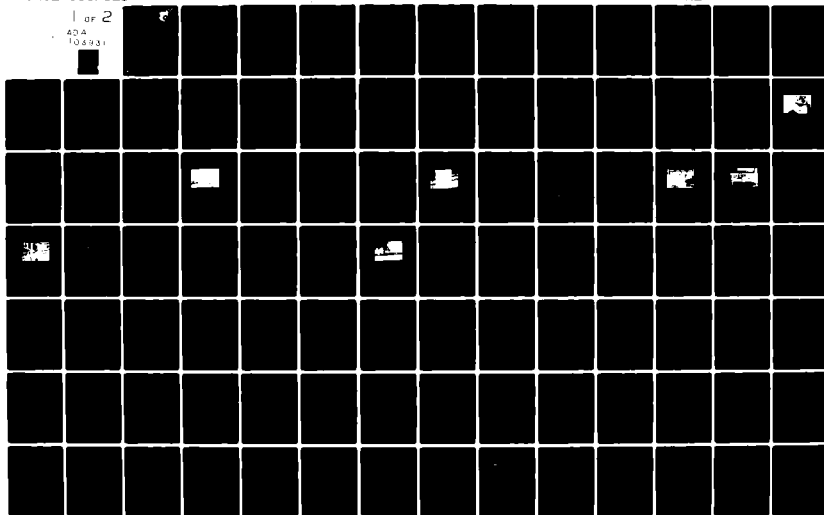
AIR FORCE WRIGHT AERONAUTICAL LABS WRIGHT-PATTERSON AFB OH F/G 21/7
ENGINE ACOUSTIC IMPEDANCE MODELED AS A CYCLIC SERIES OF PASSIVE--ETC(U)
JUL 81 T J LAGNESE
AFWAL-TR-80-4203

UNCLASSIFIED

NL

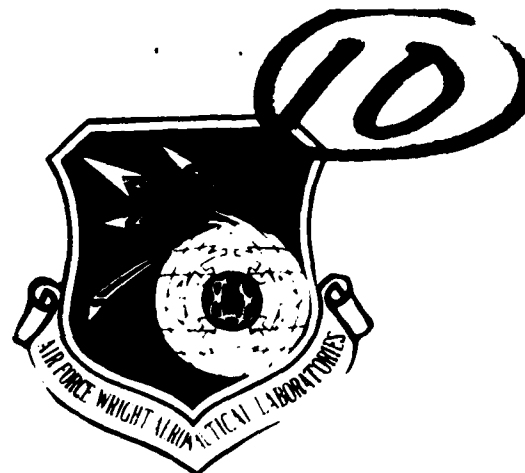
1 of 2

ADA
104931



AD A103931

AFWAL-TR-80-4203 ✓



ENGINE ACOUSTIC IMPEDANCE MODELED AS A CYCLIC SERIES OF PASSIVE SYSTEM IMPEDANCES

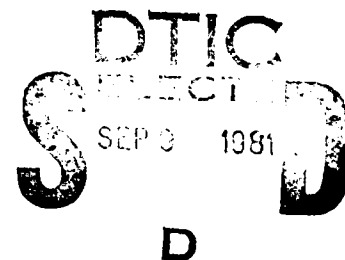
Thomas J. Lagnese, Jr.

Metals Behavior Branch
Metals and Ceramics Division

July 1981

Final Report for Period January 1978 to February 1980

Approved for public release; distribution unlimited.



MATERIALS LABORATORY
AIR FORCE WRIGHT AERONAUTICAL LABORATORIES
AIR FORCE SYSTEMS COMMAND
WRIGHT-PATTERSON AIR FORCE BASE, OHIO 45433

81 9 09 095


DTIC FILE COPY

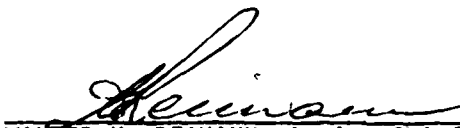
NOTICE

When Government drawings, specifications, or other data are used for any purpose other than in connection with a definitely related Government procurement operation, the United States Government thereby incurs no responsibility nor any obligation whatsoever; and the drawings, specifications, or other data, is not to be regarded by implication or otherwise as in any manner licensing the holder or any other person or corporation, or conveying any rights or permission to manufacture use, or sell any patented invention that may in any way be related thereto.

This report has been reviewed by the Office of Public Affairs (ASD/PA) and is releasable to the National Technical Information Service (NTIS). At NTIS, it will be available to the general public, including foreign nations.

This technical report has been reviewed and is approved for publication.


Lt. T. Lagnese
Metals Behavior Branch
Metals and Ceramics Division


WALTER H. REIMANN, Acting Chief
Metals Behavior Branch
Metals and Ceramics Division

If your address has changed, if you wish to be removed from our mailing list, or if the addressee is no longer employed by your organization, please notify AFVAL/MLLN, W-PAFB, OH 45433 to help us maintain a current mailing list.

Copies of this report should not be returned unless return is required by security considerations, contractual obligations, or notice on a specific document.

SECURITY CLASSIFICATION OF THIS PAGE (When Data Entered)

REPORT DOCUMENTATION PAGE		READ INSTRUCTIONS BEFORE COMPLETING FORM
1. REPORT NUMBER 14 AFWAL-TR-80-4203	2. GOVT ACCESSION NO. AD-A103 937	3. RECIPIENT'S CATALOG NUMBER
4. TITLE (and Subtitle) 6 ENGINE ACOUSTIC IMPEDANCE MODELED AS A CYCLIC SERIES OF PASSIVE SYSTEM IMPEDANCES.	5. TYPE OF REPORT/PERIOD COVERED Final Rept.	
7. AUTHOR(s) 10 Thomas J. Lagnese, Jr.	6. PERFORMING ORG. REPORT NUMBER Jan 78 - Feb 80	
9. PERFORMING ORGANIZATION NAME AND ADDRESS Materials Laboratory Air Force Wright Aeronautical Laboratories Wright-Patterson Air Force Base, Ohio 45433		10. PROGRAM ELEMENT, PROJECT, TASK AREA & WORK UNIT NUMBERS
11. CONTROLLING OFFICE NAME AND ADDRESS Materials Laboratory Air Force Wright Aeronautical Laboratories Air Force Systems Command Wright-Patterson Air Force Base, Ohio 45433		12. REPORT DATE 11 July 1981
13. NUMBER OF PAGES 128		14. SECURITY CLASS. (of this report) Unclassified
15. DISTRIBUTION STATEMENT (of this Report) 17 F1 Approved for public release; distribution unlimited.		15a. DECLASSIFICATION DOWNGRADING SCHEDULE
17. DISTRIBUTION STATEMENT (of the abstract entered in Block 20, if different from Report)		
18. SUPPLEMENTARY NOTES		
19. KEY WORDS (Continue on reverse side if necessary and identify by block number) Acoustic Impedance Engine Impedance Acoustic Impedance Measurement Acoustic Engine Impedance Modeling Engine Noise Combustion Noise		
20. ABSTRACT (Continue on reverse side if necessary and identify by block number) The objective of this project was to utilize a recently proposed two sensor sampling technique for attaining certain acoustic properties of an internal combustion engine. Particular interest will be in attempting to define the acoustic source impedance characteristics of an internal combustion engine. The two sensor method of analysis incorporates a Digital Signal Analyzer system to analyze the sensor signals and to calculate incident-reflected acoustic properties. The laboratory method of experimentation includes exposure of the		

DD FORM 1 JAN 73 1473 EDITION OF 1 NOV 65 IS OBSOLETE

SECURITY CLASSIFICATION OF THIS PAGE (When Data Entered)

372.662

engine to a broadband random noise while performing signal analysis using a transfer function technique. The acoustic source impedance results obtained from this analysis for the engine are then interpreted within a format of passive acoustic systems.

It was a hypothesis of this experimentation that the operating engine can be modeled as a series of cyclic passive systems. This hypothesis has been assessed from experimental results obtained from impedance studies of the motored and powered engine. Modeling of the engine as a cyclic series of passive systems was found to be quite useful for interpreting experimental acoustic impedances for motored engines. This acoustic engine model was found to be less applicable for powered engine studies.

PREFACE

This report was prepared by the Metals Behavior Branch, Metals and Ceramics Division, Materials Laboratory, Air Force Wright Aeronautical Laboratories, Wright-Patterson Air Force Base, Ohio. The research report herein was conducted under Project No. 2307, "Solid Mechanics," Task 2307P102, "Failure Prediction in Metals." The work was performed during the period January 1978 to February 1980.

The author wishes to extend his gratitude and appreciation to his thesis advisor, Dr. John Edward Sneckenberger, of the Department of Engineering Mechanics, West Virginia University, Morgantown, West Virginia, for his technical assistance and encouragement. He also expresses his deepest thanks to Nelson's Industries for their sponsorship of this work.

Accession For	
NTIS GRA&I	<input checked="checked" type="checkbox"/>
DTIC TAB	<input type="checkbox"/>
Unannounced	<input type="checkbox"/>
Justification	
By	
Distribution/	
Availability Codes	
Dist	Avail and/or Special
A	

DTIC
SELECTED
SEP 9 1981
D

TABLE OF CONTENTS

SECTION	PAGE
I INTRODUCTION	1
1. Need for Powered Engine Acoustic Studies	1
2. Previous Approaches to Acoustic Impedance Evaluation	2
a. Approaches Before Digital Signal Analysis	2
b. Approaches Since Digital Signal Analysis	3
3. Formulated Approach Toward Powered Engine Acoustic Impedance Evaluation	4
a. Experimental Assessment of Engine Impedance	4
b. Analytical Modeling of Engine Impedance	5
c. Agreement Between Analytical and Experimentally Defined Impedances	6
II EXPERIMENTAL DEVELOPMENT	7
1. Test Engine Selection and Operational Development	7
a. Motored Engine Operation	9
b. Powered Engine Operation	11
2. Measurand Tube Facility Development	11
a. Acoustic Pressure Sensor Selection	13
b. External Acoustic Signal System	17
3. Anechoic Tailpipe Termination	22
4. Acoustic Signal Measurement System	25
a. Signal Monitoring and Recording System	25
b. Signal Analysis System	28
III THEORY	29
1. Introduction	29
2. Defining Impedance	29
3. Acoustic Phenomena in the Measurand Tube	30

TABLE OF CONTENTS (Continued)

SECTION	PAGE
4. Particular Cases of Acoustic Passive Systems	33
5. Adaptation of Passive System Impedances to the Experimental Case	36
6. Supportive Theory for Digital Signal Analyzer Calculation of Acoustic Impedance Using Transfer Techniques	39
IV RESULTS	42
1. Experimental Passive System Impedances	42
a. Passive Acoustic Impedance Evaluation for Fixed Geometry Configurations	42
b. Engine Acoustic Impedance at Various Crankangles - A Passive System Study	45
2. Experimental Active System Impedances	53
a. Motored Engine Acoustic Impedance Study	53
b. Powered Engine Acoustic Impedance Study	53
3. Analytical Passive System Acoustic Impedances	62
4. Analytical Active System Impedances	62
V EVALUATION OF ANALYTICAL AND EXPERIMENTAL RESULTS	86
1. Passive System Impedance Evaluation	86
a. Evaluation of Computer Modeling Efforts for Passive Systems	86
b. Evaluation of Experimental Results of Standard Passive Acoustic Systems	90
c. Evaluation of Experimental Engine Crank-angle Studies	91
2. Active System Impedance Evaluation	93
a. Analysis of Computer Modeling Effort of an Active Engine Acoustic System	93
b. Analysis of Motored Engine Studies	94

TABLE OF CONTENTS (Concluded)

SECTION	PAGE
c. Analysis of Operating Engine Data	99
VI DISCUSSION AND RECOMMENDATIONS	101
1. General Remarks	101
2. Success of Project's Approach	102
3. Recommendations	103
REFERENCES	105
APPENDIX A ACOUSTIC PRESSURE SENSOR SPACING	107
APPENDIX B COMPUTER ACOUSTIC MODELING EFFORT FOR AN INTERNAL COMBUSTION ENGINE	110

LIST OF ILLUSTRATIONS

FIGURE		PAGE
1	Test Facility for Powered Engine Experimentation	8
2	Crankangle Position Defining the Engine's Analogous Acoustic Passive Systems	10
3	Measurand Tube with Anechoic Tailpipe Termination	12
4	Pressure Transducers and Condenser Microphones as Mounted to the Measurand Tube	15
5	Pressure Transducers with Water-Cooling System and Thermocouple Shown Adapted to Measurand Tube	16
6	Motored Engine Sound Pressure Levels Compared with those Sound Pressure Levels Produced by the Horn Driver	18
7	Attachment of the Horn Driver to the Measurand Tube	19
8	Horn Driver Mounted to the Side of the Measurand Tube by Adapter with Water Cooling	20
9	External Acoustic Signal Generation for Horn Driver and Amplification	21
10	Anechoic Tailpipe Termination	23
11	Cross Section View of the Anechoic Tailpipe Termination	24
12	Schematic Representation of the Experimental Facility	26
13	Signal Monitoring and Recording System	27
14	The X-Ordinate System and Appropriate Dimensions for the Location of the Measured and Terminating Impedances	31
15	Dimensionless Resistive Impedance of Close Ended Measurand Tube	43
16	Dimensionless Reactive Impedance of Close Ended Measurand Tube	43
17	Dimensionless Resistive Impedance of Open Ended Measurand Tube	44
18	Dimensionless Reactive Impedance of Open Ended Measurand Tube	44
19	Dimensionless Resistive Impedance of Engine at 90° Crankangle	46

LIST OF ILLUSTRATIONS (Continued)

FIGURE		PAGE
20	Dimensionless Reactive Impedance of Engine at 90° Crankangle	46
21	Dimensionless Resistive Impedance of Engine at 130° Crankangle	47
22	Dimensionless Reactive Impedance of Engine at 130° Crankangle	47
23	Dimensionless Resistive Impedance of Engine at 170° Crankangle	48
24	Dimensionless Reactive Impedance of Engine at 170° Crankangle	48
25	Dimensionless Resistive Impedance of Engine at 260° Crankangle	49
26	Dimensionless Reactive Impedance of Engine at 260° Crankangle	49
27	Dimensionless Resistive Impedance of Engine at 340° Crankangle	50
28	Dimensionless Reactive Impedance of Engine at 340° Crankangle	50
29	Dimensionless Resistive Impedance of Engine at 360° Crankangle	51
30	Dimensionless Reactive Impedance of Engine at 360° Crankangle	51
31	Dimensionless Resistive Impedance of Engine at 400° Crankangle	52
32	Dimensionless Reactive Impedance of Engine at 400° Crankangle	52
33	Dimensionless Resistive Impedance of Engine Motored at 2 RPM	54
34	Dimensionless Reactive Impedance of Engine Motored at 2 RPM	54
35	Dimensionless Resistive Impedance of Engine Motored at 24 RPM	55

LIST OF ILLUSTRATIONS (Continued)

FIGURE		PAGE
36	Dimensionless Reactive Impedance of Engine Motored at 24 RPM	55
37	Dimensionless Resistive Impedance of Engine Motored at 370 RPM	56
38	Dimensionless Reactive Impedance of Engine Motored at 370 RPM	56
39	Dimensionless Resistive Impedance of Engine Motored at 390 RPM	57
40	Dimensionless Reactive Impedance of Engine Motored at 390 RPM	57
41	Dimensionless Resistive Impedance of Engine Motored at 450 RPM	58
42	Dimensionless Reactive Impedance of Engine Motored at 450 RPM	58
43	Dimensionless Resistive Impedance of Engine Motored at 475 RPM	59
44	Dimensionless Reactive Impedance of Engine Motored at 475 RPM	59
45	Dimensionless Resistive Impedance of Engine Motored at 555 RPM	60
46	Dimensionless Reactive Impedance of Engine Motored at 555 RPM	60
47	Dimensionless Resistive Impedance of Engine Motored at 560 RPM	61
48	Dimensionless Reactive Impedance of Engine Motored at 560 RPM	61
49	Dimensionless Resistive Impedance of Engine Operating at 1600 RPM at Full Load	63
50	Dimensionless Reactive Impedance of Engine Operating at 1600 RPM at Full Load	63
51	Dimensionless Resistive Impedance of Engine Operating at 2100 RPM with No Load	64

LIST OF ILLUSTRATIONS (Continued)

FIGURE		PAGE
52	Dimensionless Reactive Impedance of Engine Operating at 2100 RPM with No Load	64
53	Dimensionless Resistive Impedance of Engine Operating at 2200 RPM with Full Load	65
54	Dimensionless Reactive Impedance of Engine Operating at 2200 RPM with Full Load	65
55	Dimensionless Resistive Impedance of Engine Operating at 2400 RPM with No Load	66
56	Dimensionless Reactive Impedance of Engine Operating at 2400 RPM with No Load	66
57	Dimensionless Resistive Impedance of Engine Operating at 2700 RPM with No Load	67
58	Dimensionless Reactive Impedance of Engine Operating at 2700 RPM with No Load	67
59	Dimensionless Resistive Impedance of Engine Operating at 2950 RPM with No Load	68
60	Dimensionless Reactive Impedance of Engine Operating at 2950 RPM with No Load	68
61	Dimensionless Resistive Impedance of Engine Operating at 3520 RPM with No Load	69
62	Dimensionless Reactive Impedance of Engine Operating at 3520 RPM with No Load	69
63	Dimensionless Resistive Impedance of Engine Operating at 3600 RPM with No Load	70
64	Dimensionless Reactive Impedance of Engine Operating at 3600 RPM with No Load	70
65	Schematic of Computer Simulated Experimental Engine's Acoustic Components, with each Component Dimensions	71
66	Theoretically Predicted Close Ended Tube Dimensionless Resistive Impedance Response	72
67	Theoretically Predicted Close Ended Tube Dimensionless Reactive Impedance	73

LIST OF ILLUSTRATIONS (Continued)

FIGURE		PAGE
68	Theoretically Predicted Volume Resonator Dimensionless Resistive Impedance	74
69	Theoretically Predicted Volume Resonator Dimensionless Reactive Impedance	75
70	Simulated Engine Dimensionless Resistive Impedance Using a 40% Volume Resonator Effect and a 60% Close Ended Tube Effect	78
71	Simulated Engine Dimensionless Reactive Impedance Using a 40% Volume Resonator Effect and a 60% Close Ended Tube Effect	79
72	Simulated Engine Dimensionless Resistive Impedance Using a 60% Volume Resonator Effect and a 40% Close Ended Tube Effect	80
73	Simulated Engine Dimensionless Reactive Impedance Using a 60% Volume Resonator Effect and a 40% Close Ended Tube Effect	81
74	Simulated Engine Dimensionless Resistive Impedance Using a 5% Volume Resonator Effect and a 95% Close Ended Tube Effect	82
75	Simulated Engine Dimensionless Reactive Impedance Using a 5% Volume Resonator Effect and a 95% Close Ended Tube Effect	83
76	Simulated Engine Dimensionless Resistive Impedance Using a 90% Volume Resonator Effect and a 10% Close Ended Tube Effect	84
77	Simulated Engine Dimensionless Reactive Impedance Using a 90% Volume Resonator Effect and a 10% Close Ended Tube Effect	85
78	Dimensionless Resistive Impedance of 90° Crankangle Study (B) and 2 RPM Motored Engine Study (A)	96
79	Dimensionless Reactive Impedance of 90° Crankangle Study (B) and 2 RPM Motored Engine Study (A)	96
80	Dimensionless Resistive Impedance of 90° Crankangle Study (B) and 24 RPM Motored Engine Study (A)	97

LIST OF ILLUSTRATIONS (Concluded)

FIGURE		PAGE
81	Dimensionless Reactive Impedance of 90° Crankangle Study (B) and 24 RPM Motored Engine Study (A)	97
82	Thermodynamic Cycle Completion Time as a Function of the Engine Speed	98
A-1	Temperature Effects on Acoustic Sensor Position	109
B-1	Cyclic Volume Variation with the Engine Crankangle	113
B-2	Computer Program which Simulates the Engine Acoustically	114

LIST OF TABLES

TABLE		PAGE
1	Exhaust and Intake Valve Position with Engine Crankangle	9
2	Listing of Volume Ratios and Corresponding Closed Tube Ratios Used in Various Acoustic Engine Simulations	77
3	Experimental Pursuit Taken to Evaluate Engine Source Impedance	101
B-1	Cylinder Volume with Engine Crankangle Variation	112

NOMENCLATURE

a	Inside Radius of Measurand Tube and/or Volume Resonator
A	Arbitrary Complex Amplitude
B	Arbitrary Complex Amplitude
c	Speed of Sound
e	Exponential Power Designation
f	Frequency
F	Fourier Transform
H	Transfer Function
i	Imaginary Quantity Operator
j	Imaginary Quantity Operator
k	Wavelength Constant
L	Length Designation where $x = L$
ℓ	Length Designation where $x = \ell$
L'	Length of Exponential Horn
ℓ'	Modified or Effective Acoustic Length
m	Exponential Horn Flare Constant
p	Acoustic Pressure of Plane Waves
P	Total Acoustic Pressure
r	Specific Acoustic Resistance
R	Acoustic Resistance
R'	Resistance Function
S	Area
S'	Cross-Section Area of Exponential Horn at $x = L'$
t	Time
T	Temperature

NOMENCLATURE (Continued)

U	Volume Velocity
v	Particle Velocity
V	Volume
x	Indicates x - Ordinate Axis
x	Specific Acoustic Reactance
X	Acoustic Reactance
z	Specific Acoustic Impedance
Z	Acoustic Impedance
α	Attenuation Constant
β	Attenuation Constant
γ	Frictionally Damped Propagation Constant
ρ	Density of Acoustic Transmission Medium
ω	Angular Frequency

SUBSCRIPTS AND SUPERSCRIPTS

BDC	Bottom Dead Center (Abbreviation)
c	Close Ended Tube Case
H	Helmholtz and/or Volume Resonator Case
j or i	Imaginary Value Operators
i	Incident Wave Information
ℓ	Information where $x = \ell$
L	Information where $x = L$
n	Reference to Natural Frequency
o	Used as a Subscript, Information where $x = 0$
o	Used as a Superscript, Refers to Open Ended Tube Case

NOMENCLATURE (Concluded)

r	Reflected Wave Information
s	Characteristic Impedance
TDC	Top Dead Center (Abbreviation)
1 or 2	As Subscripts, Indicate Information at Positions 1 or 2, respectively
^	Indicates a Peak Value
*	Defines a Dimensionless Quantity

SECTION I

INTRODUCTION

1. NEED FOR POWERED ENGINE ACOUSTIC STUDIES

Interest in engine acoustic's research has been stimulated through increased concern to reduce combustion related noise from the exhaust system of an internal combustion engine. The impetus for this particular project stemmed from the often expressed need to understand the engine as an acoustic source. In particular, identification of the engine's exhaust port acoustic characteristic of source impedance would contribute significantly towards meeting this increasingly more important need.

The main emphasis in this study was placed on further definition of an engine model for interpreting source impedance. Source impedance, rather than source strength, was modeled because the transfer phenomena of acoustic energy from the engine to the exhaust system was considered to depend primarily on the relative values of the engine source impedance and impedance of the exhaust system (Reference 2). In the engine modeling effort, interpretation of the engine's valve positions and cylinder volume time histories were important considerations.

The modeled source impedance of an active internal combustion engine, if available, could be analytically investigated in conjunction with known passive acoustic impedance of modeled muffler systems toward improved definition of attenuation efficiency for an engine's exhaust system. This project's technique for developing a model for engine source impedance utilized an experimental acoustic impedance measurement facility along with some analytical and computer disclosures. The experimental facility for this project was developed to permit measurement of acoustic source impedance for a powered engine, i.e., an engine operating under its own combustion power. This required provisions to account for the effects of hot exhaust gas and an appreciable velocity head as a direct result of the incurred products of the engine's combustions process.

2. PREVIOUS APPROACHES TO ACOUSTIC IMPEDANCE EVALUATION

a. Approaches Before Digital Signal Analysis

An example of earlier experimental investigations of engine acoustics is the reported work by Alfredson and Davies (Reference 1) where the acoustic radiation impedance from an engine's exhaust system was evaluated using the tailpipe as the impedance tube and the engine noise as an acoustic source. Their investigation included such considerations as mean gas flow, the temperature gradient along the exhaust system, and boundary conditions at the termination of the exhaust system's tailpipe. Their results concluded among other findings that the mean flow produced by the engine's exhaust had a considerable effect on the radiation impedance for the tailpipe. This work is also informative concerning the complexities associated with conducting an experimental investigation of engine acoustics.

A theoretical formulation toward determination of acoustic impedance for an engine has been proposed by Kathuriya and Munjal (Reference 3). This formulation has been developed to include consideration of the effects of mean exhaust gas flow. The related experimental approach suggested by Kathuriya and Munjal's analytical development involved utilization of an impedance tube. Standing waves can develop in the impedance tube even with mean flow. However, the theoretical analysis of standing waves suggested by Kathuriya and Munjal was difficult to duplicate in the laboratory with an experimental facility. Several disadvantages inherent within the method of standing wave analysis are:

- a) Discrete frequency excitation in the impedance tube by an external source yields a time consuming evaluation for broad-band frequency assessment.
- b) The traversing acoustic pressure sensor position must be accurately detected to resolve the magnitude and phase complements of the investigated acoustic properties. This becomes increasingly difficult at higher frequencies due to smaller wavelengths (e.g., $\pm .03$ in. @ 6000 hz).

- c) Measurements must be made within a relatively long impedance tube along which acoustic energy dissipation does occur at the side walls. Therefore, any signal generated within the tube is attenuated, particularly at higher frequencies.
- d) The microphone or pressure transducer must be moved more than a half wavelength at each frequency to record the acoustic pressure maxima and minima values. This requires a very long and cumbersome probe system particularly for the lower frequency measurements.
- e) The required probe creates an acoustic discontinuity along the length of the impedance tube.

Most methods of acoustic impedance evaluation developed during the early stages of engine acoustic analysis utilized discrete frequency excitation. As previously indicated impedance evaluation was a time consuming endeavor when a broadband frequency analysis was desired. A method developed by Singh and Katra (Reference 11) utilized an acoustic impulse method. This method eliminated the problem of a time consuming analysis inherent in acoustic evaluation with discrete frequency excitation. However, producing an acoustic pulse with sufficient acoustic energy, particularly with high frequency content, is difficult. There were additional problems reportedly with signal attenuation and transients due to underdamped driver systems. The combination of these problems make it impractical to use impulse testing.

b. Approaches Since Digital Signal Analysis

Recent methods of evaluating acoustic impedance have incorporated a digital signal analyzer which uses the input from two stationary wall-mounted acoustic sensors to give amplitude and phase information of the acoustic signal. Seybert and Ross (Reference 6) were one of the first to implement the digital signal analyzer in acoustic impedance analysis. Seybert and Ross utilized an auto- and cross-spectral analysis

included in a mathematical formulation to yield the special acoustic impedance and reflection coefficient at the termination of an impedance tube. However, the analysis and mathematics involved limited the applicability of this method more to research experimentation rather than to laboratory engine testing. The digital signal analyzer approach was considered by Blaser and Chung (Reference 10) who utilized a transfer-function method which provides a direct readout of quantities such as transmission loss, reflection coefficient, and acoustic impedance. The method proposed by Blaser and Chung eliminates much of the spectral computation involved in Seybert and Ross' technique.

3. FORMULATED APPROACH TOWARD POWERED ENGINE ACOUSTIC IMPEDANCE EVALUATION

a. Experimental Assessment of Engine Impedance

Utilizing Blaser's and Chung's work as a basis for experimental development, the first efforts were focused on application of their experimental endeavors to powered engine acoustic evaluation. Several modifications had to be made in the experimental facility so the elevated temperatures caused by the engine's exhaust would have no adverse effects on any measurements or measurement instrumentation. Such auxiliary facilities as water-cooling systems for the acoustic pressure sensors and a horn driver unit had to be built. A heat retardant anechoic tailpipe termination and an adjustable pressure sensor, hermetically sealed to the impedance tube were also newly applied experimental developments.

This measurement facility has the potential of measuring several acoustic characteristics, such as transmission loss. But its use centered about defining acoustic source impedance. The integral part of this measurement system is the digital signal analyzer which performs the acoustic analysis on the acoustic signal and by way of transfer functions defines the acoustic source impedance. An additional consideration towards this measurement technique identifies the acoustic impedance evaluated as the measured impedance at the acoustic sensors

and not the impedance of the engine. Consequently, some mathematics are involved to interpret the source impedance at the engine and to qualify the measured impedance.

Initial engine tests utilized the engine as a passive system by completing acoustic impedance analysis at varying engine crankangles. Further acoustic impedance testing included motoring the engine with a starting motor and completing impedance analysis at various motored engine speeds. Engine testing climaxed with efforts to perform acoustic impedance evaluation.

b. Analytical Modeling of Engine Impedance

Initial investigation of engine crankangle acoustic impedance studies and those acoustic impedance evaluations of standard passive system (open and close ended impedance tube) led to a conceptualized model for engine acoustic impedance. The model consisted of passive systems where the dimensions of these passive systems were dictated by the engine's internal geometry. It was the hypothesis of this model that the engine, as it completes each thermodynamic cycle, also cycles through several passive acoustic systems. For example, when the engine is stopped at a crankangle identified at 180 degrees from top dead center, the exhaust valve is opened and the engine is expected to acoustically resemble a volume resonator. That is, the exhaust valve is opened and the piston is at its lowest position in the cylinder, so that the volume resonator would be the vacated cylinder. The analytical modeling of the engine was acoustically achieved by mathematically determining the impedance characteristics of the passive systems in the model. Further, fundamental idealizations were involved which defined the passive system impedance as a terminating impedance and associated this impedance at the acoustic pressure sensors with the measured impedance. These theoretical cases were necessary to simulate the experimental case more accurately. The entire theoretical analysis was summarized into a computer program which would simulate the engine's acoustic impedance characteristics.

c. Agreement Between Analytical and Experimental Defined Impedances

The first comparisons between analytically and experimentally attained impedance characteristics were of standard passive systems. Good agreement was shown between experimental and analytical results. Also, several responses in the experimental impedance characteristics could be predicted by changing particular theoretical variables, thereby learning how the physical dimensions of the passive acoustic system affects its impedance characteristics.

The experimental studies of motored engine and powered engine source impedance evaluation were less conclusive. Several trends developed within these experimental results were sporadic until compared with the analytical results. The flexibility within the computer simulated model assisted in identifying the variability of the experimentally attained source impedance. The usefulness of the computer model was further affirmed in the identification of the basic cyclic behavior of acoustic impedance characteristics for the internal combustion engine evaluated.

This application of computer modeling efforts could be extended further to encompass the combined engine/muffler exhaust system. By modeling the engine accurately along with the muffler acoustic characteristics, one could possibly predict the insertion loss for an engine/exhaust system. The design of better mufflers was not a consideration in this work.

SECTION II

EXPERIMENTAL DEVELOPMENT

1. TEST ENGINE SELECTION AND OPERATIONAL DEVELOPMENT

Towards the pursuit of identifying certain acoustic characteristics of an internal combustion engine, it was necessary to select an engine for experimentation. On the basis of its simpler construction and operation, a single cylinder Tucumseh, Model HH-120, engine was used for powered engine experimentation (Figure 1). The engine was a 12 horsepower, 3600 rpm, 28 cubic inch displacement engine with a compression ratio of 6. Some additional engine specifications of importance to this project were:

Piston Stroke: 2.8 inches

Cylinder Bore: 3.5 inches

Internal Manifold Length: 1 inch (approximate)

Internal Manifold Diameter: 2-1/4 inches (approximate)

This information was used to develop dimensions for the acoustic passive systems that were conceptualized to simulate various engine internal geometries, i.e., manifold and cylinder volumes during engine operation.

The concept of acoustic passive system engine simulation is identified in the engine internal cyclic geometry changes which occur during one thermodynamic cycle. Within the thermodynamic cycle, for example, when the engine begins its power stroke, the exhaust valve was closed. The engine then physically resembles a close ended tube with the length of the manifold volume being the length of the closed tube. The exhaust valve, by the way of the exhaust manifold, is the only connection to the engine's internal piston cavity acoustic phenomena. Consequently, it is essential that the exhaust valve's open/close operation be known so that the entire physical resemblance of the engine is known, i.e., with regards to an acoustic passive system complement.



Figure 1. Test Facility for Powered Engine Experimentation

The exhaust and intake valve positions are monitored by way of crankangle identification in correlation with the thermodynamic cycle of the engine (Table 1).

Table 1

EXHAUST AND INTAKE VALVE POSITION WITH ENGINE CRANKANGLE

Crankangle Position (Angular Degrees from Top Dead Center)	Exhaust Valve Position	Intake Valve Position
0° - 110°	Closed	Closed
110° - 360°	Open	Closed
360° - 400°	Open	Open
400° - 540°	Closed	Open
540° - 720°	Closed	Open

Particular interest occurs when the exhaust valve is open, i.e., 110° through 400°. It is for these crankangles that the acoustic source (i.e., the engine) is most geometrically active. The schematic shown in Figure 2 identifies the thermodynamic cycle, piston position, exhaust valve position, intake valve position and analogous passive acoustic system, all as a function of the engine's crankangle. The schematic also includes a column titled "Description" which provides justification for the choice of the passive system.

a. Motored Engine Operation

To eliminate some of the complexities of the engine's acoustic output contributed by the combustion process, the engine was connected to a starting motor unit so that the engine could be motored. Motored engine acoustic impedance studies could then be completed without the pressure dynamics generated by combustion. Flexibility in motored engine speeds was attained by varying the current to the starter motor by means of an adjustable battery recharging unit (Figure 1).

The range of speed variation offered by this system was constrained to a maximum motored engine speed of 600 rpm and a minimum of 300 rpm.

Schematic of Engine Operation		Analogous Acoustic System		Description
<p>Thermodynamic Cycle Compression A/R Intake Exhaust Stroke Power Stroke</p>			<p>Transducer Ports Anechoic Tailpipe Horn Driver</p>	The exhaust valve is closed and the engine will look acoustically like a closed ended tube
	110			With the exhaust valve open an expanding volume with possible resonator effects are expected.
	180			The exhaust valve is open and a decreasing volume with possible resonator effects are expected.
	360	<p>Intake Valve Exhaust Valve</p>		With the exhaust and intake valves open, possible expansion chamber effects are expected.
	400			The exhaust valve is again closed and the engine will acoustically resemble a closed ended tube.

Figure 2. Crankangle Position Defining the Engine's Analogous Acoustic Passive Systems

The power made available by the starting motor was rather limited so that loading the engine while being motored was not attempted.

The length of time that the engine could be motored was restricted since the starting motor would overheat after a certain period of usage. Consequently, the starting motor was carefully monitored so that a series of motored engine studies could be completed without seriously damaging the starting motor.

b. Powered Engine Operation

Powered engine operation was achieved by operating the engine at its normal running conditions. Variation in engine speed was attained by throttling the engine. The engine facility also had the capability of being loaded. Loading was achieved by having the engine drive an electric generator unit. The voltage produced by the generator could be dissipated by a load cell comprised of a series of high power light bulbs (500 watt). As each light was turned on, the lighting unit drained more power from the generator, which in turn, further loaded the engine (engine loading by this system had a potential of 6000 watts, which was 100% of the engine's maximum brake horsepower). This loading system was used in several of the powered engine tests.

The range of engine speed available was a maximum of 3600 rpm to a minimum of 1500 rpm. The capability of loading the engine when operating at lower speeds was limited to approximately 1000 watts since the engine could stall if heavily loaded; however, maximum loading was available when engine speed exceeded 3000 rpm.

2. MEASURAND TUBE FACILITY DEVELOPMENT

Once the engine with motoring capability was developed, the principle measurement tool, known as a measurand tube, was designed. The measurand tube, which is similar to the classical impedance tube, provides a transmission line where engine acoustic properties may be evaluated (Figure 3). The transmission line allows propagation of



Figure 3. Measurand Tube with Anechoic Tailpipe Termination

acoustic pressure signals to travel along its length in either direction. Acoustic discontinuities, such as:

- 1) Cross-sectional area changes, which cause a change in the acoustic impedance within the tube;
- 2) Varying dimension in wall thickness, particularly for tube walls which are thin, which causes a dissipation of acoustic energy due to vibration of the tube walls. (ASTM (Reference 19) requires the wall thickness of an impedance tube to be at least 8% of the tube inside diameter.);
- 3) Varying roughness along the length inside the impedance tube which causes varying acoustic energy losses along the length.
- 4) Any holes or loose connections, (if the measurand tube is two pieces), which cause acoustic energy leaks at the discontinuity;

were considered in the design for acoustic pressure sensors access ports, external acoustic source adapter, and tube tailpipe termination.

a. Acoustic Pressure Sensor Selection

Acoustic sensing elements were selected primarily to be able to detect acoustic pressure disturbances within the pressure environment of the measurand tube. Two types of pressure sensor devices were considered; the first was acoustic microphones and the second was low impedance pressure transducers with dynamic ranges which include acoustic pressure levels. Experimentation with pressure transducers is generally constrained to higher dynamic ranges than microphones. The lower limit of measurable acoustic pressure levels for pressure transducers is approximately 85 decibels (dB) because internal instrument noise masks the acoustic signal. The dynamic range afforded when using small diameter acoustic microphones is approximately 40 dB to 170 dB. A second consideration toward acoustic pressure selection was the thermal environment in which the measurement was to be made. During powered engine operation the acoustic pressure sensors were expected to subject to very sooty exhaust gases with temperatures in excess of 1100°F.

Piezoelectric pressure transducers (Kistler 202A5) were chosen for powered engine studies, while condenser microphones were selected for passive system and motored engine studies. The pressure transducers had water-cooling jackets enabling them to withstand flash temperatures in excess of 2000°F.

The pressure transducers and microphones were mounted as flush as possible to the outside wall of the measurand tube at the acoustic access ports, as shown in Figure 4. It can be seen that the two pressure transducers were temperature and vibration isolated using an ablative silicone (General Electric RTV560) to form a rubber gasket sealing the sensors into position while eliminating possible dissipation of acoustic energy. The location of the pressure transducers and microphones from the exhaust port of the engine was approximately 250 millimeters (mm). This distance was deemed appropriate to minimize both the undesired near-field effects of chamber combustion and the attenuation effects of extended tube distance. Relative location of the pressure transducers and microphone access ports to each other was dependent upon several factors. One important factor, related to digital signal analysis capabilities, was that an available time delay (78 microseconds) had to be selected. This time delay was the time needed to establish the transfer functions for right and left traveling waves within the measurand tube. The condenser microphones were spaced 27 mm apart while pressure transducer spacings could be varied from 35 mm to 47 mm. One pressure transducer position remained fixed while the second pressure transducer position was adjustable (Figure 5). This flexibility was needed so that as the exhaust temperature varies with such conditions as engine speed and load, the speed of sound varies with the exhaust temperature and the distance over which right- and left-traveling waves propagate in 78 microseconds varies with the speed of sound. The temperature was monitored by a thermocouple inserted within the mainstream of the measurand tube near pressure transducers (Figure 5). As the temperature changed, the spacing between the pressure transducers was correspondingly adjusted according to a precalculated position curve (Appendix A).

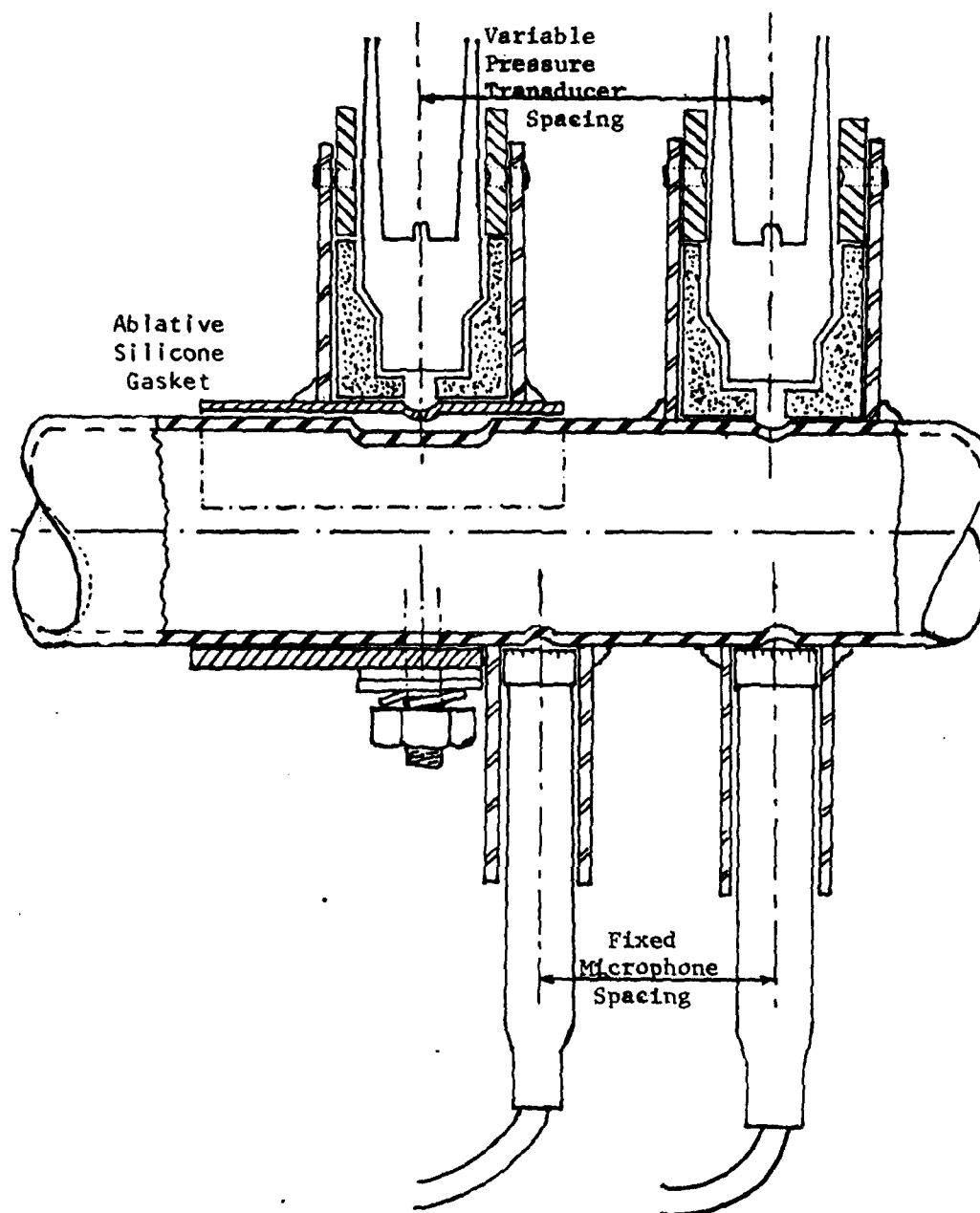


Figure 4. Pressure Transducers and Condenser Microphones as Mounted to the Measurand Tube



Figure 5. Pressure Transducers with Water-Cooling System and Thermocouple Shown Adapted to Measurand Tube

b. External Acoustic Signal System

This experimentation required that an adequate external acoustic signal be introduced into the measurand tube. This acoustic signal was made to propagate down the measurand tube toward the engine. The resultant incident-reflected acoustic phenomena was then assessed by monitoring the two pressure sensors. It was desired to externally produce an acoustic signal with a sound pressure level 10 dB above the sound pressure level of the operating engine for all spectrum frequencies of interest. The noise spectrum level at the acoustic pressure sensors produced by the engine varied from 110 dB at the lower frequencies to 90 dB at the higher frequencies.

A 60 watt electromagnetic acoustic horn driver (LTV Ling Altec) was chosen because of its frequency range and maximum sound pressure level capabilities. This horn driver provided a sound pressure level of 135 dB within the measurand tube over the desired 500 Hz to 6000 Hz bandwidth. Figure 6 shows the monitored horn driver signal compared to the corresponding noise spectrum for the motored engine.

The acoustic horn driver was mounted perpendicular to the measurand tube to decrease interaction between the combustion dynamics produced by the engine and the diaphragm of the horn driver (Figure 7). This arrangement reduced possible signal distortion and lessened diaphragm deterioration. A screen with asbestos fiber and steel wool was placed in front of the diaphragm to collect some of the combustion particulates and inhibit the convection heat transferred by the engine's exhaust. Harmful conduction heat transfer from the measurand tube horn driver was minimized by implementing a cooling-water jacket around the horn driver adapter (Figure 8). The acoustic signal was generated by a random noise generator (filtered) using a bandpass from 500 Hz to 6000 Hz and then power amplified to drive the acoustic horn (Figure 9).

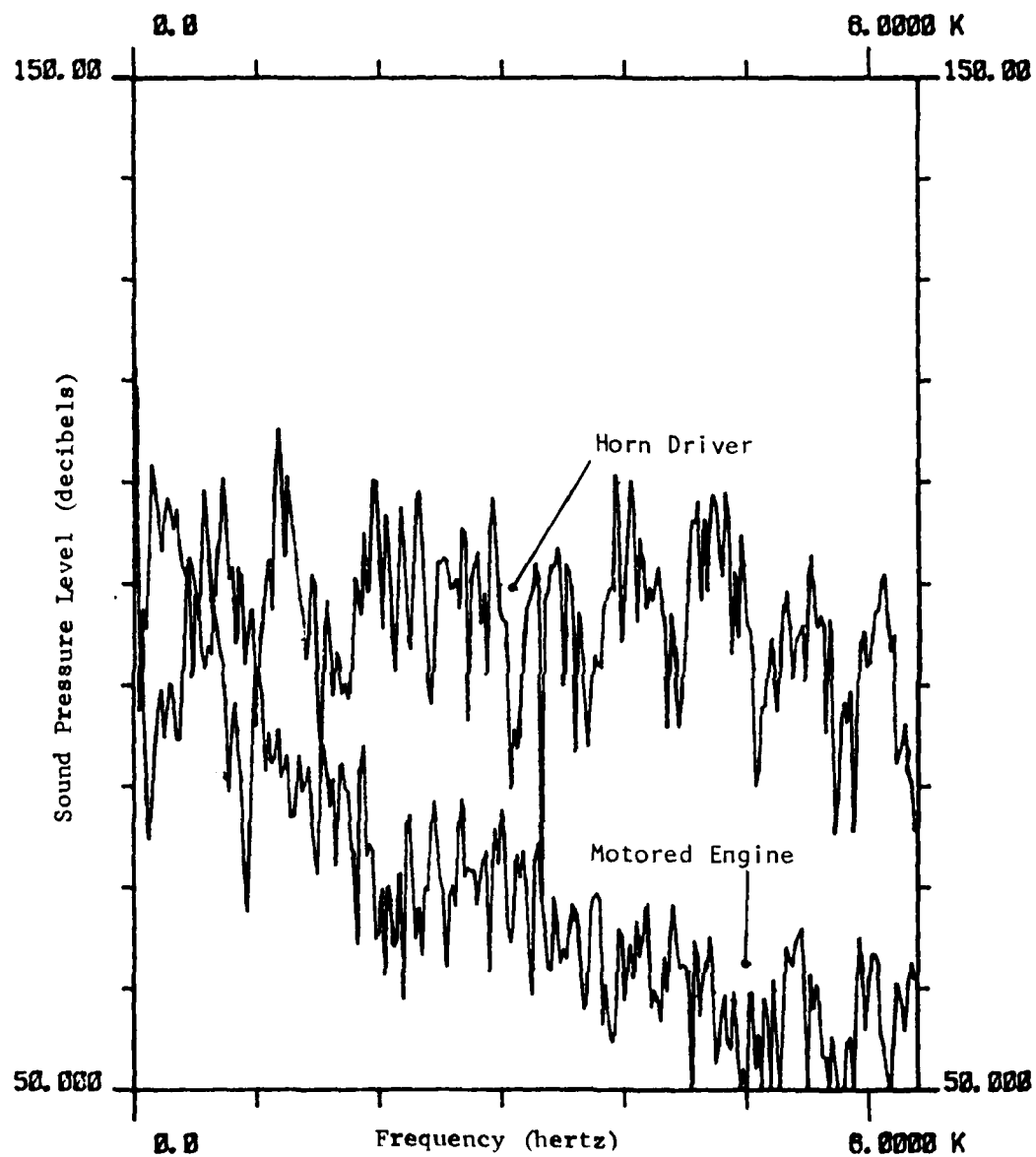


Figure 6. Motored Engine Sound Pressure Levels Compared with those Sound Pressure Levels Produced by the Horn Driver

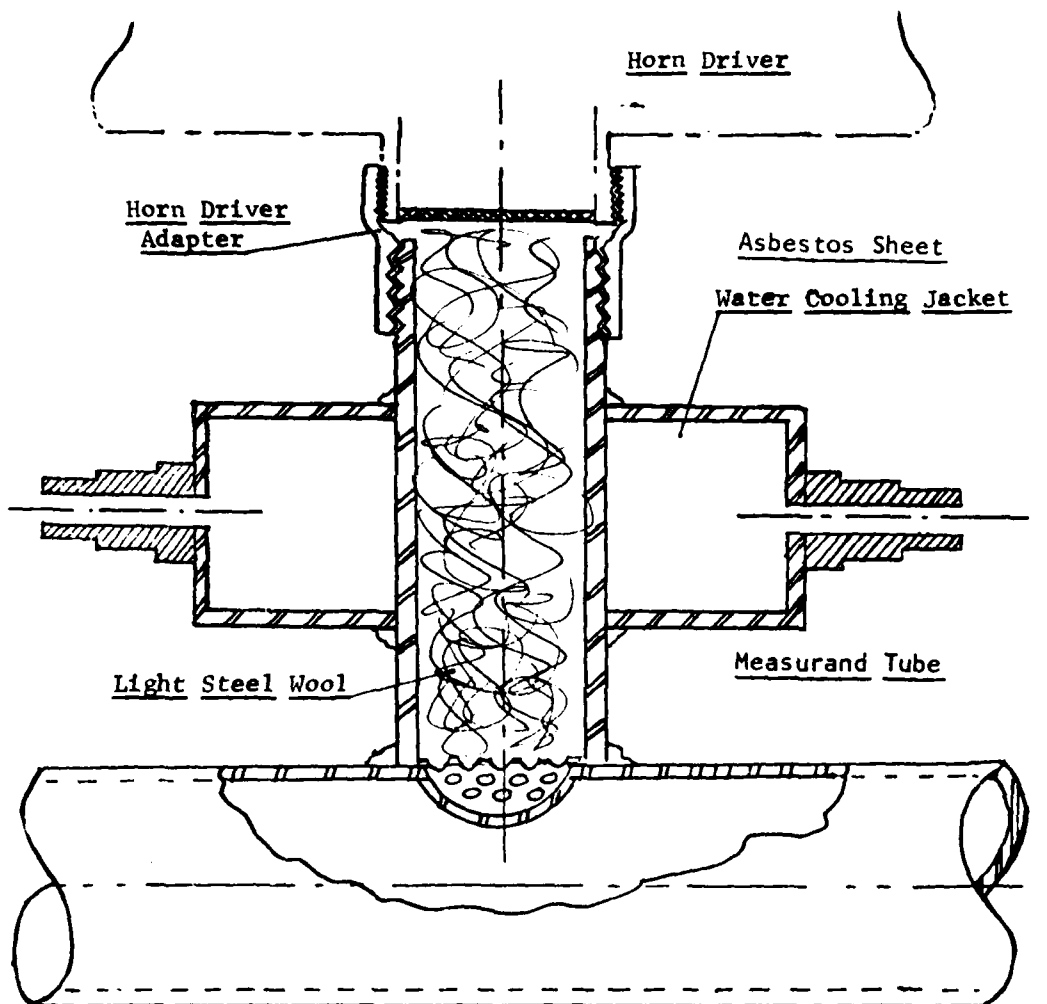


Figure 7. Attachment of the Horn Driver to the Measurand Tube



Figure 8. Horn Driver Mounted to the Side of the Measurand Tube by Adapter with Water Cooling

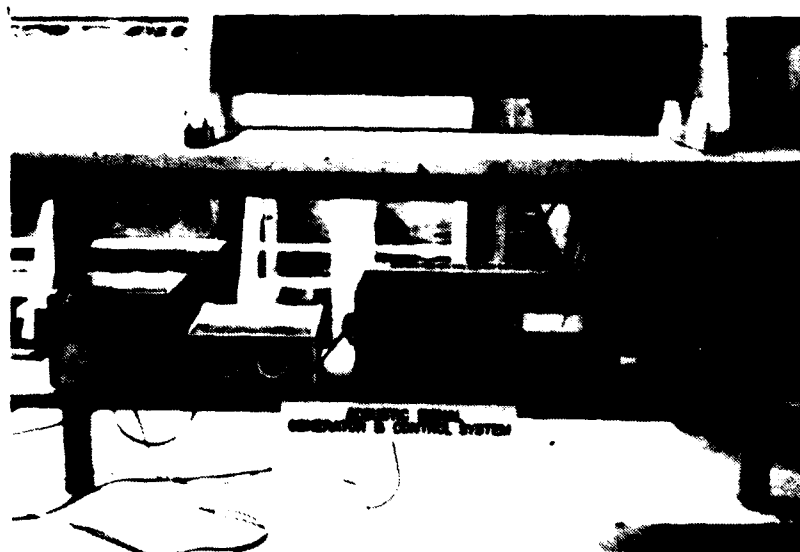


Figure 9. External Acoustic Signal Generation for Horn Driver and Amplification

3. ANECHOIC TAILPIPE TERMINATION

Control of the engine's contribution to the acoustic environment within the measurand tube required that a method be devised by which engine noise would not be reflected back to the engine after interfacing the tailpipe end of the measurand tube. Elimination of reflected engine noise is necessary so that the incident-reflected characteristics of the externally generated acoustic horn driver signal can be detected and easily monitored and not be masked by engine noise. As a tailpipe termination, an exponential horn geometry followed by an attached cylinder was designed (Figure 10). Thus, with the termination, longer wavelengths, i.e., lower frequencies of interest, would not be reflected at the tailpipe end of the measurand tube.

The effectiveness of an exponential horn at transmitting sound is defined in terms of cut-off frequency (f_c). The cut-off frequency for an exponential horn is dependent on the flare constant (m) of the horn. This flare constant, indicative of the rate of exponential expansion of the horn, can be calculated from the equation (Reference 9):

$$m = \frac{1}{L_1} \ln \frac{S_1}{S_0}$$

where

S_1 is the cross-sectional area at the distance L_1 from the throat of the horn,

S_0 is the cross-sectional area at the throat of the horn. The experimental horn developed (Figure 11) had a flare constant of 1.84 ft^{-1} .

The cut-off frequency for an exponential horn can be evaluated using the equation (Reference 9):

$$f_c = \frac{mc}{4}$$



Figure 10. Anechoic Tailpipe Termination

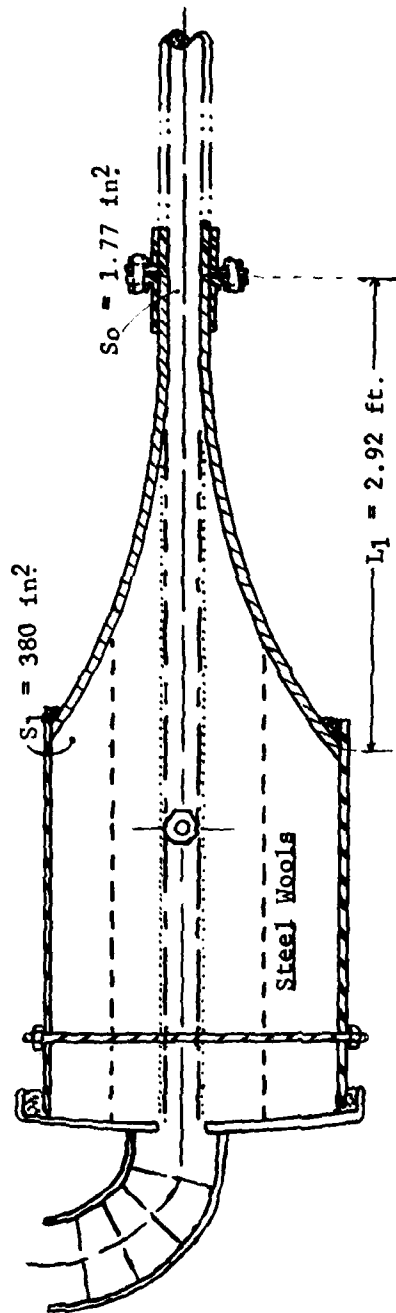


Figure 11. Cross Section View of the Anechoic Tailpipe Termination

where

c is the speed of sound

Using the above flare constant, it was assessed that the exponential tailpipe termination should absorb sound energy with frequencies above 167 Hz for motored engine studies and should absorb sound energy with frequencies above 280 Hz for powered engine studies.

To enhance the effectiveness of the tailpipe termination, the cavity of the exponential horn and attached cylinder were filled with varying grades of steel wool. The acoustic energy thus propagated by the horn would be dissipated in the steel wool (Figure 11). The packing order for the several grades of steel wool used was determined by a detailed study of steel wools as effective anechoic terminations. The exponential horn with attached cylinder was attached by a flexible exhaust duct to a powered exhaust vent.

4. ACOUSTIC SIGNAL MEASUREMENT SYSTEM

a. Signal Monitoring and Recording System

The facility developed for performing acoustic impedance evaluation of the engine included the incorporation of monitoring devices for engine speed and exhaust temperature, as well as record capabilities for acoustic pressure (Figures 12 and 13).

The engine speed during experimentation was monitored using a strobe tachometer (Figure 1). The strobe tachometer permitted inspection of the engine speed stability throughout a particular evaluation of acoustic impedance.

The temperature of the exhaust gas was monitored by means of a thermocouple (Section II.2.a). The temperature was indirectly read from a temperature potentiometer (Leed's and Northrup) that indicated a voltage potential which was then translated to a temperature reading.

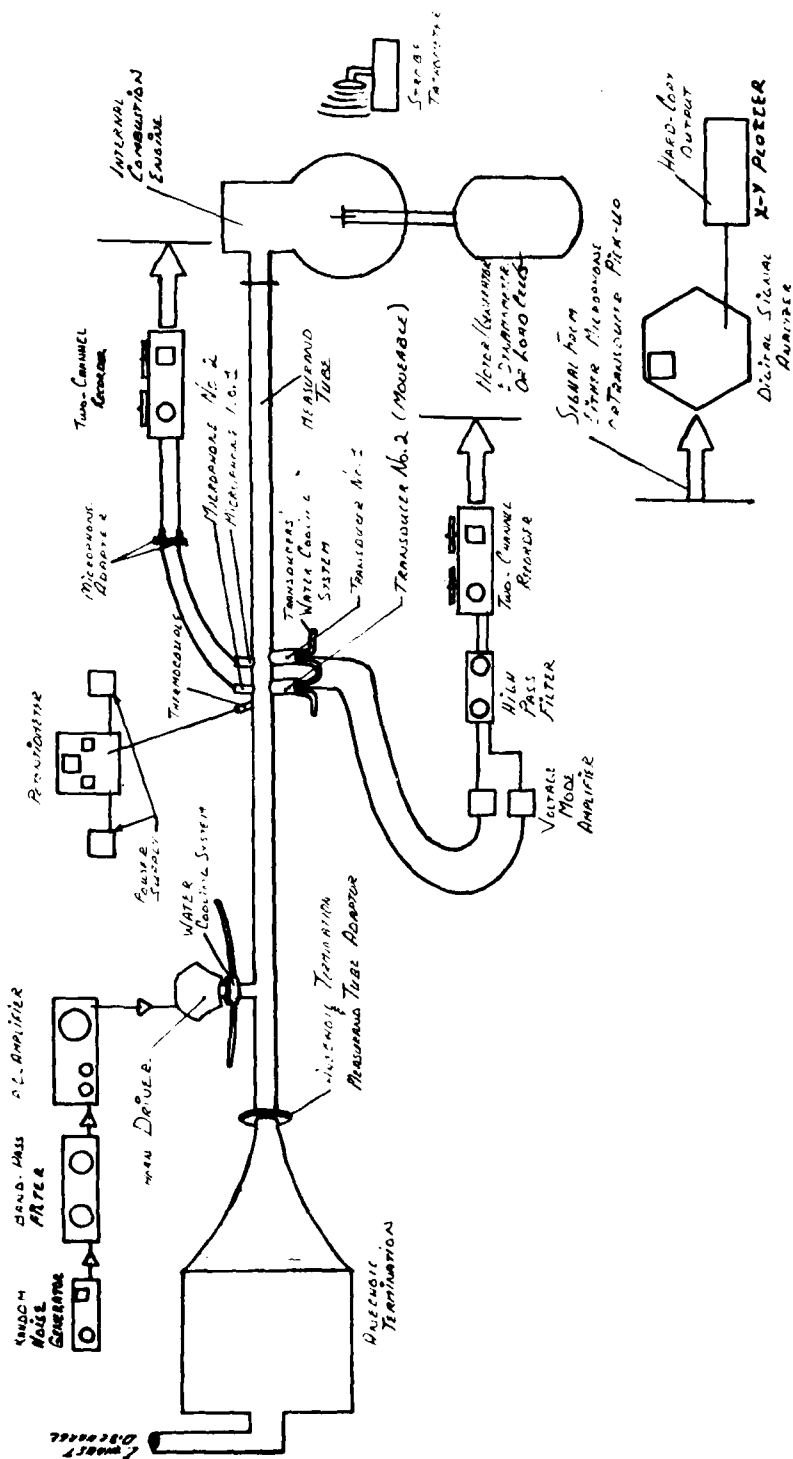


Figure 12. Schematic Representation of the Experimental Facility

where

c is the speed of sound

Using the above flare constant, it was assessed that the exponential tailpipe termination should absorb sound energy with frequencies above 167 Hz for motored engine studies and should absorb sound energy with frequencies above 280 Hz for powered engine studies.

To enhance the effectiveness of the tailpipe termination, the cavity of the exponential horn and attached cylinder were filled with varying grades of steel wool. The acoustic energy thus propagated by the horn would be dissipated in the steel wool (Figure 11). The packing order for the several grades of steel wool used was determined by a detailed study of steel wools as effective anechoic terminations. The exponential horn with attached cylinder was attached by a flexible exhaust duct to a powered exhaust vent.

4. ACOUSTIC SIGNAL MEASUREMENT SYSTEM

a. Signal Monitoring and Recording System

The facility developed for performing acoustic impedance evaluation of the engine included the incorporation of monitoring devices for engine speed and exhaust temperature, as well as record capabilities for acoustic pressure (Figures 12 and 13).

The engine speed during experimentation was monitored using a strobe tachometer (Figure 1). The strobe tachometer permitted inspection of the engine speed stability throughout a particular evaluation of acoustic impedance.

The temperature of the exhaust gas was monitored by means of a thermocouple (Section II.2.a). The temperature was indirectly read from a temperature potentiometer (Leed's and Northrup) that indicated a voltage potential which was then translated to a temperature reading.

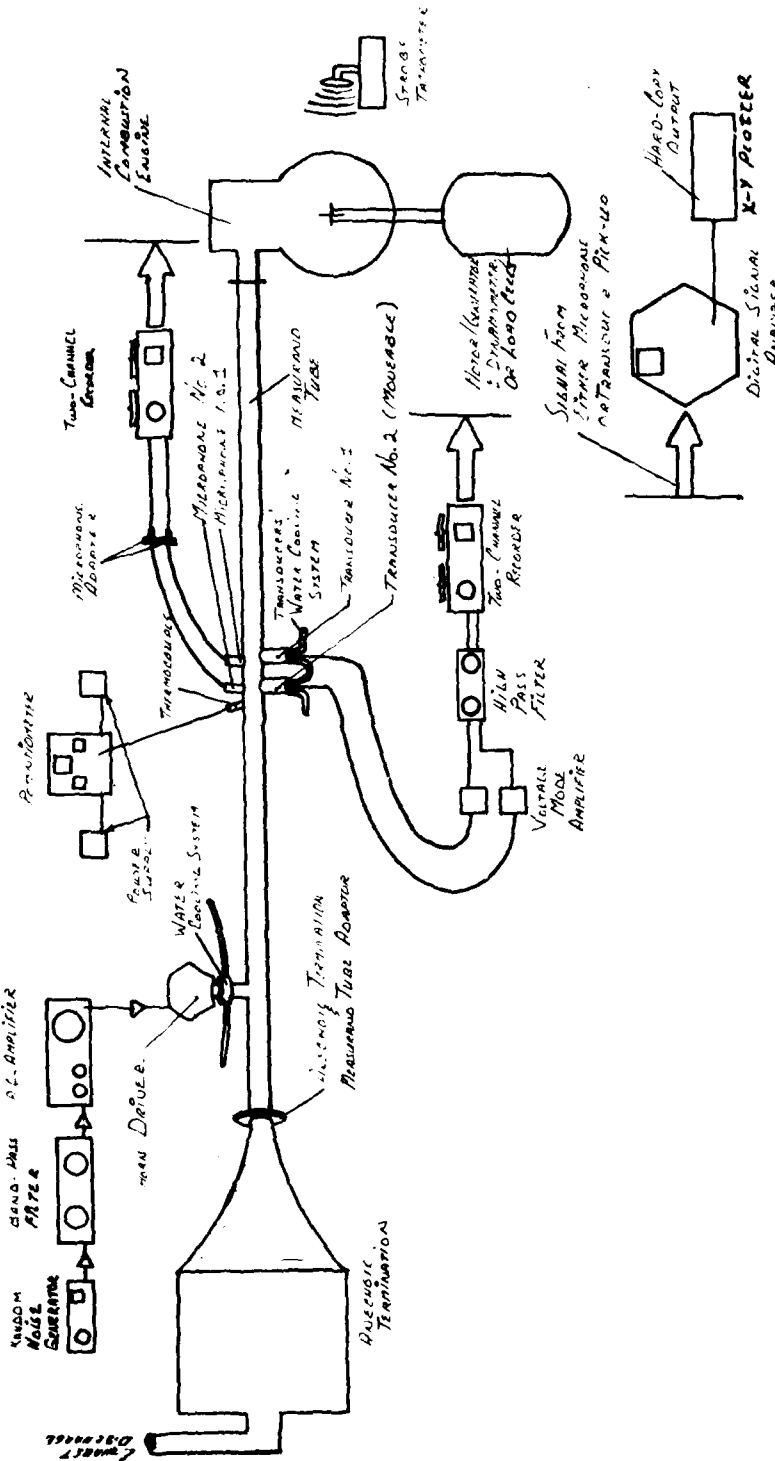


Figure 12. Schematic Representation of the Experimental Facility

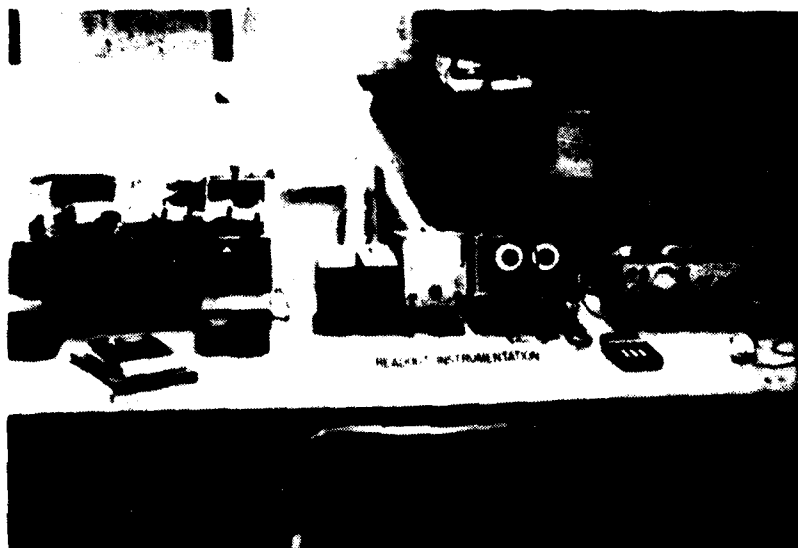


Figure 13. Signal Monitoring and Recording System

The temperature was obtained so that the appropriate pressure transducer spacing could be known for each engine test.

The acoustic pressure signal conditioning system consisted of several intermediate devices connected to the pressure transducers. After the acoustic signal from the pressure transducer was conditioned by a charge amplifier (Kisler 504A), the amplified signal was fed into an RMS voltmeter. The voltmeter was monitored so that excessive RMS voltages would not be inputted into succeeding intermediate devices. Once the acoustic signal was appropriately amplified, the acoustic signal was bandpass filtered using a 500 Hz to 6000 Hz bandwidth. The filtering was performed to attenuate those low frequency components of the overall acoustic spectrum level which were largely contributed by engine noise. The filtered acoustic signal was monitored and recorded.

b. Signal Analysis System

The recorded acoustic signals were fed into a digital signal analyzer (HP 5420A) which could evaluate the reflection coefficient and acoustic source impedance as a function of frequency. A hard copy of the generated reflection coefficient and acoustic source impedance was obtained as plotted functions of frequency using an X-Y plotter. The corrected results of this analysis/copy process are shown in Sections IV.1.a through IV.1.d.

SECTION III

THEORY

1. INTRODUCTION

The notion that an engine can be modeled as a cyclic series of passive systems was supported in Section II by the identification of both a closed tube and the varying size internal volumes of the engine as it completed one thermodynamic cycle. Now that certain conceptualized passive systems have been identified for the engine, it will be helpful to theoretically appreciate the acoustic impedances for each of these passive systems. These analytically predicted impedances can then be compared to experimentally obtained acoustic impedances for actual passive systems. The theoretical passive system acoustic impedances can then be further utilized to interpret motored engine impedance data. It might be additionally possible to extend this evaluative comparison between modeled engine passive system acoustic impedances and experimentally obtained acoustic impedances to explain the active acoustic impedances for various powered engine conditions.

2. DEFINING IMPEDANCE

In general, theoretical investigations dealing with acoustical impedance usually involve such acoustic identifications as specific acoustic impedance. The specific acoustic impedance (z) by definition is the complex ratio of the acoustic pressure (P) to the particle velocity (v). The specific acoustic impedance can be interpreted as a complex quantity composed of a resistive (real) component and a reactive (imaginary) component, as shown in the following relationship:

$$z = \frac{P}{v} = r + ix \quad (1)$$

where

r defines the specific acoustic resistance

x defines the specific acoustic reactance

This specific acoustic impedance identifies the impedance at a point and is considered a property of the medium for the type of wave being propagated through the medium. For example, the specific acoustic impedance for simple plane harmonic waves forward propagating in a fluid within a tube is shown to be equal to ρc . The product ρc is a real quantity and a function of specific properties for the medium. For this reason, the product is often known simply as the characteristic impedance (z_s) or characteristic resistance for the medium. For cross-sectional areas within tubes, etc., acoustic impedance (Z) is defined as the complex ratio of the uniform acoustic pressure to the associated volume velocity (U), and thus can be used to describe the acoustical impedance at a particular surface. The acoustic impedance at a specific surface can be related to the uniform specific acoustic impedance (z) at the surface by:

$$Z = \frac{P}{U} = \frac{z}{S} = R + jX \quad (2)$$

where

U is equivalent to vS with the particle velocity (v) uniform over the surface (S).

S is the area of the designated surface.

R is the acoustic resistive impedance.

X is the acoustic reactive impedance.

The acoustic impedance which defines the impedance where the engine's manifold interfaces the measurand tube will be identified as the acoustic source impedance (Z_{source}).

3. ACOUSTIC PHENOMENA IN THE MEASURAND TUBE

The dominant type of incident and reflected waveforms propagating in the measurand tube at the pressure sensors was considered to be linear harmonic plane waves subject to amplitude attenuation (Figure 14). The incident pressure plane waves (p_i) traveling in the positive

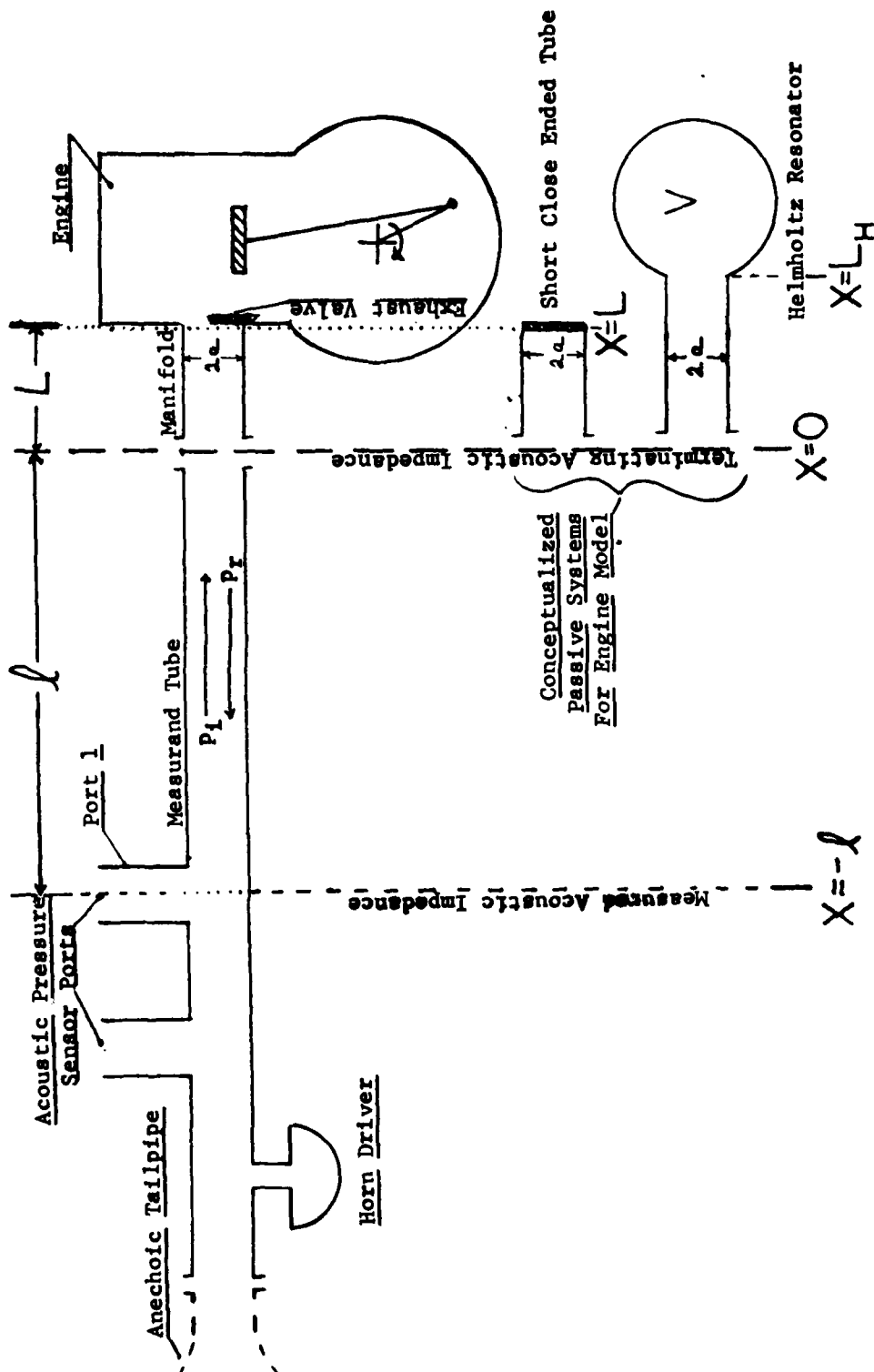


Figure 14. The X-ordinate System and Appropriate Dimensions for the Location of the Measured and Terminating Impedances

x-direction theoretically possess a phase relationship where the particle velocity and acoustic pressure are almost in phase. However, for reflected (negative x-direction propagation) pressure plane waves (p_r), the particle velocity will theoretically lag the acoustic pressure by about 180° .

The steady state interaction between positive traveling plane waves from the acoustic source and negative traveling plane waves from a passive termination results in the formation of a standing wave. For the standing wave, the acoustic pressure and particle velocity are a combination of the incident and reflected plane wave fields. If, for the cross-section of the sound field at $x = L$, the peak values of acoustic pressure (\hat{P}_L) and particle velocity (\hat{v}_L) are known, then the acoustic pressure (P_o) and particle velocity (v_o) at the origin where $x = 0$ can be expressed in complex phasor form as (Reference 16):

$$P_o(L,t) = \hat{P}_o e^{i\omega t} \quad (3)$$

where

$$\hat{P}_o = [\hat{P}_L \cosh(\gamma L) - z_s \hat{v}_L \sinh(\gamma L)] \quad (3a)$$

and

$$v_o(L,t) = \hat{v}_o e^{i\omega t} \quad (4)$$

where

$$\hat{v}_o = \left[\frac{\hat{P}_L}{z_s} \sinh(\gamma L) - \hat{v}_L \cosh(\gamma L) \right] \quad (4a)$$

Here,

$\gamma = \alpha + i\beta$ is the propagation constant which incorporates attenuation and phase information at the particular frequency.

Thus, the acoustic impedance Z_o at $x = 0$ can be calculated using the equation

$$Z_o = \frac{P_o}{S v_o} \quad (5)$$

4. PARTICULAR CASES OF ACOUSTIC PASSIVE SYSTEMS

Certain types of acoustic passive systems were investigated to identify distinguishing acoustic impedance characteristics. The two most frequently applied cases in the literature are that of a close ended tube and open ended tube. Also, due to its application in conceptualized passive engine geometries in this project, the helmholtz (or volume) resonator was considered.

In an ideal close ended tube (or acoustically hard termination) the peak particle velocity (v_L) is zero at the termination where $x = L$. Consequently, the particle velocity and acoustic pressure developed in Equations 3 and 4 become:

$$P_o = \hat{P}_L \cosh (\gamma L) e^{i\omega t} \quad (6)$$

$$v_o = \hat{v}_L \sinh (\gamma L) e^{i\omega t} \quad (7)$$

These equations can be further simplified if negligible attenuation ($\alpha \sim 0$) is assumed. Further if $\alpha \ll k$, where $k = \omega/c$ is the wavelength constant with ω the rotational harmonic frequency and c the speed of sound propagation, then

$$\beta \sim k$$

and hence,

$$\gamma = i k \quad (8)$$

upon substitution of Equation 8 in Equations 6 and 7, and using circular trigonometric identities, the equations become:

$$P_o = \hat{P}_L \cos (kL) e^{i\omega t} \quad (9)$$

$$v_o = i \frac{\hat{P}_L}{Z_s} \sin (kL) e^{i\omega t} \quad (10)$$

Note that the acoustic pressure amplitude varies as a cosine function of length and frequency while the particle velocity amplitude varies as a sine function of length and frequency. The acoustic pressure and particle velocity are shifted in phase with respect to time by 90° from each other.

For the close ended tube case, the acoustic impedance (Z_0^c) can thus be expressed as,

$$Z_0^c = i \frac{Z_s}{S} \cot(k\ell) \quad (11)$$

Noting that $\frac{\rho c}{S}$ is the acoustic impedance for a plane wave (Z_s), then the ratio of close ended tube impedance divided by the plane wave impedance defines a dimensionless acoustic impedance Z_0^{c*} for a close ended tube as:

$$Z_0^{c*} = \frac{Z_0^c}{Z_s} = -i \cot(k\ell) \quad (12)$$

Thus, the acoustical impedance for an attenuation-free tube with an acoustically hard termination is a purely imaginary negative cotangent function of tube length and frequency. Attenuation-free propagation specifies there be no viscous wall damping of the acoustic signal or energy dissipation within the propagation medium.

For the open tube case (or acoustically soft termination), the acoustic pressure becomes zero at the open end where $x = 0$. From Equations 3 and 4, expressions for the acoustic pressure and particle velocity at $x = 0$, again assuming negligible attenuation, are:

$$p_0 = z_s \hat{v}_L i \sin(k\ell) e^{i\omega t} \quad (13)$$

$$v_0 = \hat{v}_L \cos(k\ell) e^{i\omega t} \quad (14)$$

Consequently, the acoustic impedance for the open tube case is:

$$Z_o^{o*} = \frac{P}{Sv_o} = i \frac{\rho c}{S} \tan(kl) \quad (15)$$

The dimensionless form of the acoustic impedance for the open tube case is:

$$Z_o^{o*} = i \tan(kl) \quad (16)$$

Hence, the acoustical impedance for a tube with an acoustically soft termination, in this attenuation-free case, is purely imaginary, since there is no viscous damping of the acoustic signal or energy dissipation within the propagation medium. The acoustic impedance characteristics have the form of a tangent function of the tube length and the frequency. The tube length should be small to eliminate attenuation for this analysis to hold true.

Another passive acoustic system which is of importance in this project is the helmholtz or volume resonator (Figure 14). The simple helmholtz resonator consists of a rigid enclosure of volume V , with radiation of sound into the volume medium through a small opening of radius (a) and length L_H .

A feature of an ideal helmholtz resonator is that there is very little energy absorbed or dissipated, other than energy lost by viscous effects. Consequently, the resistive component of impedance is negligible. The reactive component of impedance is dependent upon the physical dimensions of the resonator such as the area of the opening, length of the neck, total volume in the resonator, etc.

From basic acoustic theory, the acoustic reactance at $x = 0$ is shown to be (Reference 9):

$$X_o^H = \frac{Z_s}{S} (\ell'k - \frac{S}{kV}) \quad (17)$$

where:

$$\ell' = L_H + .85a,$$

is the effective length of the neck.

Thus, the acoustic impedance at $x = 0$ can be expressed as:

$$Z_o^H = i \frac{Z_s}{S} (\ell'k - \frac{S}{kV}) \quad (18)$$

The corresponding dimensionless acoustic impedance can be written as:

$$Z_o^{H*} = i(\ell'k - \frac{S}{kV}) \quad (19)$$

Note that this acoustic impedance does not have a cyclic behavior as did the impedances in previous open and close ended passive systems.

5. ADAPTATION OF PASSIVE SYSTEM IMPEDANCES TO THE EXPERIMENTAL CASE

Now that certain passive acoustic impedances have been evaluated at the manifold-measurand tube interface where $x = 0$, a procedure will be developed by which the acoustic impedance some distance along the measurand tube away from the passive system termination can be determined. The need for this procedure exists because the measurement technique used in this project permitted assessment of the acoustic impedance at the acoustic pressure sensors rather than where the measurand tube interfaces the engine's exhaust manifold. Therefore, the theoretical impedances Z_o must be adjusted for the length (ℓ) of measurand tube between the first acoustic sensor port and the engine's exhaust manifold.

The acoustic impedance (Z_ℓ) at the first acoustic sensor can be analytically developed by considering the incident and reflected acoustic waves that propagate within the measurand tube. The acoustic impedance Z_ℓ at the plane $x = -\ell$ (Figure 14), can be written as (Reference 9):

$$Z_\ell = \frac{\rho c}{S} \frac{Ae^{jk\ell} + Be^{-jk\ell}}{Ae^{jk\ell} - Be^{-jk\ell}} \quad (20)$$

where A and B are the complex amplitudes of the unattenuated incident and reflected waves, respectively. Both A and B are evaluated where $x = 0$. Thus, the terminating impedance Z_0 at the plane $x = 0$ is simply:

$$Z_0 = \rho \frac{c}{S} \frac{A+B}{A-B} \quad (21)$$

Solving Equation 21 for amplitude A and substituting into Equation 20 yields:

$$Z_\ell = \frac{\rho c}{S} \frac{\frac{(Z_0 + \frac{\rho c}{S})}{(Z_0 - \frac{\rho c}{S})} Be^{jk\ell} + Be^{-jk\ell}}{\frac{(Z_0 + \frac{\rho c}{S})}{(Z_0 - \frac{\rho c}{S})} Be^{jk\ell} - Be^{-jk\ell}} \quad (22)$$

rearranging, canceling common terms, and using circular function identities for sine and cosine, this equation becomes:

$$Z_\ell = \frac{\rho c}{S} \frac{Z_0 + i \frac{\rho c}{S} \tan k\ell}{\frac{\rho c}{S} + i Z_0 \tan k\ell} \quad (23)$$

by substituting:

$$Z_0 = R_0 + jX_0 = \frac{\rho c}{S} (R_0^* + jX_0^*) \quad (24)$$

and by multiplying the numerator and denominator of Equation 23 by the complex conjugate of the denominator, the resistive (R_ℓ)

component and reactive (X_ℓ) component of the acoustic impedance Z_ℓ , can be expressed in dimensionless form as:

$$R_\ell^* = \frac{R_o^* (1 + \tan^2 k\ell)}{(1 - X_o^* \tan k\ell)^2 + R_o^{*2} \tan^2 k\ell}, \quad (25)$$

and

$$X_\ell^* = \frac{-X_o^* \tan^2 k\ell + (1 + R_o^* - X_o^{*2}) \tan k\ell + X_o^*}{(1 - X_o^* \tan k\ell)^2 + R_o^{*2} \tan^2 k\ell} \quad (26)$$

Theoretical analysis of the acoustic impedance for the passive helmholtz resonator studied in Section III.4 has revealed that the resistive impedance R_o will be negligible. But, it was desirable in computer analysis for Z_ℓ not to let resistance R_o be exactly zero. The acoustic resistance was chosen to be defined as (Reference 9):

$$R_o = \frac{Z_s}{S} R'(2ka) \quad (27)$$

where

R' is a resistance function.

k is the wavelength constant.

a is the radius of the measurand tube.

Specifying the acoustic resistance as .005 at 500 Hz and .69 at 6000 Hz (Reference 9), the equation for acoustic resistance as a function of frequency (f) can be empirically approximated as:

$$R_o \sim \frac{Z_s}{S} (2.0 \times 10^{-8}) f^2 \quad (28)$$

or as a dimensionless terminating acoustic resistance:

$$R_o^* \sim (2.0 \times 10^{-8}) f^2 \quad (29)$$

6. SUPPORTIVE THEORY FOR DIGITAL SIGNAL ANALYZER CALCULATION OF ACOUSTIC IMPEDANCE USING TRANSFER TECHNIQUES

The digital signal analyzer approach to reflection coefficient evaluation as developed by Blaser and Chung (Reference 10) utilized transfer functions obtained from Fourier analysis of measured acoustic pressure signals at two sensor positions in the measurand tube.

If subscripts 1 and 2 indicate sensor locations and if i and r denote incident and reflected components of the measured acoustic pressure, then the complex phasor acoustic pressures, P_1 and P_2 at positions 1 and 2, can be written as:

$$P_1 = P_{1i} + P_{1r} \quad (30)$$

and

$$P_2 = P_{2i} + P_{2r} \quad (31)$$

The complex phasor reflection coefficients R_1 and R_2 at these sensor locations can be expressed as:

$$R_1 = F\{P_{1r}\}/F\{P_{1i}\} \quad (32)$$

and

$$R_2 = F\{P_{2r}\}/F\{P_{2i}\} \quad (33)$$

where $F\{P\}$ indicated the Fourier transform of the time history signal for acoustic pressure P .

The transfer functions with port 2 as output and port 1 as input associated with the incident and reflected pressures may be expressed individually as:

$$H_{12_r} = F\{P_{2_r}\}/F\{P_{1_r}\} \quad (34)$$

and

$$H_{12_i} = F\{P_{2_i}\}/F\{P_{1_i}\} \quad (35)$$

Also, the similar transfer function for the total acoustic pressure is:

$$H_{12} = F\{P_2\}/F\{P_1\} \quad (36)$$

From Equations 30 through 36, it follows that,

$$H_{12} = H_{12_i} (1 + R_2)/(1 + R_1) \quad (37)$$

From Equations 32 through 35 a relationship between the two reflection coefficients can be expressed as:

$$R_2 = (H_{12_i}/H_{12_r}) R_1 \quad (38)$$

Substituting Equation 38 into Equation 37 and solving for R_1 yields:

$$R_1 = (H_{12} - H_{12_r})/(H_{12_i} - H_{12}) \quad (39)$$

This equation permits the reflection coefficient in the measurand tube at $x = -l$ to be calculated when certain transfer functions have been obtained.

A relationship between acoustic impedance and the reflection coefficient for a single frequency was additionally developed from basic definitions for the acoustic particle velocity, acoustic pressure, and acoustic impedance. The acoustic impedance from Equation 2 can be expressed as the acoustic pressure divided by volume velocity, i.e.,

$$Z = \frac{P_i + P_r}{S(v_i + v_r)} \quad (40)$$

Using the relationship between acoustic pressure and acoustic particle velocity for plane waves, Equation 40 becomes:

$$Z = \frac{Z_s}{S} \frac{P_i + P_r}{P_i - P_r} \quad (41)$$

Dividing numerator and denominator by P_i and simplifying by using the definition for reflection coefficient, i.e., $R = \frac{P_r}{P_i}$, then the acoustic impedance can be expressed as:

$$Z = \frac{Z_s}{S} \frac{1 + R}{1 - R} \quad (42)$$

Hence, the dimensionless acoustic impedance Z_ℓ^* , which was obtained following digital signal analyzer evaluation of R_1 for Equation 39, was calculated using spectrum arithmetic as:

$$Z_\ell^* = \frac{1 + R_1}{1 - R_1} \quad (500 \text{ Hz} \leq f \leq 6000 \text{ Hz}) \quad (43)$$

SECTION IV

RESULTS

Both experimental and analytical results are presented in this section. The results presented, while not the total of all data collected, provide an informative collection of the major types of impedance evaluation. These evaluative impedance studies included: passive acoustic impedance for several fixed system geometries, passive acoustic impedance for various engine crankangle configurations, and active acoustic impedance for both the motored engine and the powered engine. Also included is a brief explanation on each experimental set-up particularly with regards to adjustments in the measurement system between the different types of evaluative studies. The evaluation of these results is given in Section 5.

1. EXPERIMENTAL PASSIVE SYSTEM IMPEDANCES

a. Passive Acoustic Impedance Evaluation for Fixed Geometry Configurations

The first type of acoustic impedance evaluation focused on passive systems. Particular interests were directed at identifying the impedance for the open and closed tube cases. These special cases permitted affirmation of the accuracy of the experimental measurement analysis system through a successful comparison of the acoustic impedance trends for both experimental systems with expected analytical results. Figures 15 and 16 show the impedance for the close ended tube case, which was evaluated with the reference acoustic sensor six inches from the acoustically hard termination. An identifiable theoretically predicted characteristic of this reactive impedance in Figure 16 was its negative cotangent function with an indicated effort to approach negative infinity at zero frequency. As another affirmation of the measurement analysis facility, the open tube acoustic impedance case was investigated with the results shown graphically in Figures 17 and 18. The experimental set-up was the same as in the close ended tube case, i.e., the reference acoustic sensor was six inches from the open tube termination. Referring

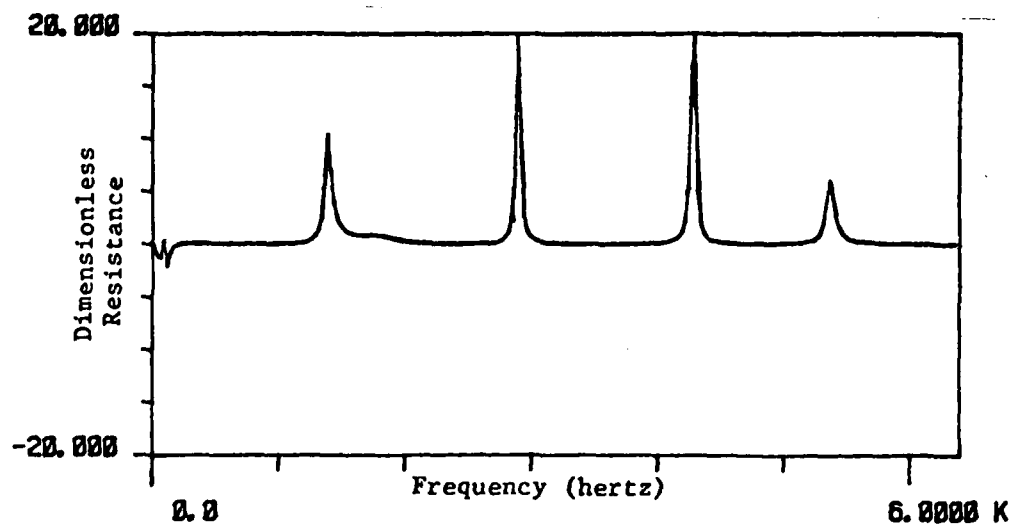


Figure 15. Dimensionless Resistive Impedance of Close Ended Measurand Tube

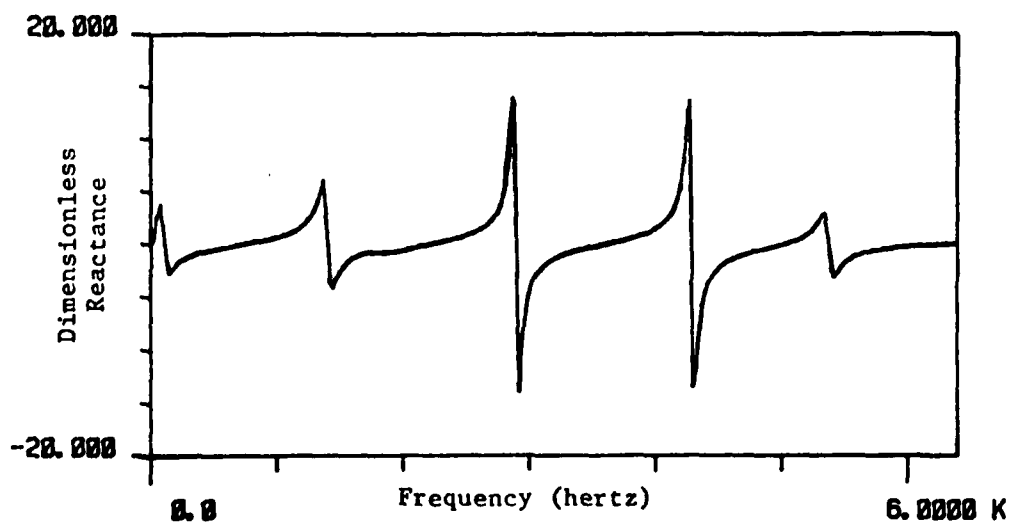


Figure 16. Dimensionless Reactive Impedance of Close Ended Measurand Tube

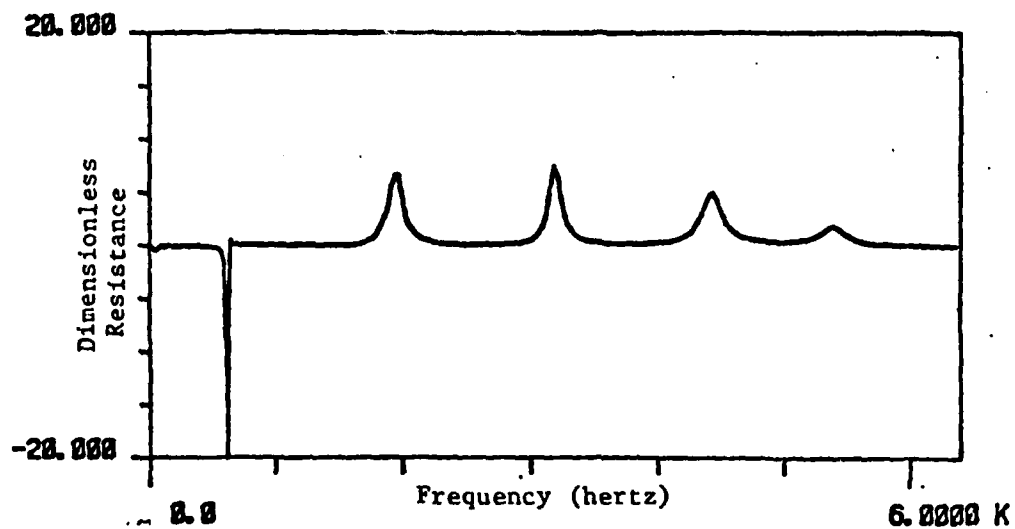


Figure 17. Dimensionless Resistive Impedance of Open Ended Measurand Tube

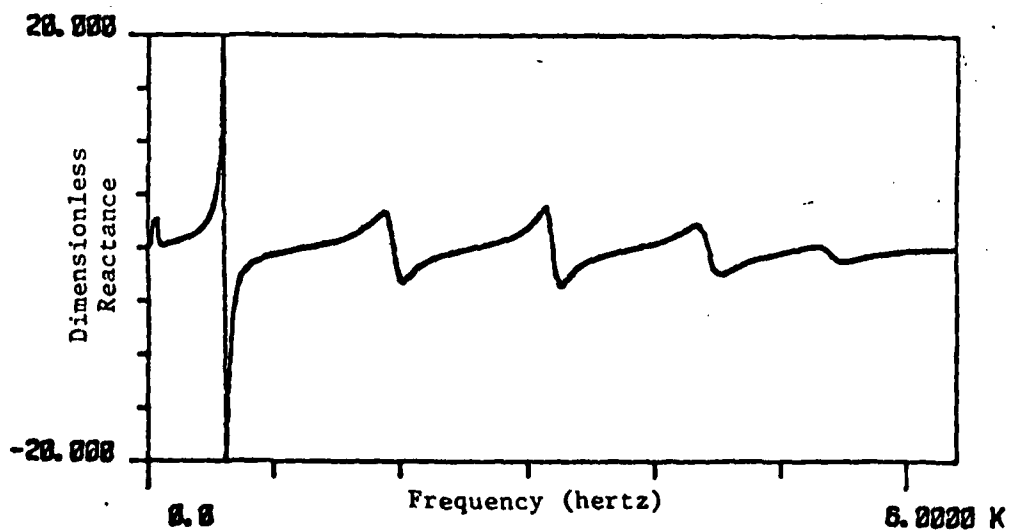


Figure 18. Dimensionless Reactive Impedance of Open Ended Measurand Tube

to the reactive impedance shown in Figure 18, the tangent function which is theoretically expected for the impedance of an open ended tube was clearly evident in the experimental results. The fact that at zero frequency the impedance approaches zero was additional evidence of the accuracy of the measurement analysis system developed to experimentally investigate acoustic impedance. In both the close and open ended tube cases, the resistive impedance was periodically non-zero near resonant conditions for the reactive impedance.

b. Engine Acoustic Impedance at Various Crankangles - A Passive System Study

The crankangle impedance study identified the acoustic impedance for various internal volume configurations as the engine progressed through one thermodynamic cycle (0° - 720°). Specific crankangles were selected to represent particular types of engine valve/chamber configurations in the thermodynamic cycle. An example was the first result presented in this section where the engine had a crankangle of 90° (Figures 19 and 20) for which the exhaust valve was known to be closed. The predominant cotangent waveform is quite evident in Figure 20 with the zero frequency value tending toward negative infinity, a characteristic effect of a close ended tube termination (Figure 16).

The engine configurations for crankangles from about 130° to 360° should represent the engine as a varying helmholtz-type volume, since it is through these crankangles that the engine's exhaust valve opens and closes (Figure 14) while the chamber volume changes substantially. Results are presented for crankangles of 130° , 170° , 260° , 340° , and 360° (Figures 20-30). The final result presented was for a crankangle of 400° (Figures 31 and 32) where the exhaust valve was again closed and remained closed through the remainder of the cycle and into the next thermodynamic cycle until past 90° where the exhaust valve again started to reopen.

In this crankangle impedance study and in the studies involving a motored or powered engine, the experimental set-up was different

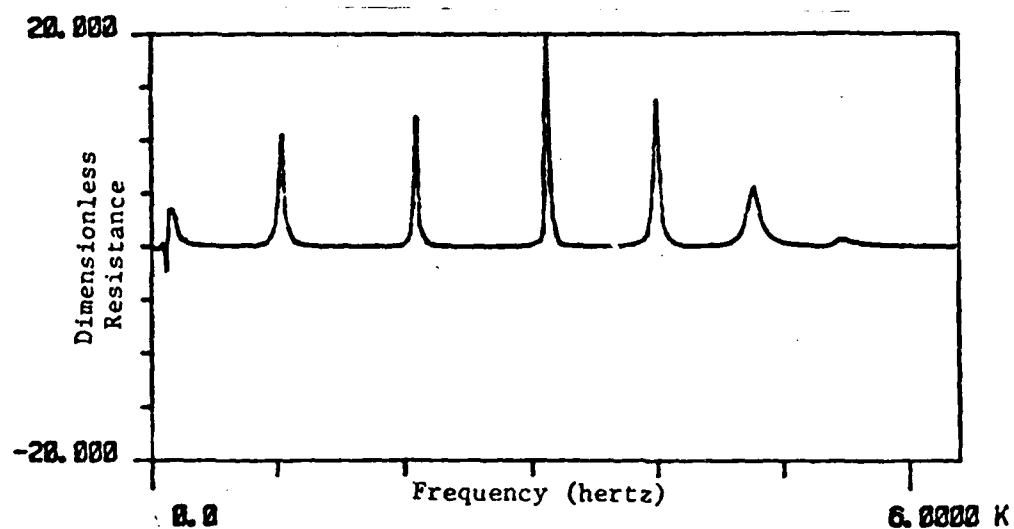


Figure 19. Dimensionless Resistive Impedance of Engine at 90° Crankangle

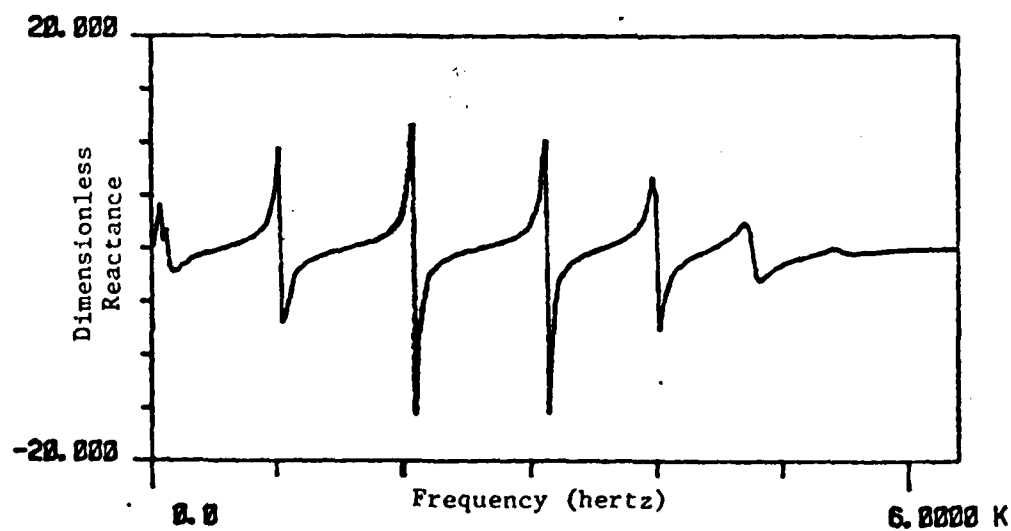


Figure 20. Dimensionless Reactive Impedance of Engine at 90° Crankangle

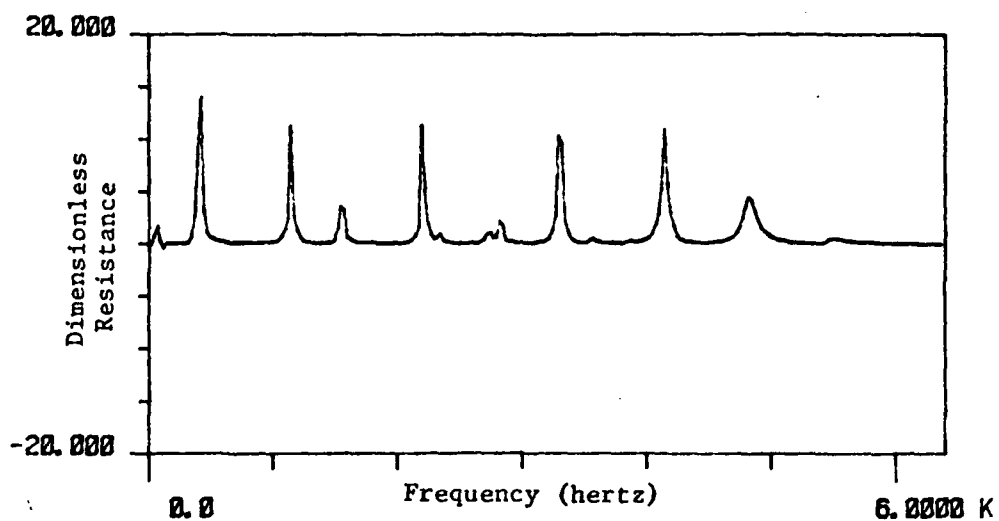


Figure 21. Dimensionless Resistive Impedance of Engine at 130° Crankangle

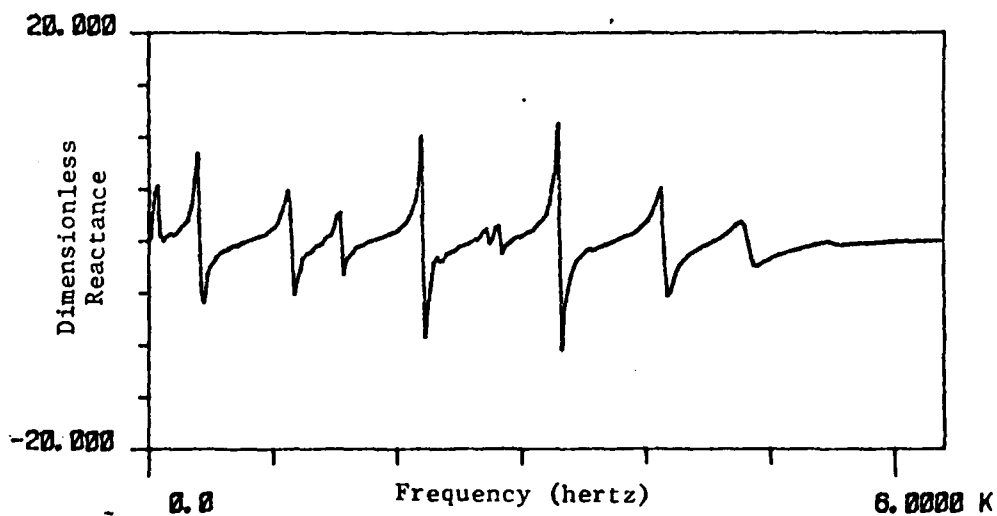


Figure 22. Dimensionless Reactive Impedance of Engine at 130° Crankangle

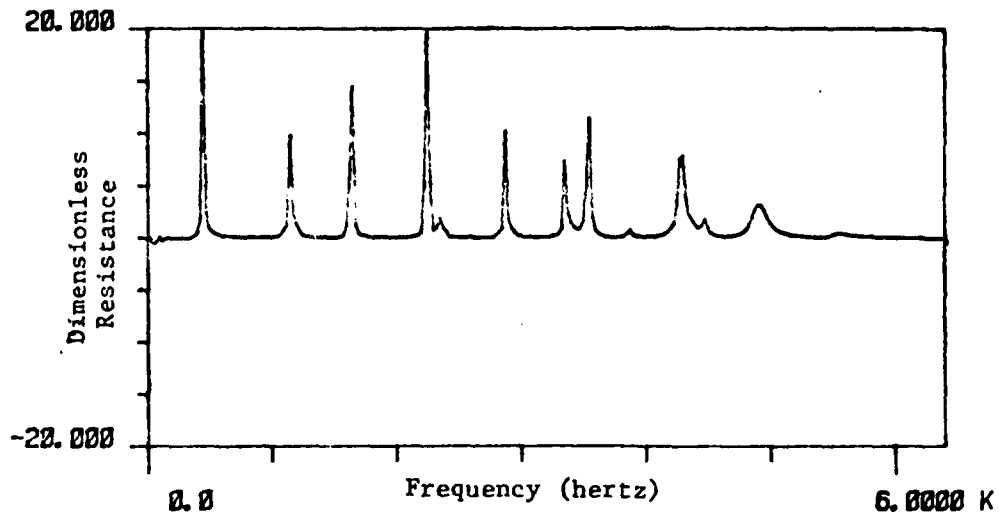


Figure 23. Dimensionless Resistive Impedance of Engine at 170° Crankangle

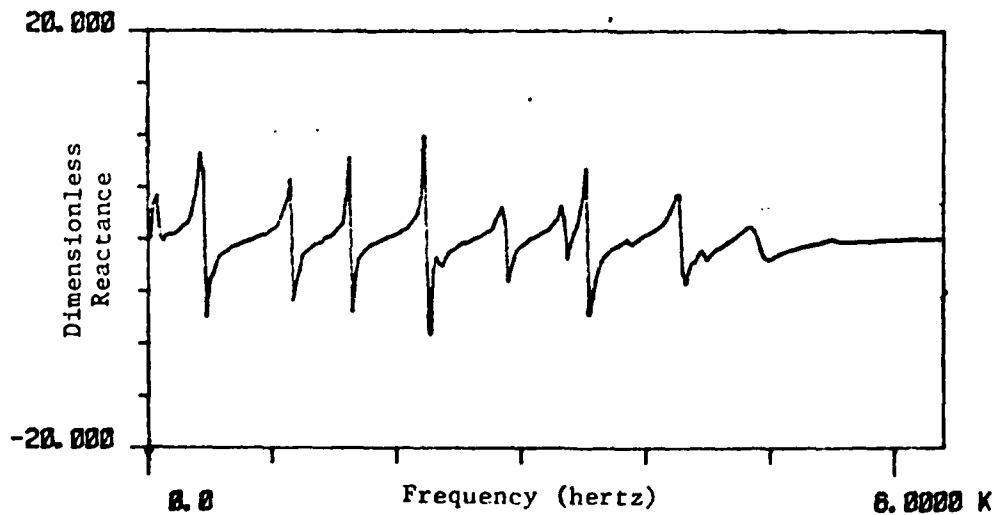


Figure 24. Dimensionless Reactive Impedance of Engine at 170° Crankangle

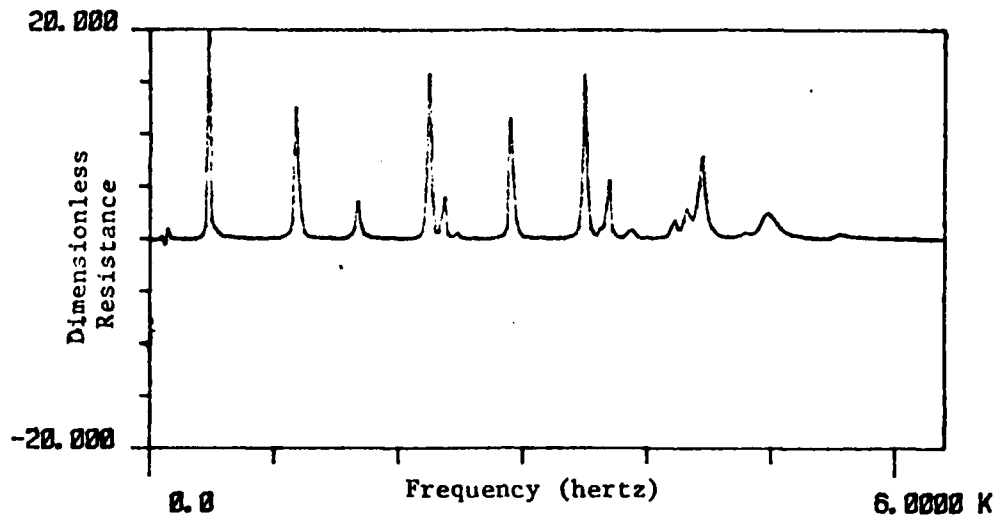


Figure 25. Dimensionless Resistive Impedance of Engine at 260° Crankangle

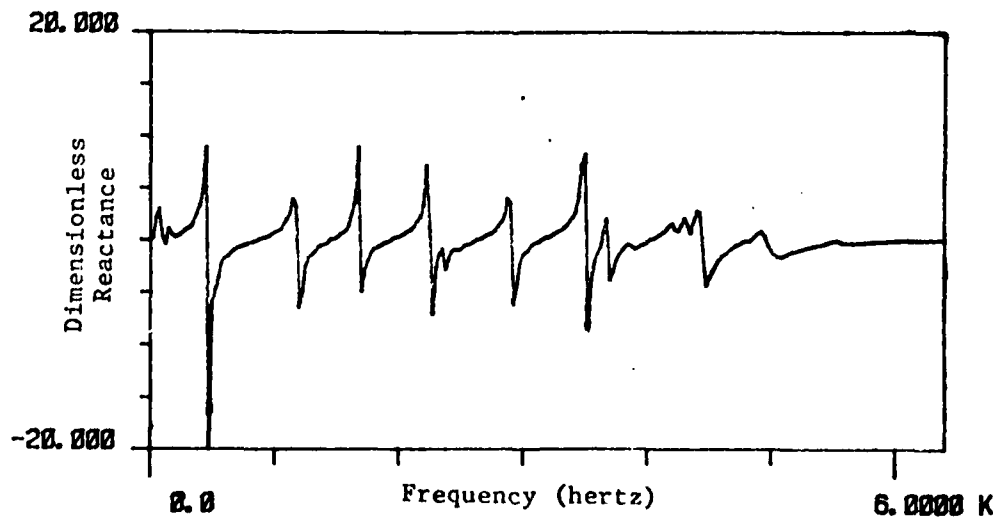


Figure 26. Dimensionless Reactive Impedance of Engine at 260° Crankangle

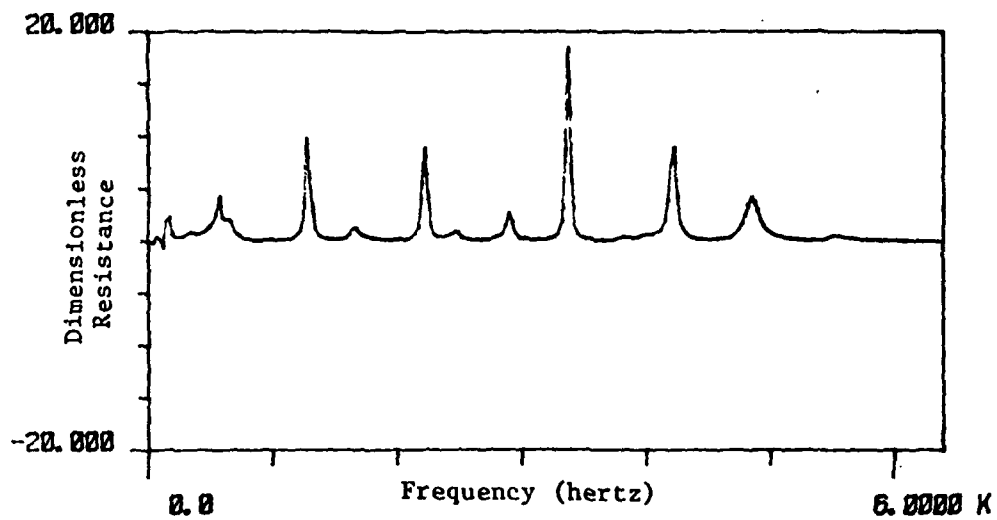


Figure 27. Dimensionless Resistive Impedance of Engine at 340° Crankangle

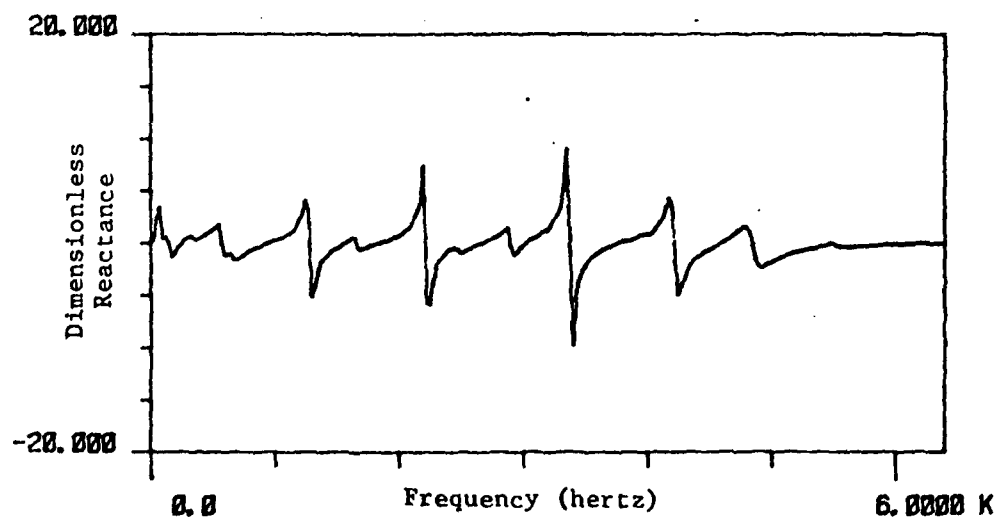


Figure 28. Dimensionless Reactive Impedance of Engine at 340° Crankangle

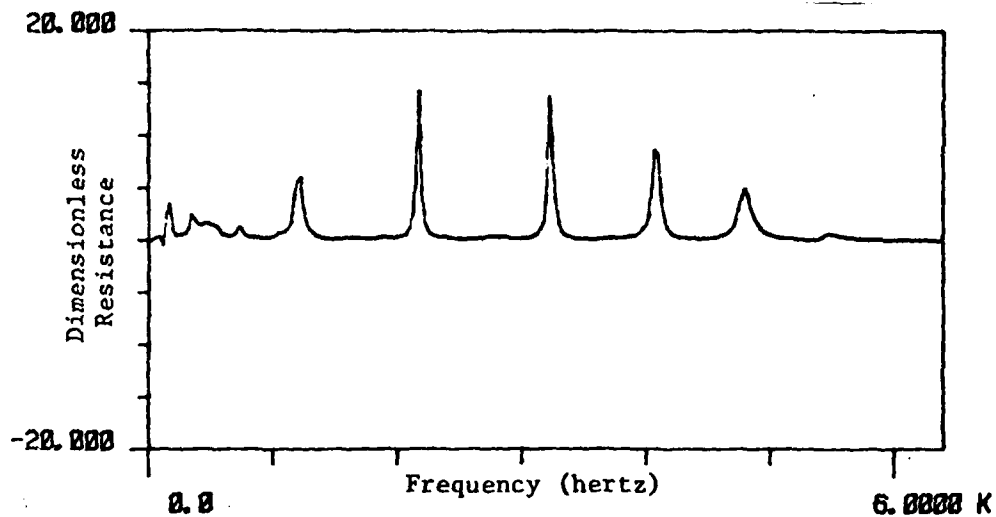


Figure 29. Dimensionless Resistive Impedance of Engine at 360° Crankangle

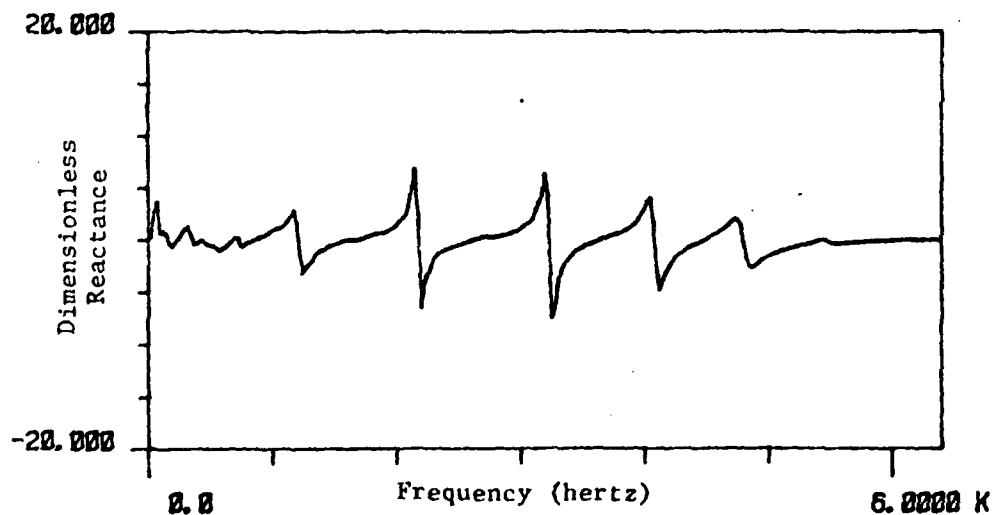


Figure 30. Dimensionless Reactive Impedance of Engine at 360° Crankangle

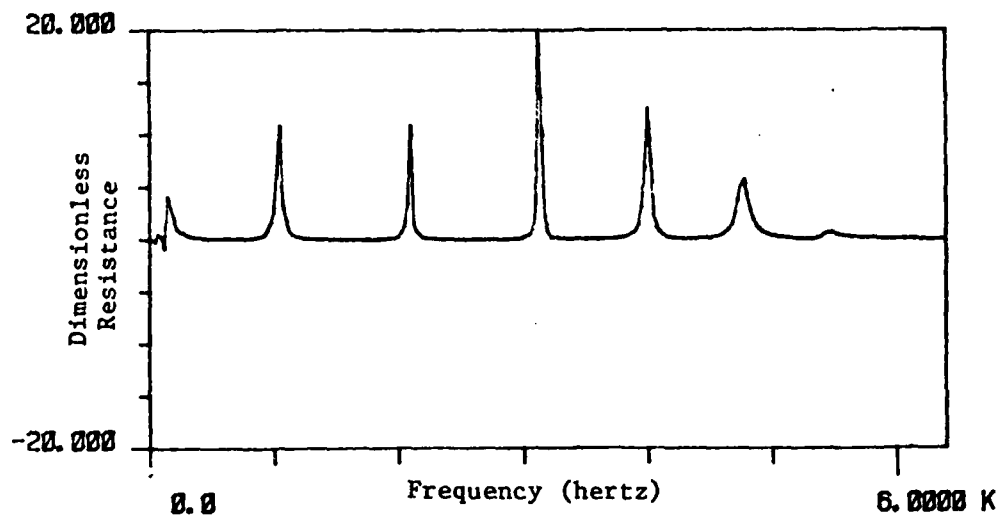


Figure 31. Dimensionless Resistive Impedance of Engine at 400° Crankangle

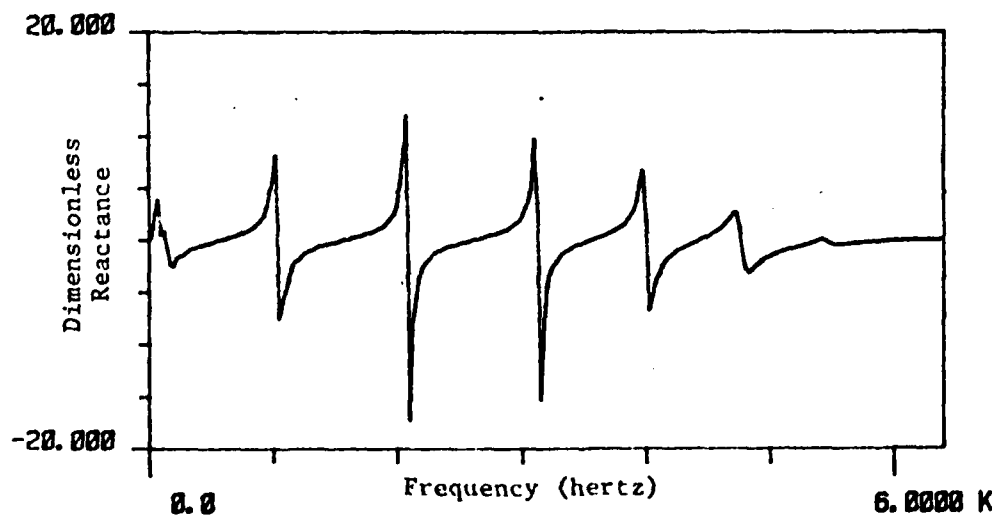


Figure 32. Dimensionless Reactive Impedance of Engine at 400° Crankangle

in one respect from the open and passive system study. The reference acoustic sensor in all engine related impedance studies was 9.25 inches away from the end of the measurand tube, and not six inches away as was the case for the passive acoustic impedance evaluation for open and close ended tube terminations. The engine for these crankangle impedance studies was a 10 horsepower Briggs and Stratton single cylinder engine.

2. EXPERIMENTAL ACTIVE SYSTEM IMPEDANCES

a. Motored Engine Acoustic Impedance Study

The results presented in this section are the first for two types of active system acoustic impedances which were evaluated. The first results presented here are for an engine hand rotated at about 2 rpm (Figures 33 and 34). The 2 rpm speed is equivalent to the completions of one thermodynamic cycle or a 0° through 720° crankangle rotation each minute. Figures 35 and 36 then show graphically the acoustic impedance of a slightly more active system with the engine speed increased to about 24 rpm. The remaining results are for an engine driven by a starter motor with successively increased engine speeds. This sequence of gradually increased engine speed was done to permit progressing patterns in the impedance characteristics to be identifiable from these lower speed motored engine studies (Figures 37-48). All experimentation was performed with an external white noise horn driver level of 130 dB or more. No major changes were made in the experimental measurement analysis system from the system used for the engine crankangle study. The speed variation for the Briggs and Stratton 10 horsepower motored engine was accomplished by using a battery recharging unit to vary the current to the starter motor which drove the engine. No external engine load was applied.

b. Powered Engine Acoustic Impedance Study

The results presented in this section represent efforts at attaining acoustic impedances for a powered engine under varying conditions. The results are primarily presented for increasing engine speeds. The

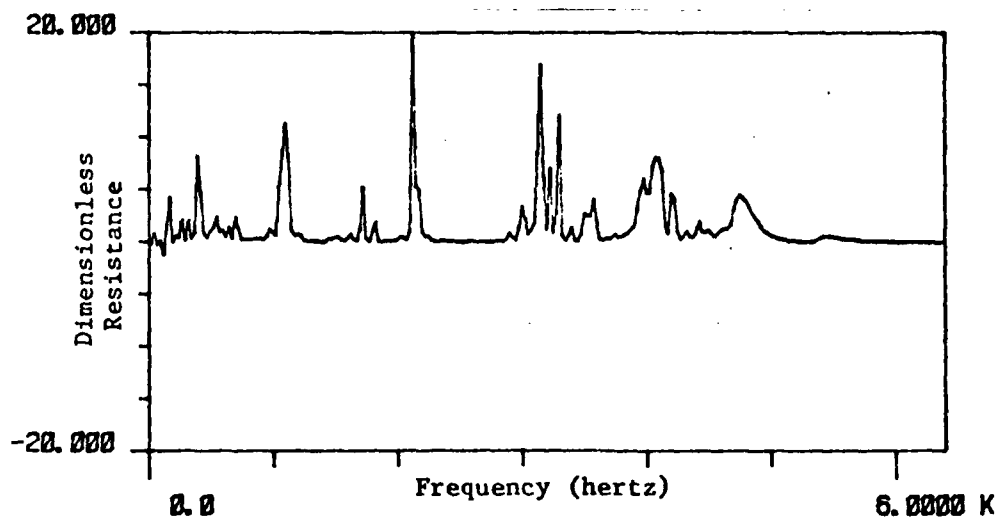


Figure 33. Dimensionless Resistive Impedance of Engine Motored at 2 RPM

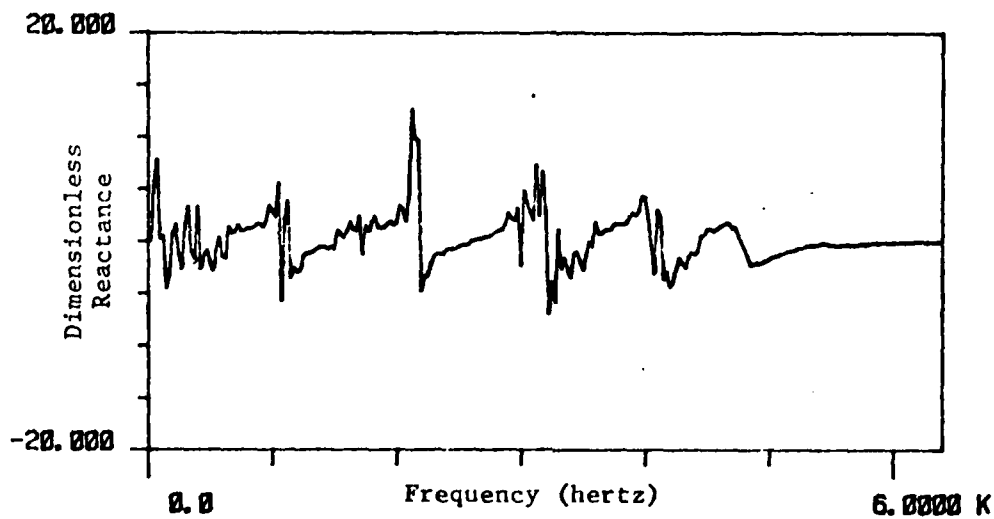


Figure 34. Dimensionless Reactive Impedance of Engine Motored at 2 RPM

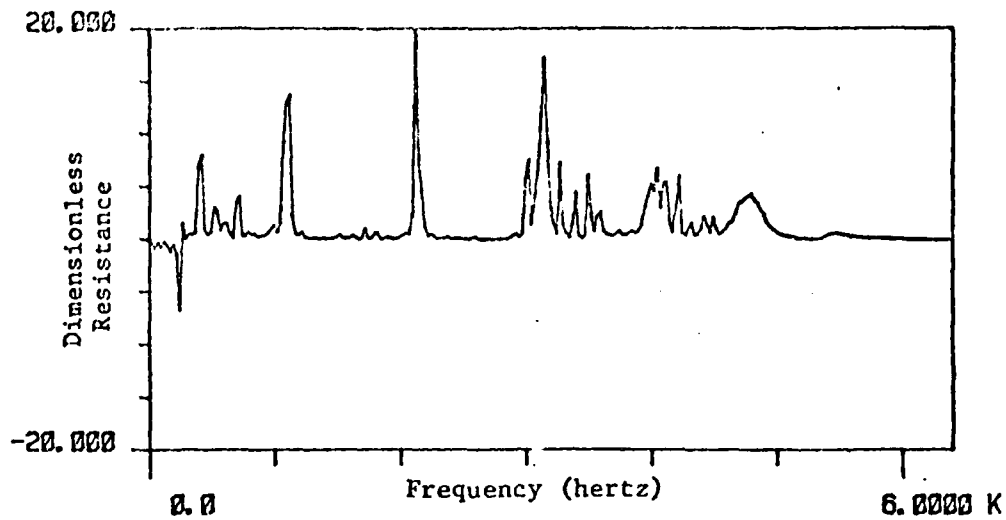


Figure 35. Dimensionless Resistive Impedance of Engine Motored at 24 RPM

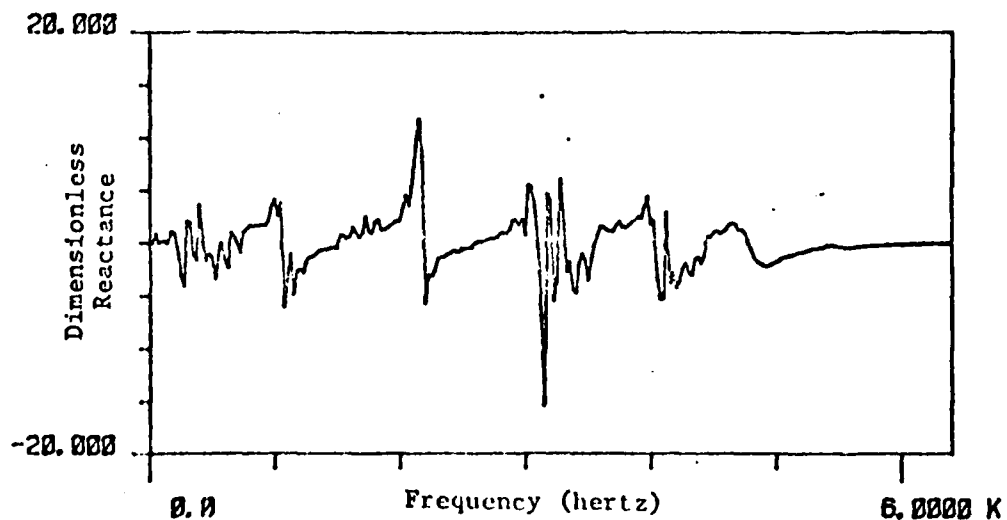


Figure 36. Dimensionless Reactive Impedance of Engine Motored at 24 RPM

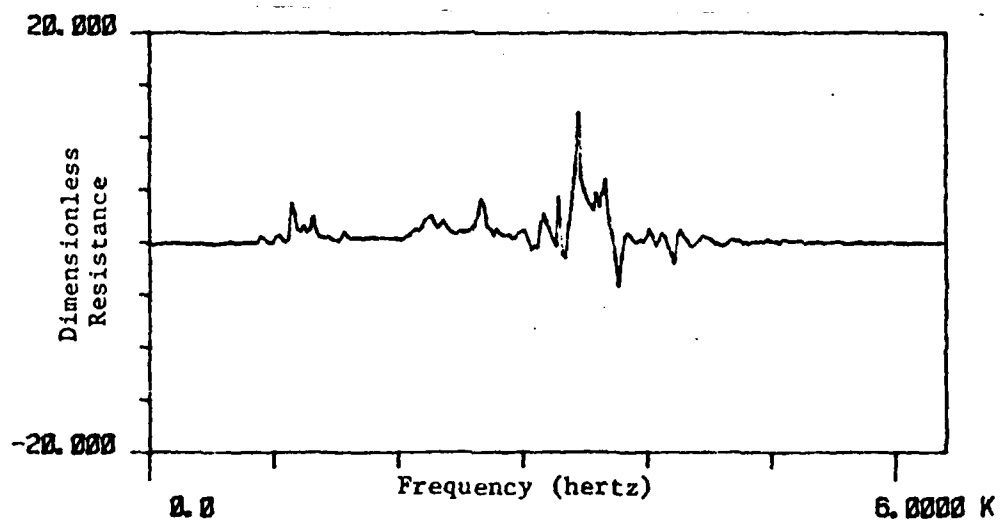


Figure 37. Dimensionless Resistive Impedance of Engine Motored at 370 RPM

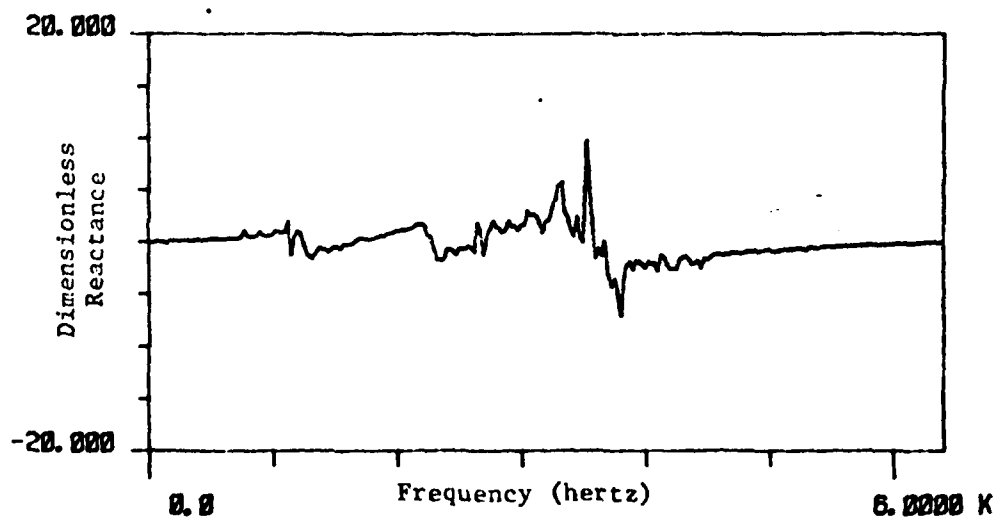


Figure 38. Dimensionless Reactive Impedance of Engine Motored at 370 RPM

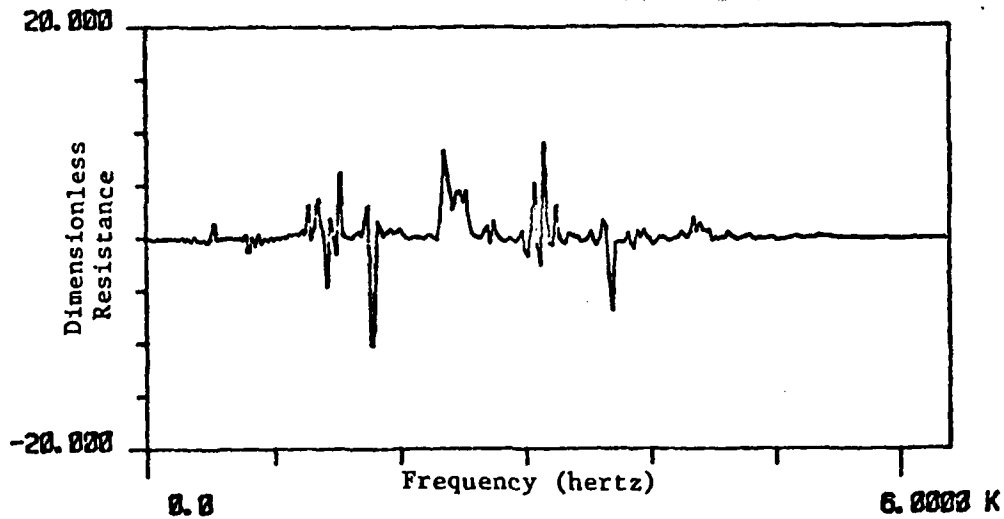


Figure 39. Dimensionless Resistive Impedance of Engine Motored at 390 RPM. Externally Generated Acoustic Signal at 120 db (10 db Below Standard Testing Levels)

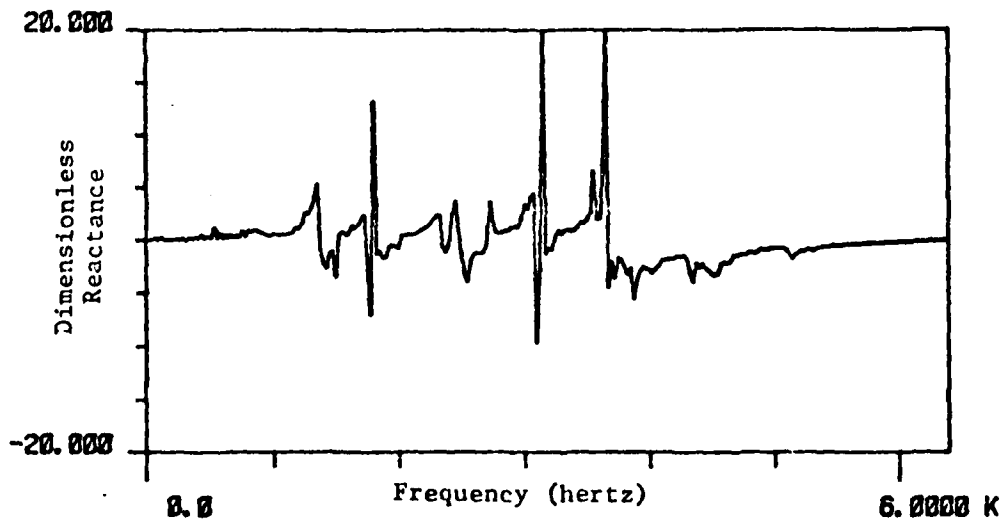


Figure 40. Dimensionless Reactive Impedance of Engine Motored at 390 RPM. Externally Generated Acoustic Signal at 120 db (10 db Below Standard Testing Levels)

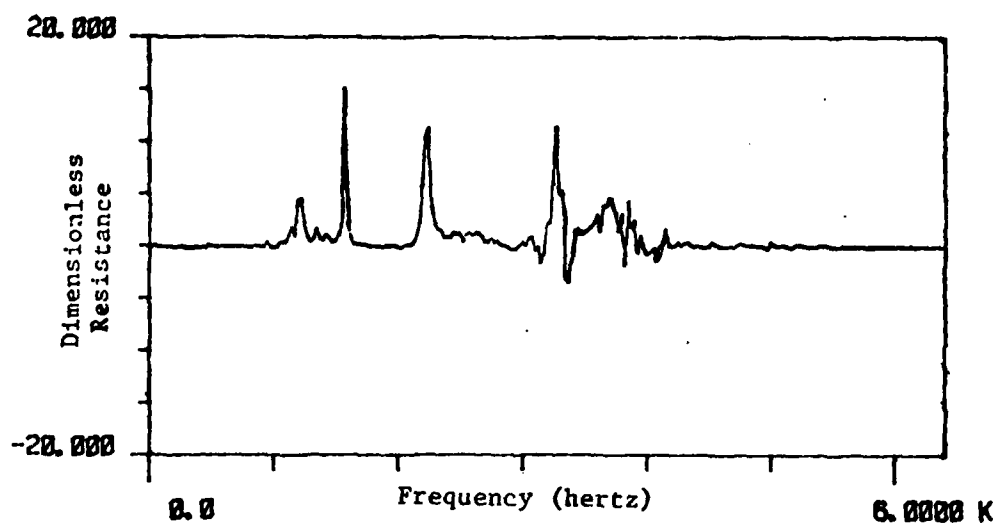


Figure 41. Dimensionless Resistive Impedance of Engine Motored at 450 RPM

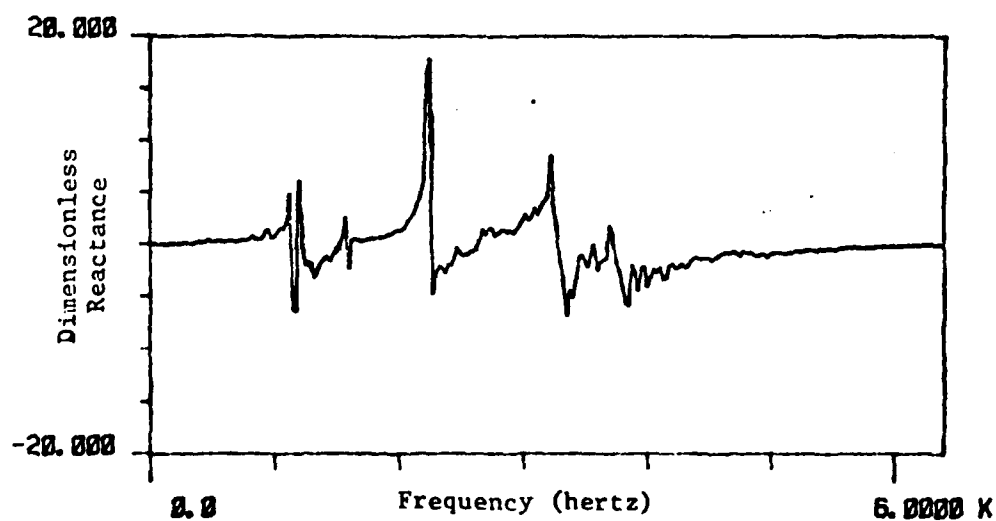


Figure 42. Dimensionless Reactive Impedance of Engine Motored at 450 RPM

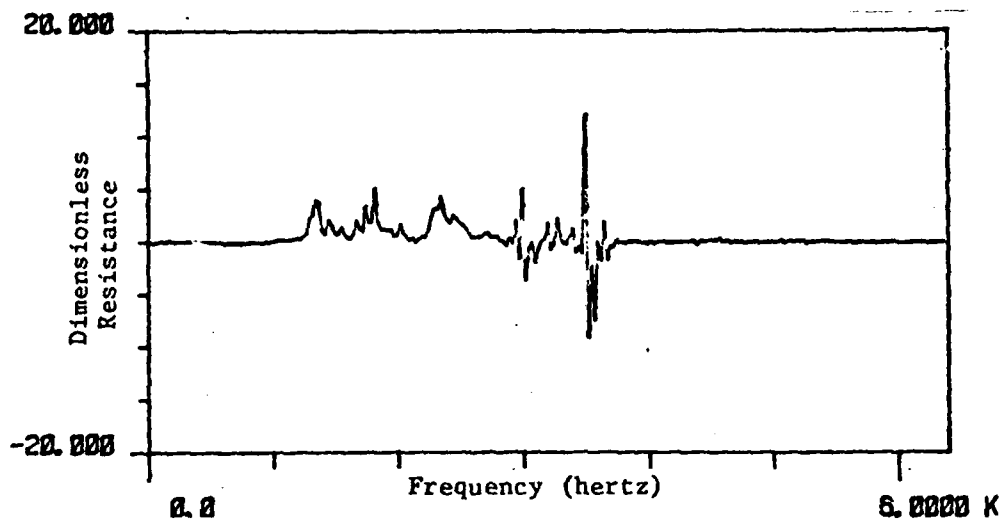


Figure 43. Dimensionless Resistive Impedance of Engine Motored at 475 RPM

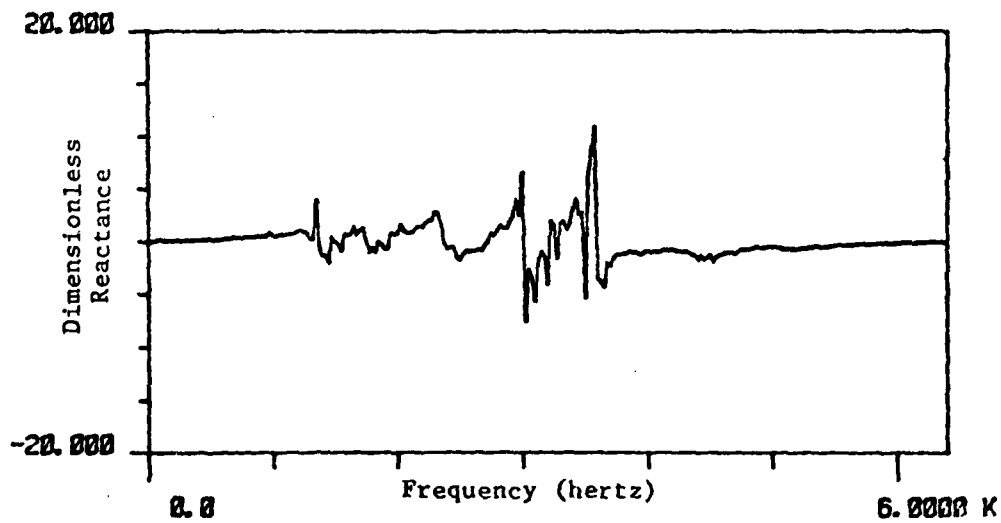


Figure 44. Dimensionless Reactive Impedance of Engine Motored at 475 RPM

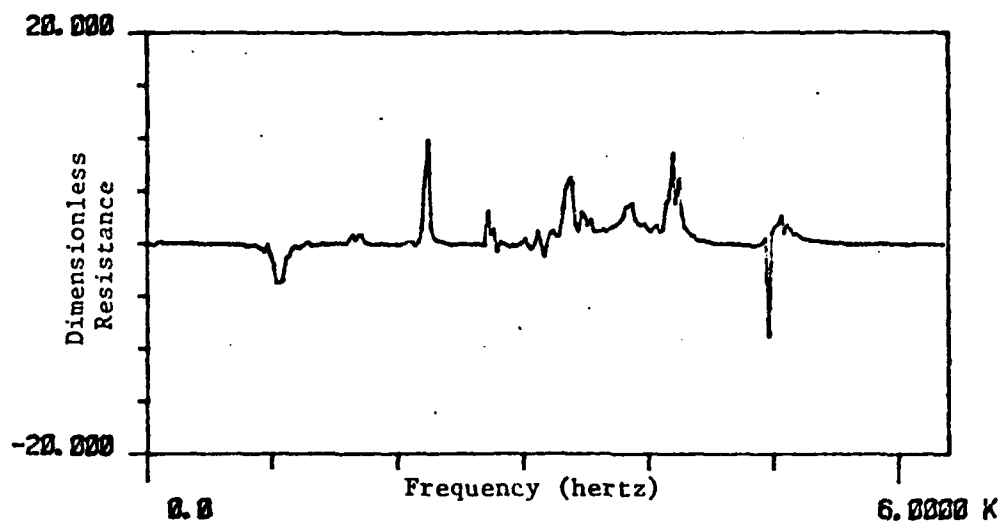


Figure 45. Dimensionless Resistive Impedance of Engine Motored at 555 RPM

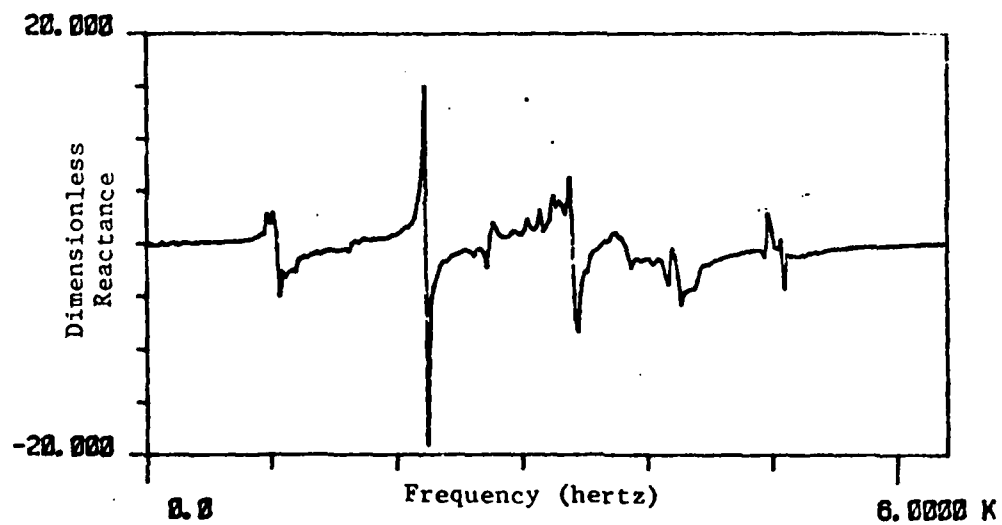


Figure 46. Dimensionless Reactive Impedance of Engine Motored at 555 RPM

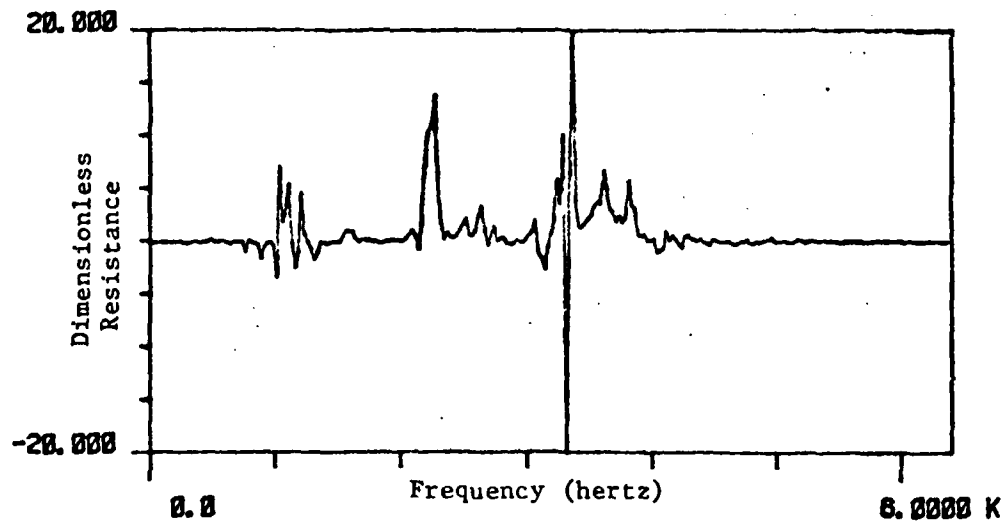


Figure 47. Dimensionless Resistive Impedance of Engine Motored at 560 RPM

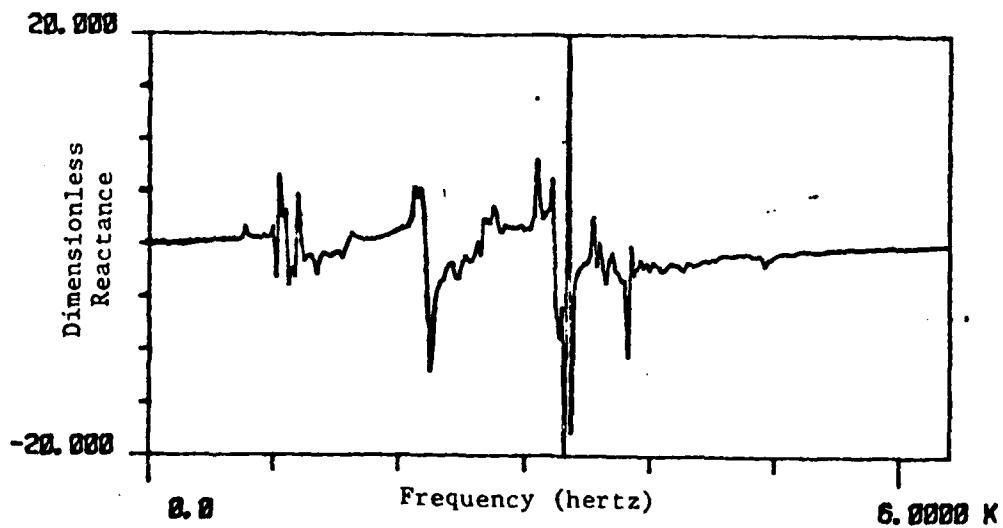


Figure 48. Dimensionless Reactive Impedance of Engine Motored at 560 RPM

engine speed was varied from a low of 1600 rpm to the high of 3600 rpm to permit possible identifiable trends in the impedance characteristics as a function of engine speed. In general, results for no-load are presented, with full-load occasionally applied (Figures 49-64).

The experimental measurement system was the same as in the motored engine study except a readjusting of the second acoustic sensor (furthest from the engine) was necessary to accommodate for the change in the speed of sound caused by elevated exhaust gas temperatures. The engine for powered experimentation was the 12 horsepower Tucumseh engine described in detail in Section II.1.

3. ANALYTICAL PASSIVE SYSTEM ACOUSTIC IMPEDANCES

The results presented in this section are for the two passive systems identified as most contributive characteristics to the acoustic impedance of the engine during its thermodynamic cycle. In the theoretical computer model the calculations for the input impedance required defining of pipe lengths, etc., as dimensions for the passive termination. Figure 65 shows the lengths and dimensions used for the analytically developed close ended tube and volume resonator impedance analysis.

Figures 66 and 67 present the close ended tube resistive impedance and the close ended tube reactive impedance for a zero to 6000 Hz bandwidth. The resistive and reactive components for the volume resonator are presented in Figures 68 and 69.

4. ANALYTICAL ACTIVE SYSTEM IMPEDANCES

Analytical results presented in this section represent efforts to simulate the actual powered engine acoustic impedance by analytical modeling.

With the significant passive system acoustic impedances for the engine identified, the passive acoustic impedances were analytically

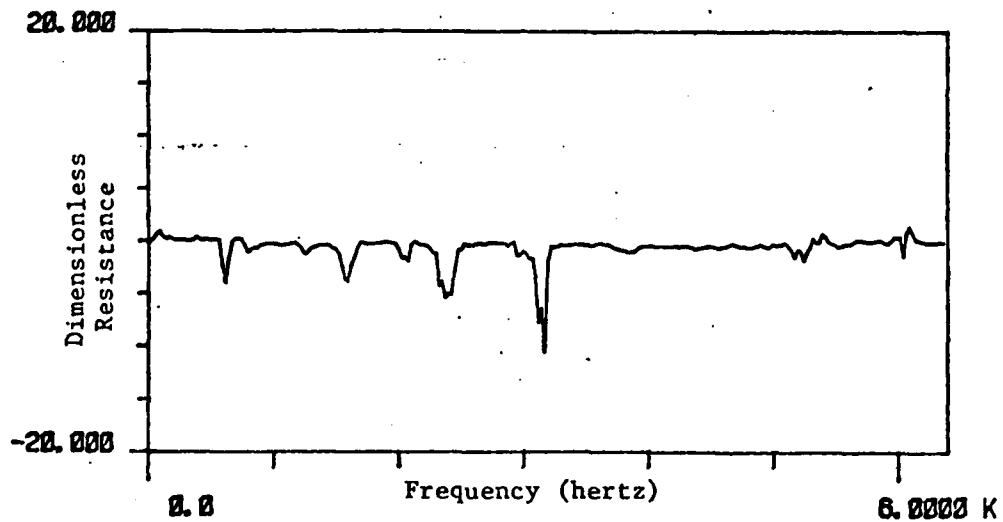


Figure 49. Dimensionless Resistive Impedance of Engine Operating at 1600 RPM at Full Load

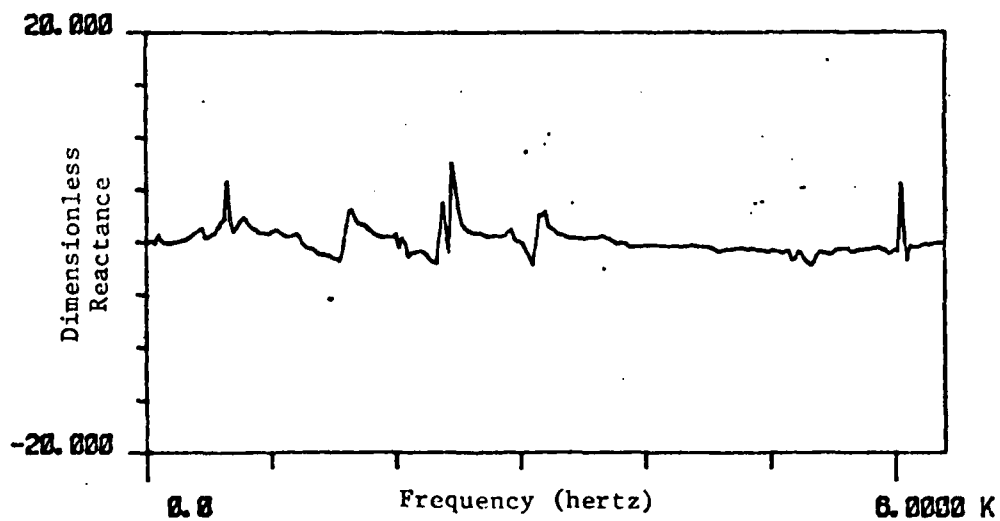


Figure 50. Dimensionless Reactive Impedance of Engine Operating at 1600 RPM at Full Load

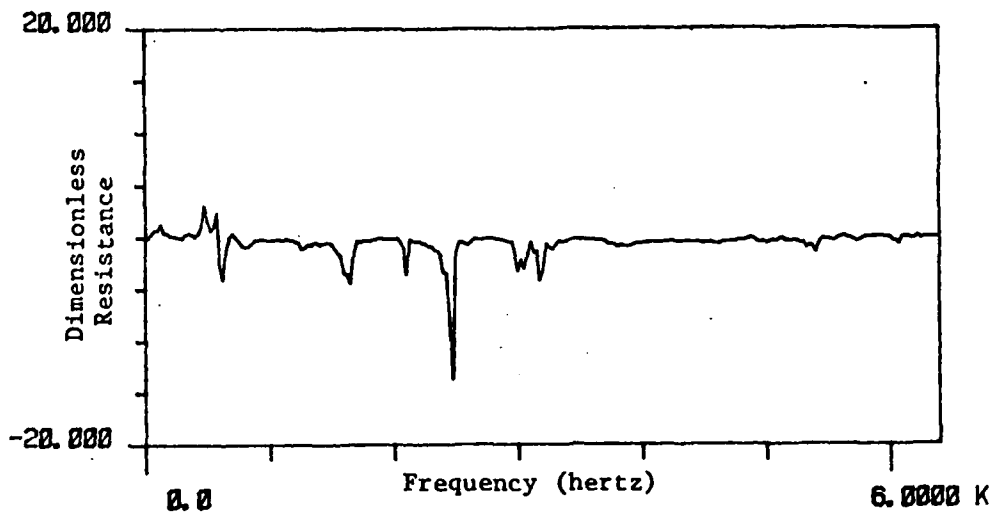


Figure 51. Dimensionless Resistive Impedance of Engine Operating at 2100 RPM with No Load

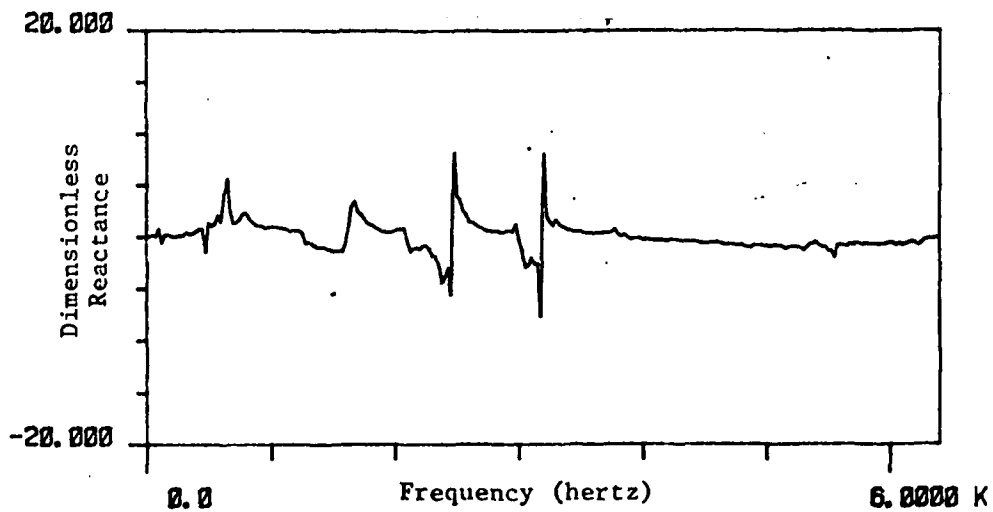


Figure 52. Dimensionless Reactive Impedance of Engine Operating at 2100 RPM with No Load

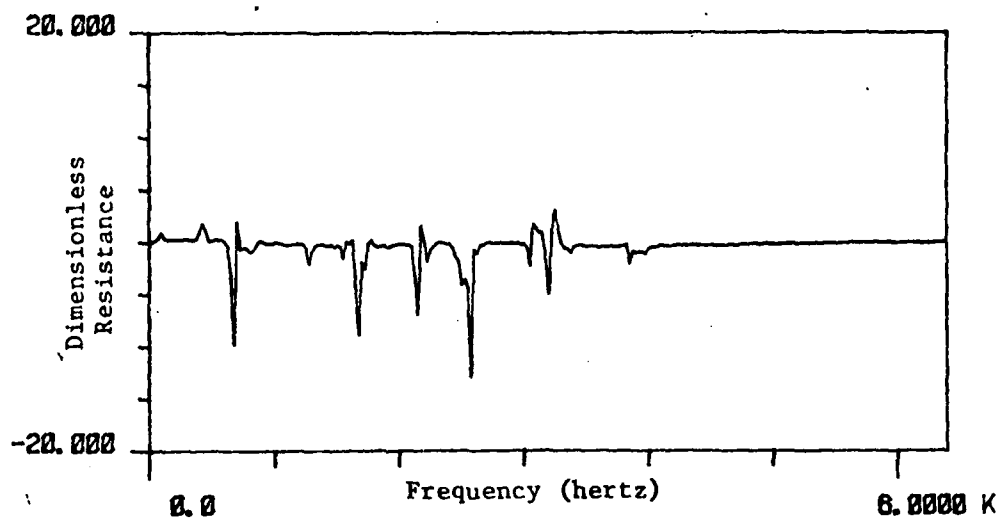


Figure 53. Dimensionless Resistive Impedance of Engine Operating at 2200 RPM with Full Load

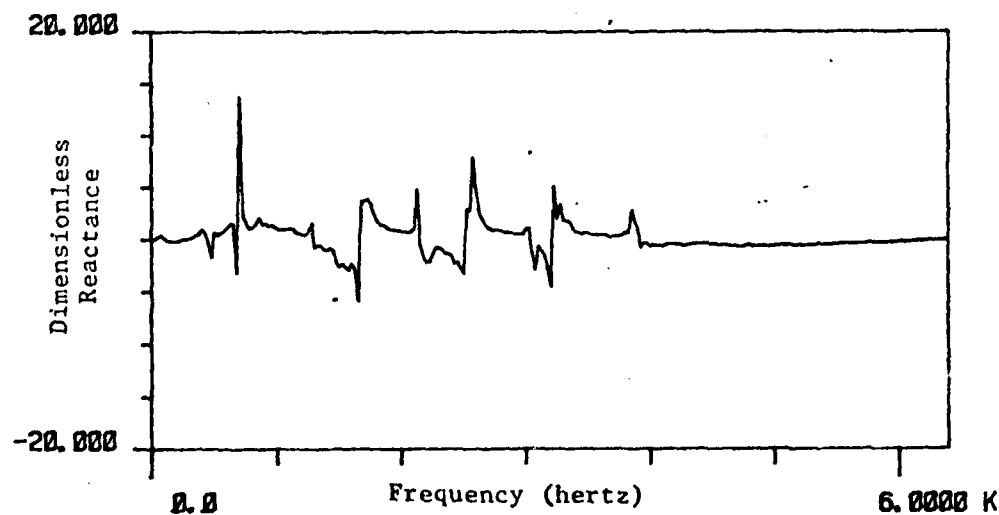


Figure 54. Dimensionless Reactive Impedance of Engine Operating at 2200 RPM with Full Load

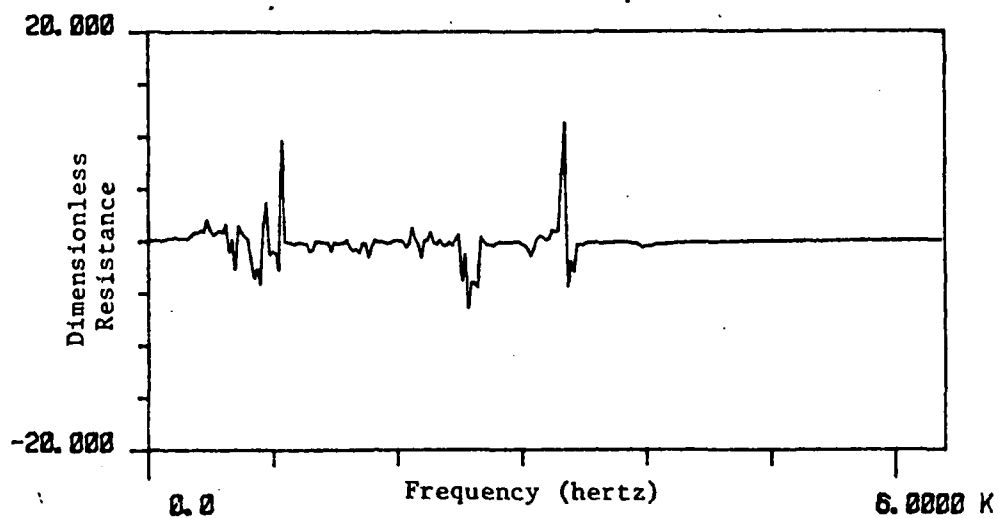


Figure 55. Dimensionless Resistive Impedance of Engine Operating at 2400 RPM with No Load

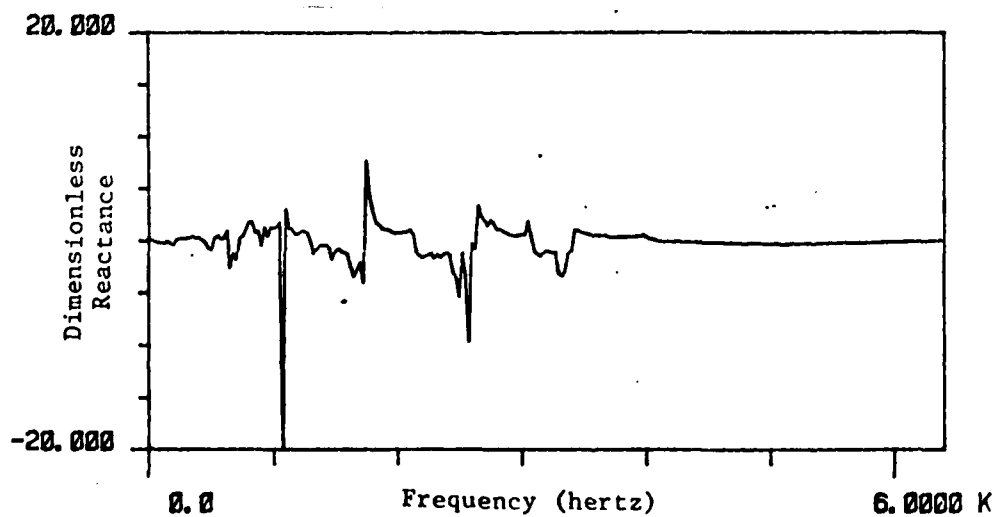


Figure 56. Dimensionless Reactive Impedance of Engine Operating at 2400 RPM with No Load

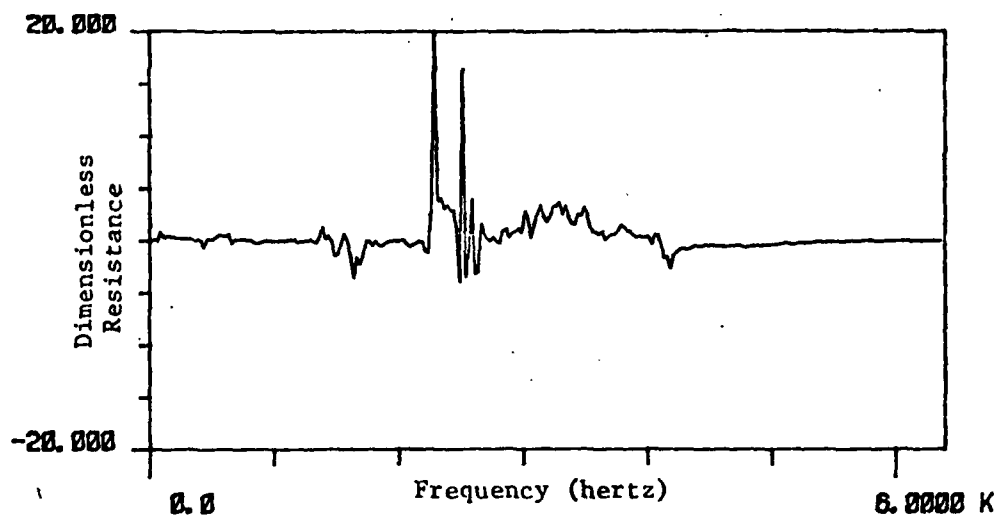


Figure 57. Dimensionless Resistive Impedance of Engine Operating at 2700 RPM with No Load

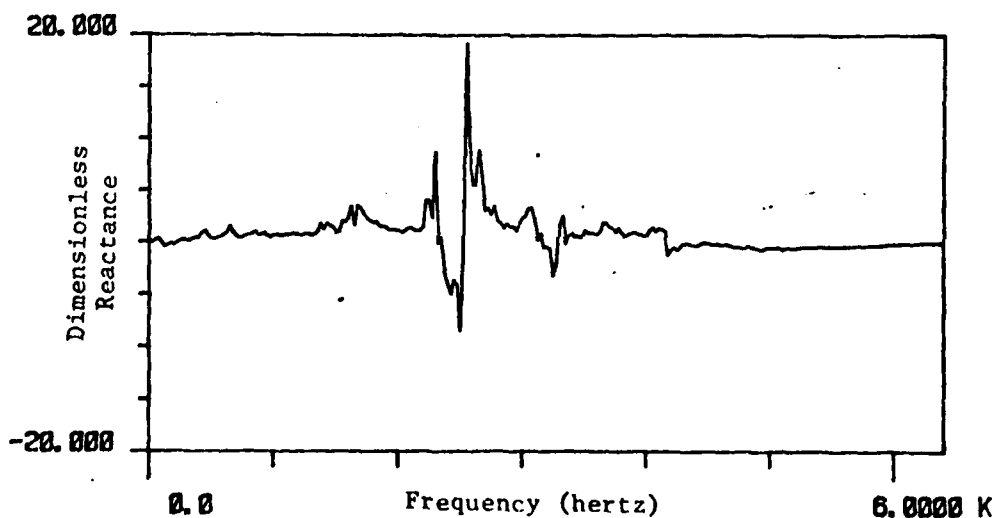


Figure 58. Dimensionless Reactive Impedance of Engine Operating at 2700 RPM with No Load

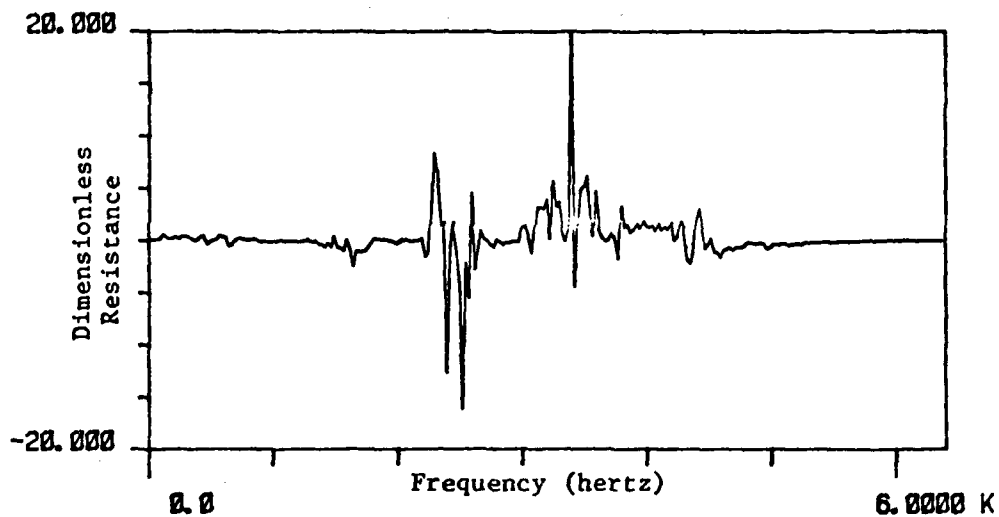


Figure 59. Dimensionless Resistive Impedance of Engine Operating at 2950 RPM with No Load

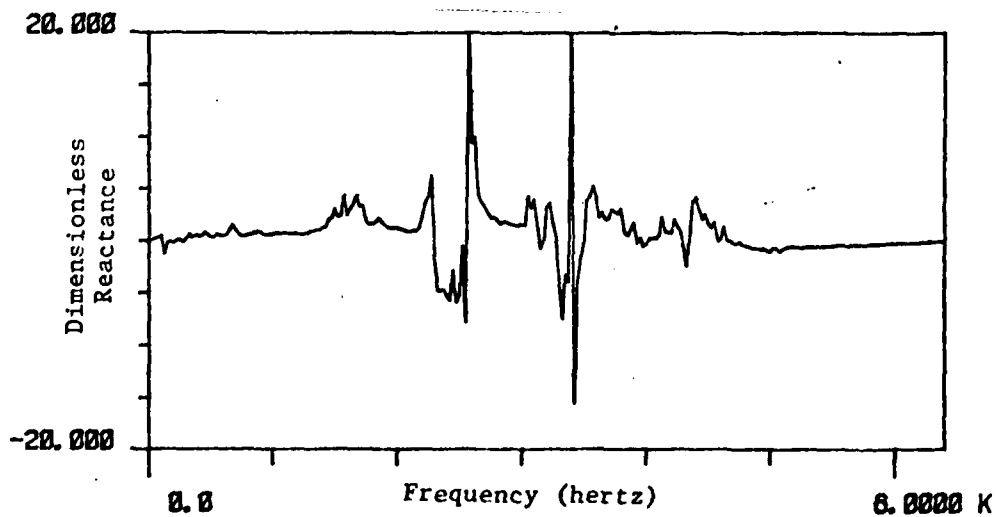


Figure 60. Dimensionless Reactive Impedance of Engine Operating at 2950 RPM with No Load

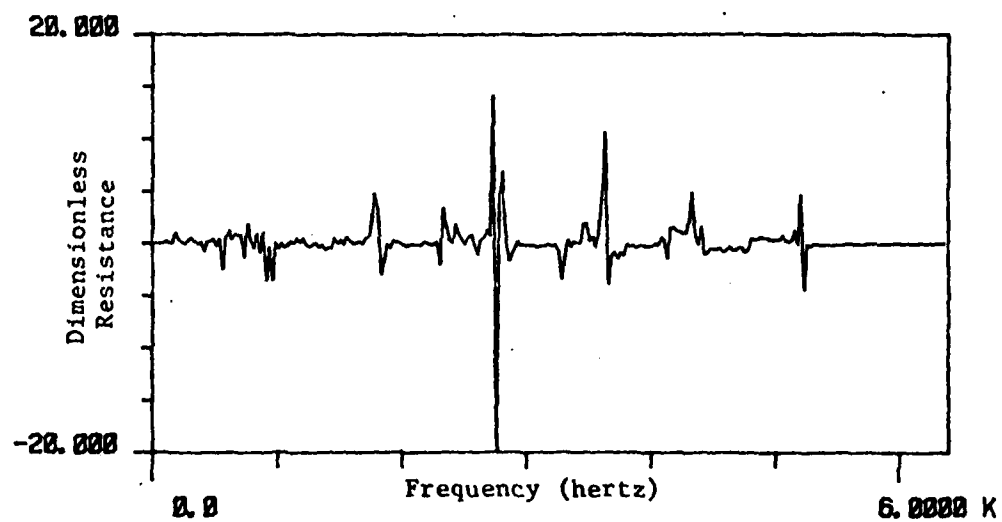


Figure 61. Dimensionless Resistive Impedance of Engine Operating at 3520 RPM with No Load

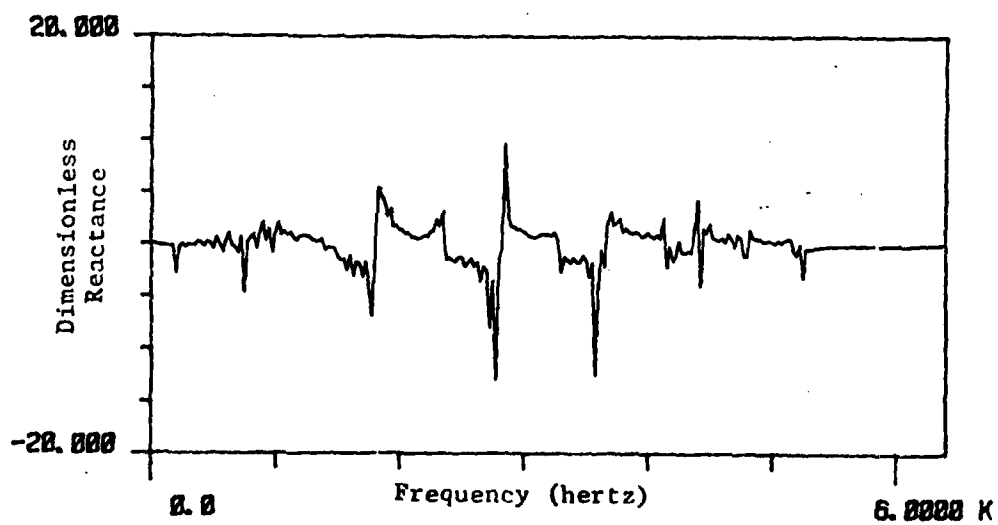


Figure 62. Dimensionless Reactive Impedance of Engine Operating at 3520 RPM with No Load

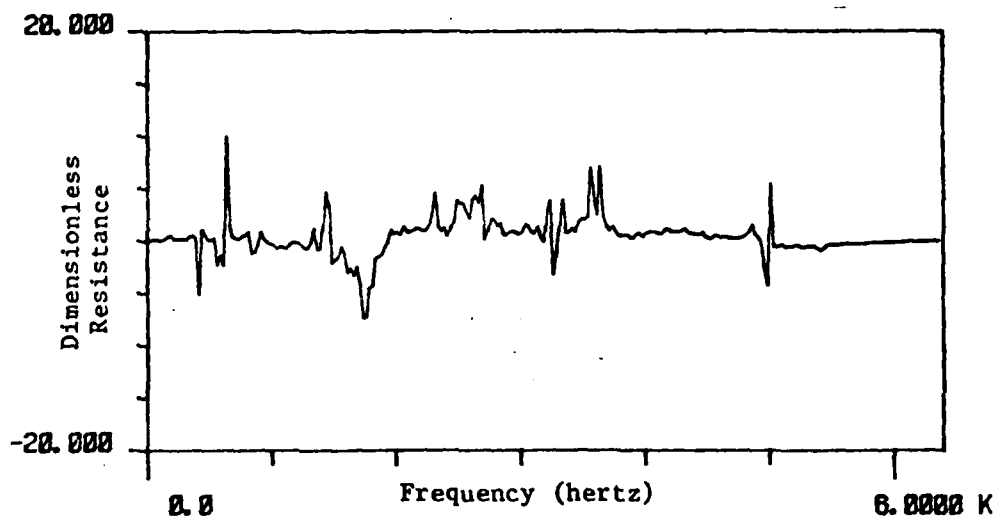


Figure 63. Dimensionless Resistive Impedance of Engine Operating at 3600 RPM with No Load

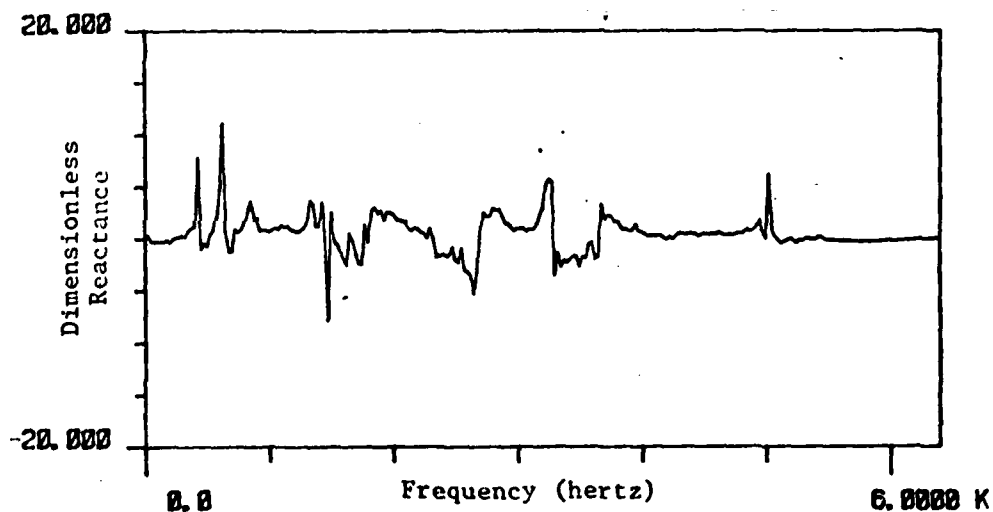
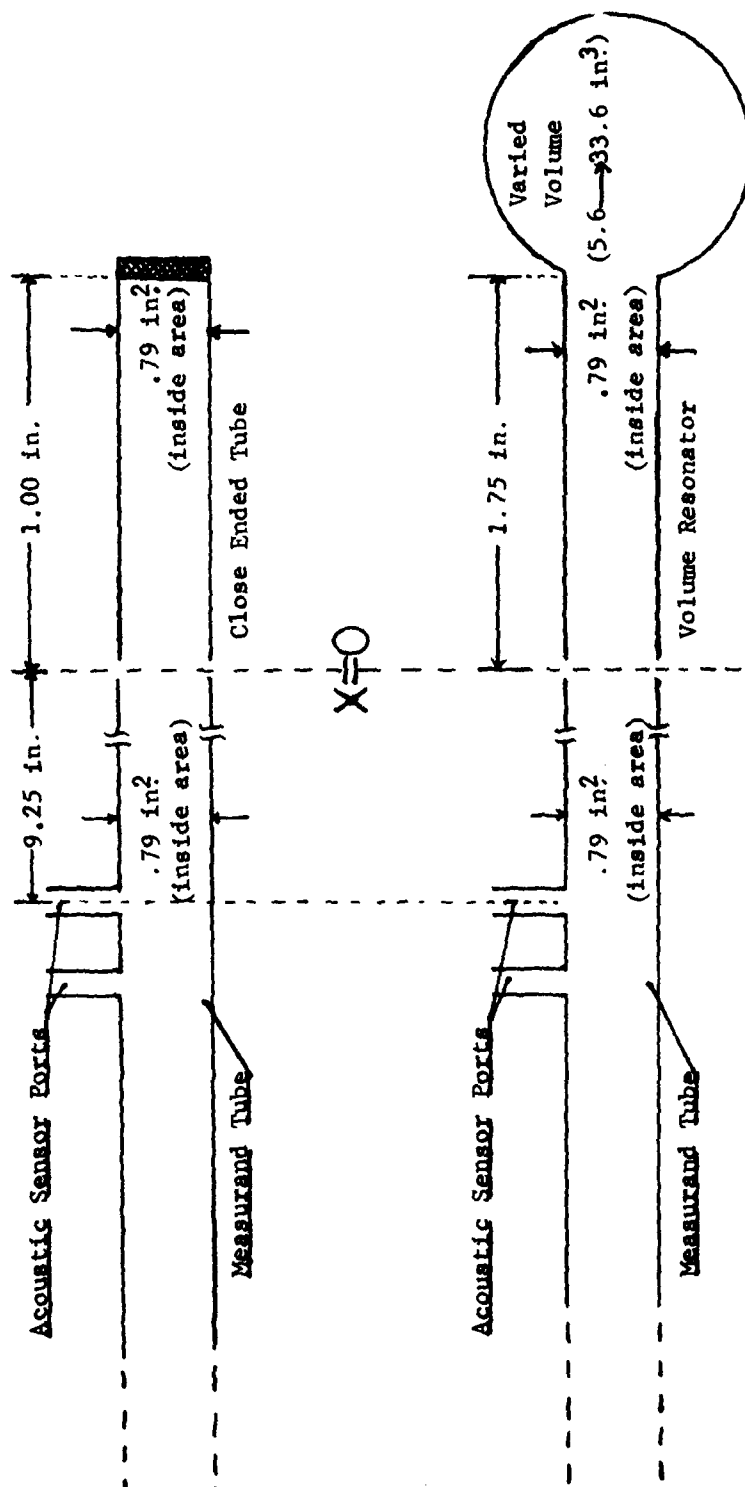


Figure 64. Dimensionless Reactive Impedance of Engine Operating at 3600 RPM with No Load



Note: Some Dimensions are distorted for Presentation Purposes.

Figure 65. Schematic of Computer Simulated Experimental Engine's Acoustic Components, with each Component Dimensions

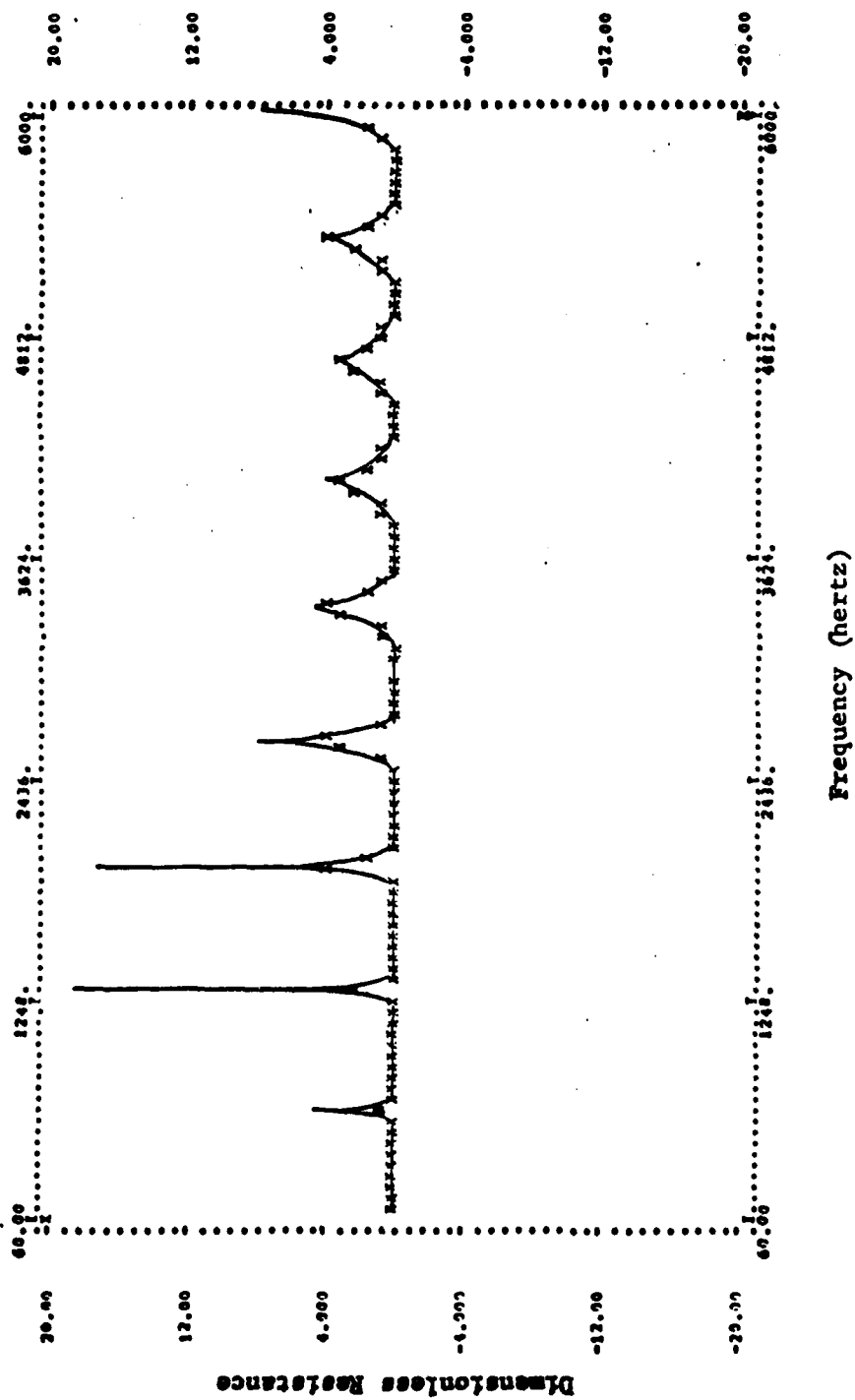


Figure 66. Theoretically Predicted Close Ended Tube Dimensionless Resistive Impedance Response

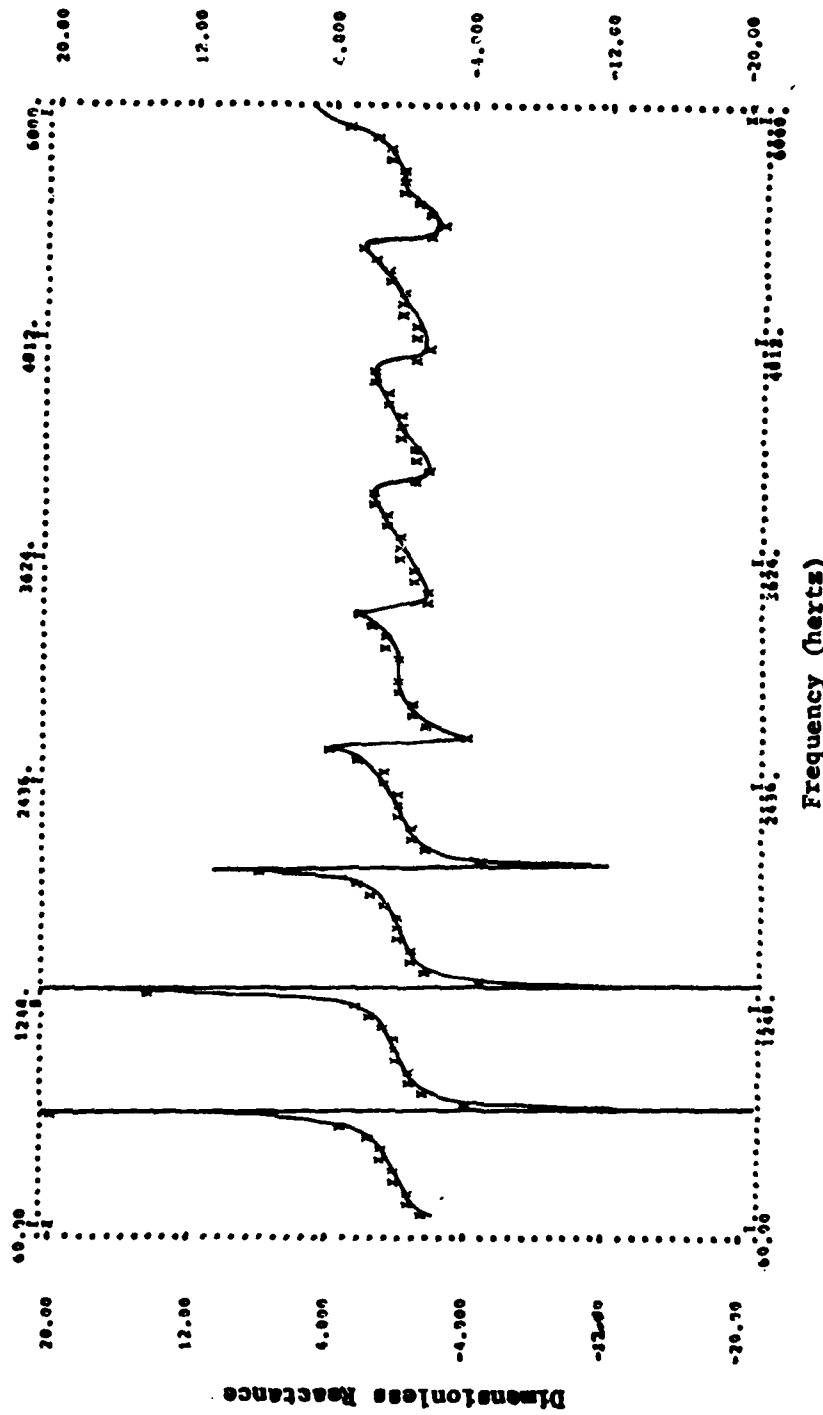


Figure 67. Theoretically Predicted Close Ended Tube
Dimensionless Reactive Impedance

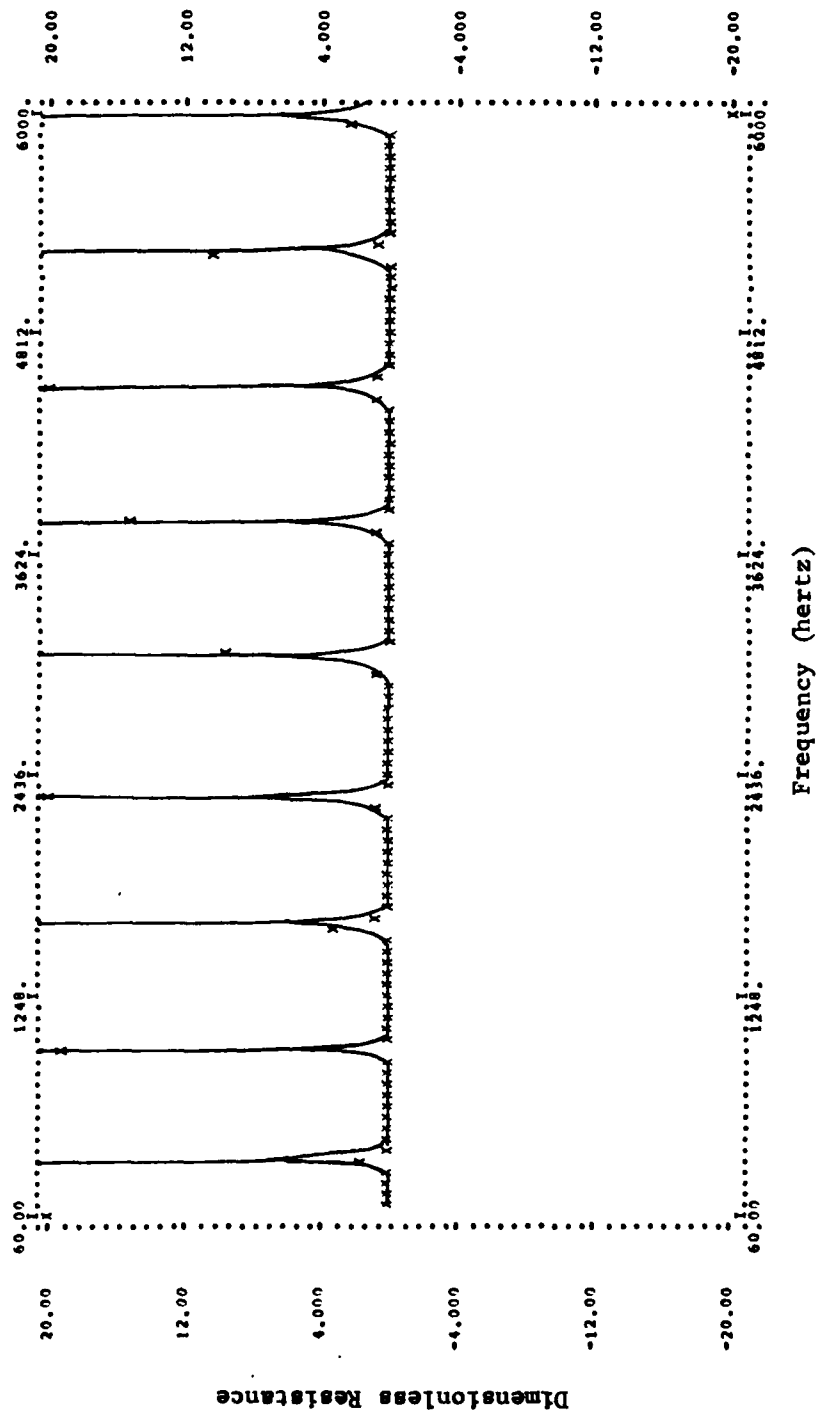


Figure 68. Theoretically Predicted Volume Resonator
Dimensionless Resistive Impedance

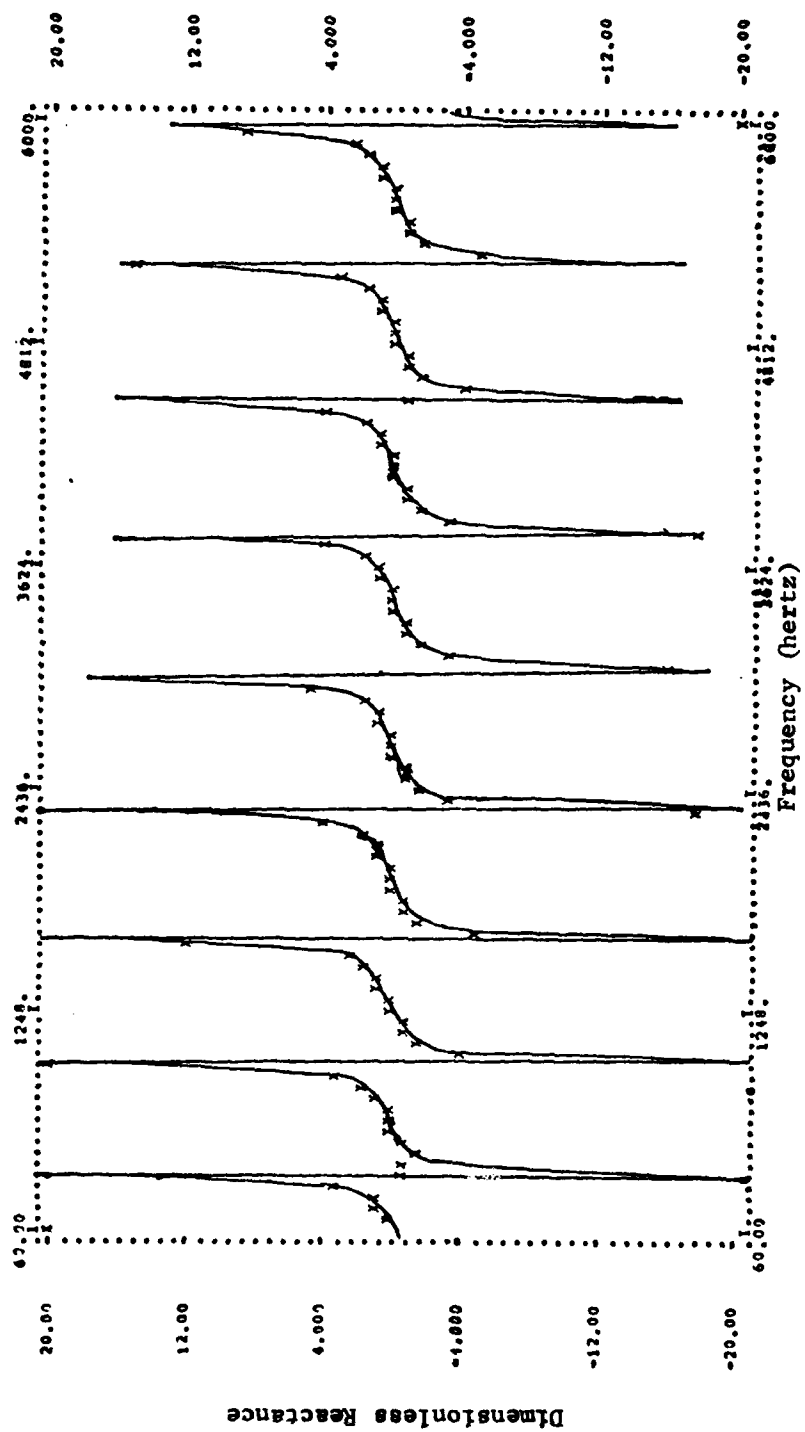


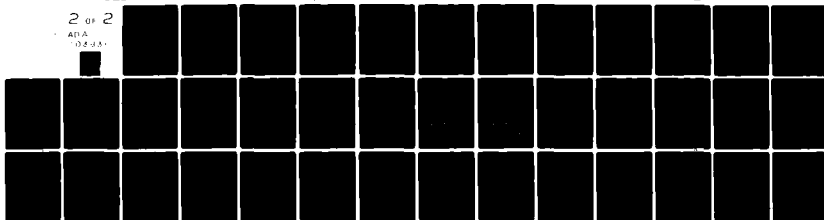
Figure 69. Theoretically Predicted Volume Resonator Dimensionless Reactive Impedance

developed into a computer program, see Appendix B. The manner in which the identified passive systems were combined to simulate the actual experimental engine was accomplished as follows: it was hypothesized that each of the passive systems should be present in the projected engine acoustic impedance in the same proportion that they were available within the thermodynamic cycle. For one thermodynamic cycle, it was projected that a closed tube passive system was present 57% of the cycle, a volume resonator effect existed 35% of the cycle, and an expansion chamber occurred 8% of the cycle. Since the expansion chamber effect was relatively small, its contribution to the total cycle was redistributed to the other two passive system configurations. Therefore, the typical simulated passive system model for the engine was selected to be 60% closed tube configuration and 40% variable volume resonator configuration. These typical percentages were used to computer generate the acoustic impedance for the engine from knowledge of the individual acoustic impedances for the passive systems. The analytical results for such passive system engine modeling are shown in Figures 70 and 71. Since other ratios of passive system contribution to the simulated engine impedance were possible, several other percentage proportions were investigated (Table 2).

AD-A103 931 AIR FORCE WRIGHT AERONAUTICAL LABS WRIGHT-PATTERSON AFB OH F/G 21/7
ENGINE ACOUSTIC IMPEDANCE MODELED AS A CYCLIC SERIES OF PASSIVE--ETC(U)
JUL 81 T J LAGNESE
UNCLASSIFIED AFwAL-TR-80-4203 NL

2 OF 2

ADA
04 JUL 81



END

DATE

FILED

10-81

DTIC

TABLE 2

LISTING OF VOLUME RATIOS AND CORRESPONDING CLOSED TUBE RATIOS
USED IN VARIOUS ACOUSTIC ENGINE SIMULATIONS

Closed Tube Configuration	Variable Volume Resonator Configuration	Figures Showing Impedances
40%	60%	72, 73
95%	5%	74, 75
10%	90%	76, 77

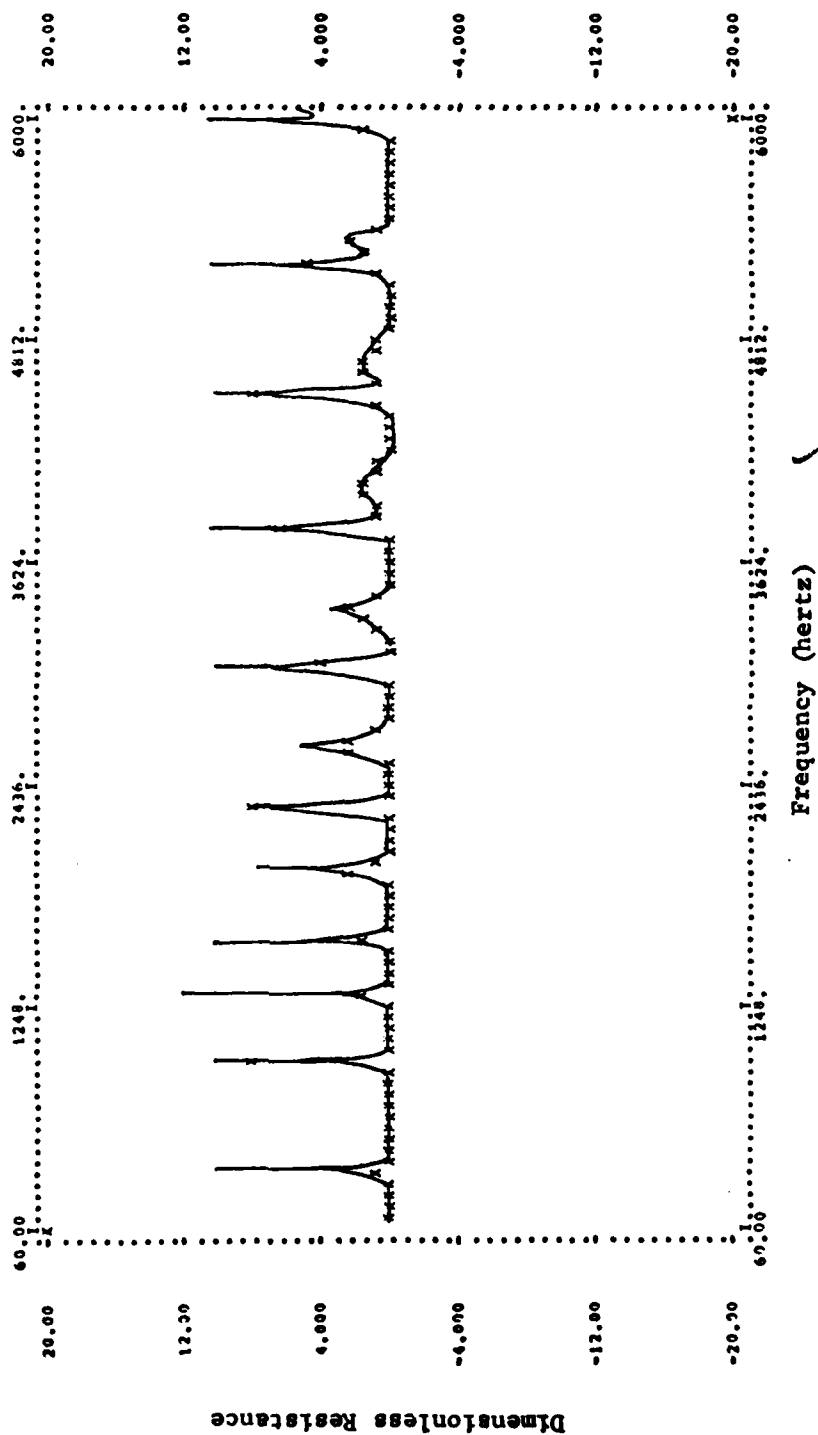


Figure 70. Simulated Engine Dimensionless Resistive Impedance
Using a 40% Volume Resonator Effect and a 60% Close
Ended Tube Effect

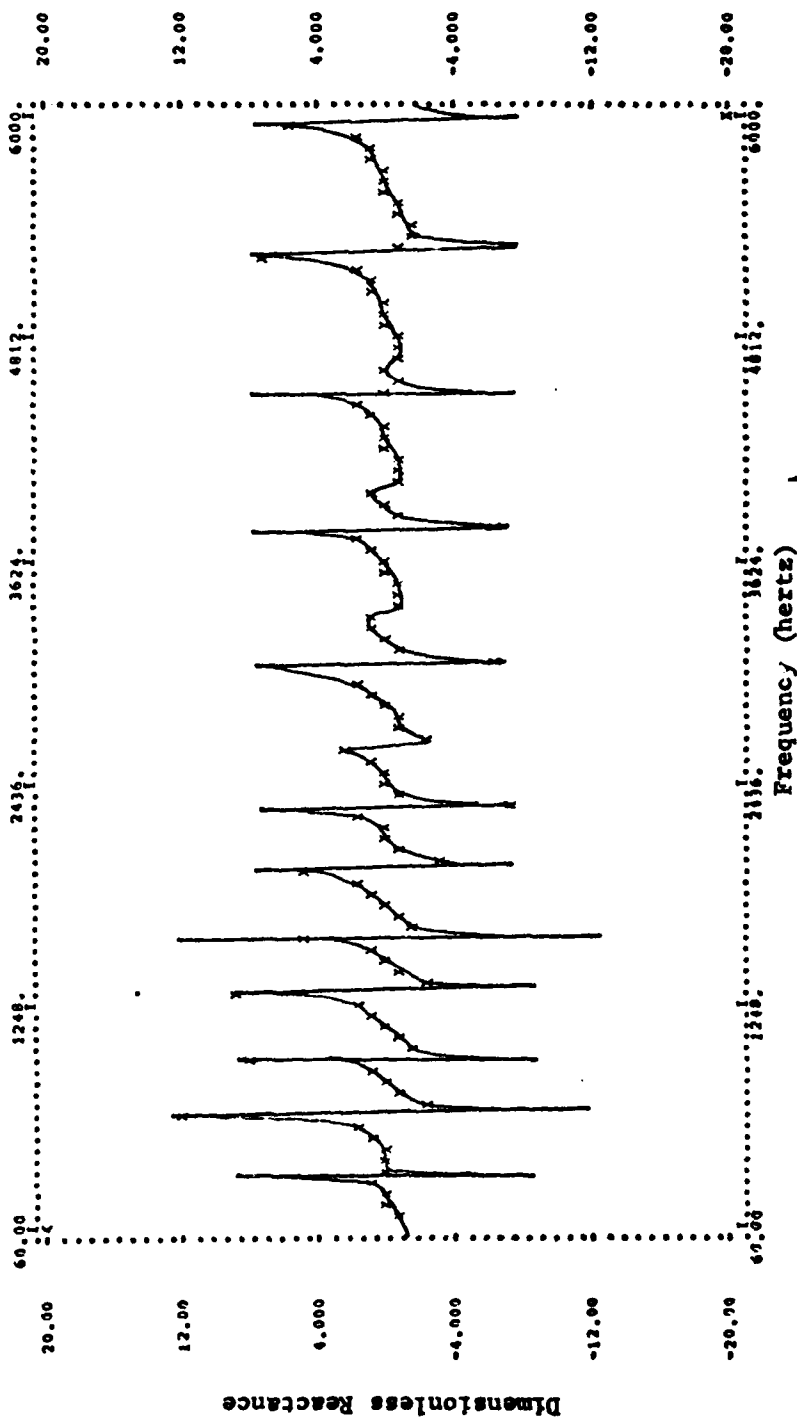


Figure 71. Simulated Engine Dimensionless Reactive Impedance
Using a 40% Volume Resonator Effect and a 60% Close
Ended Tube Effect

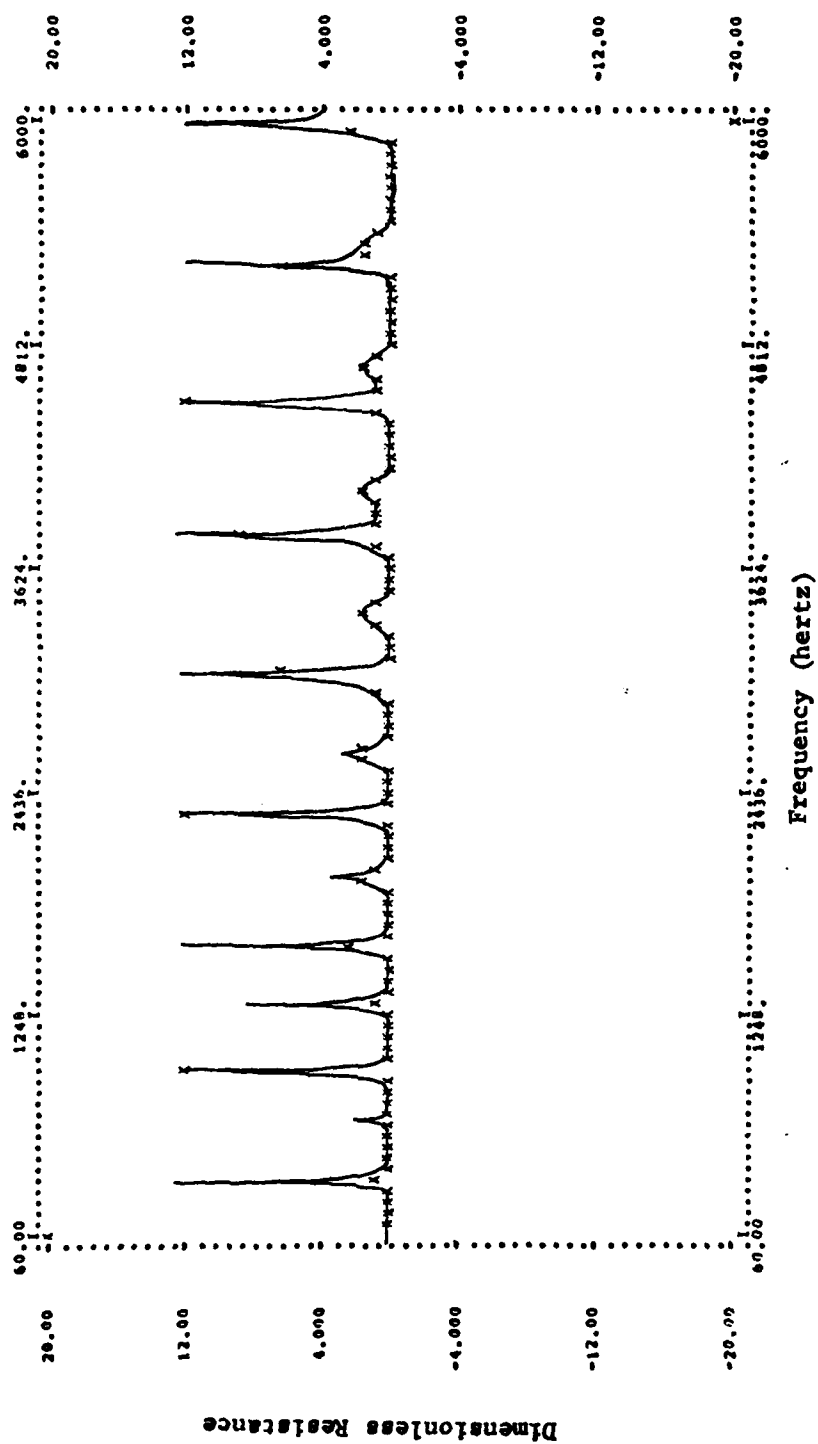


Figure 72. Simulated Engine Dimensionless Resistive Impedance
Using a 60% Volume Resonator Effect and a 40% Close
Ended Tube Effect

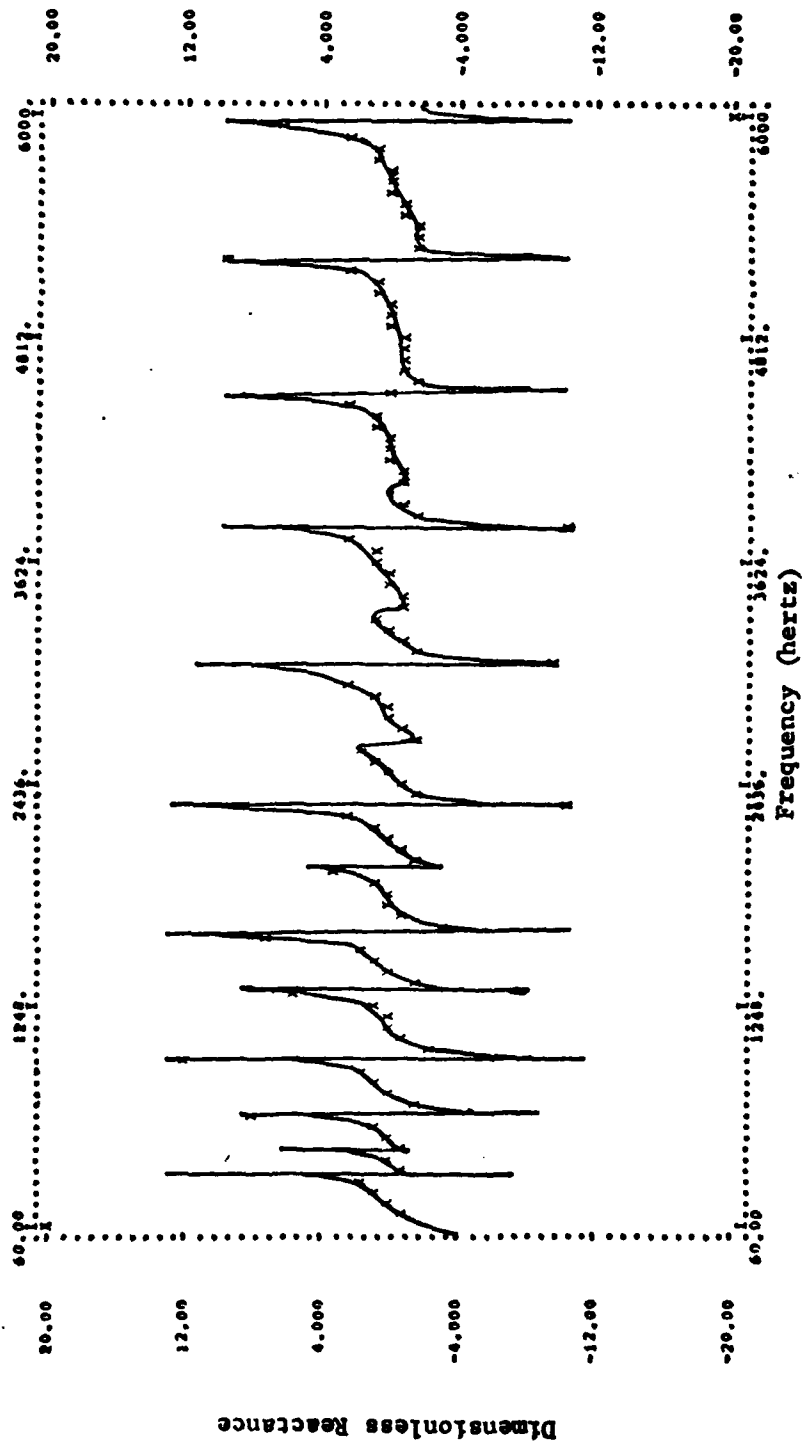


Figure 73. Simulated Engine Dimensionless Reactive Impedance
Using a 60% Volume Resonator Effect and a 40% Close
Ended Tube Effect

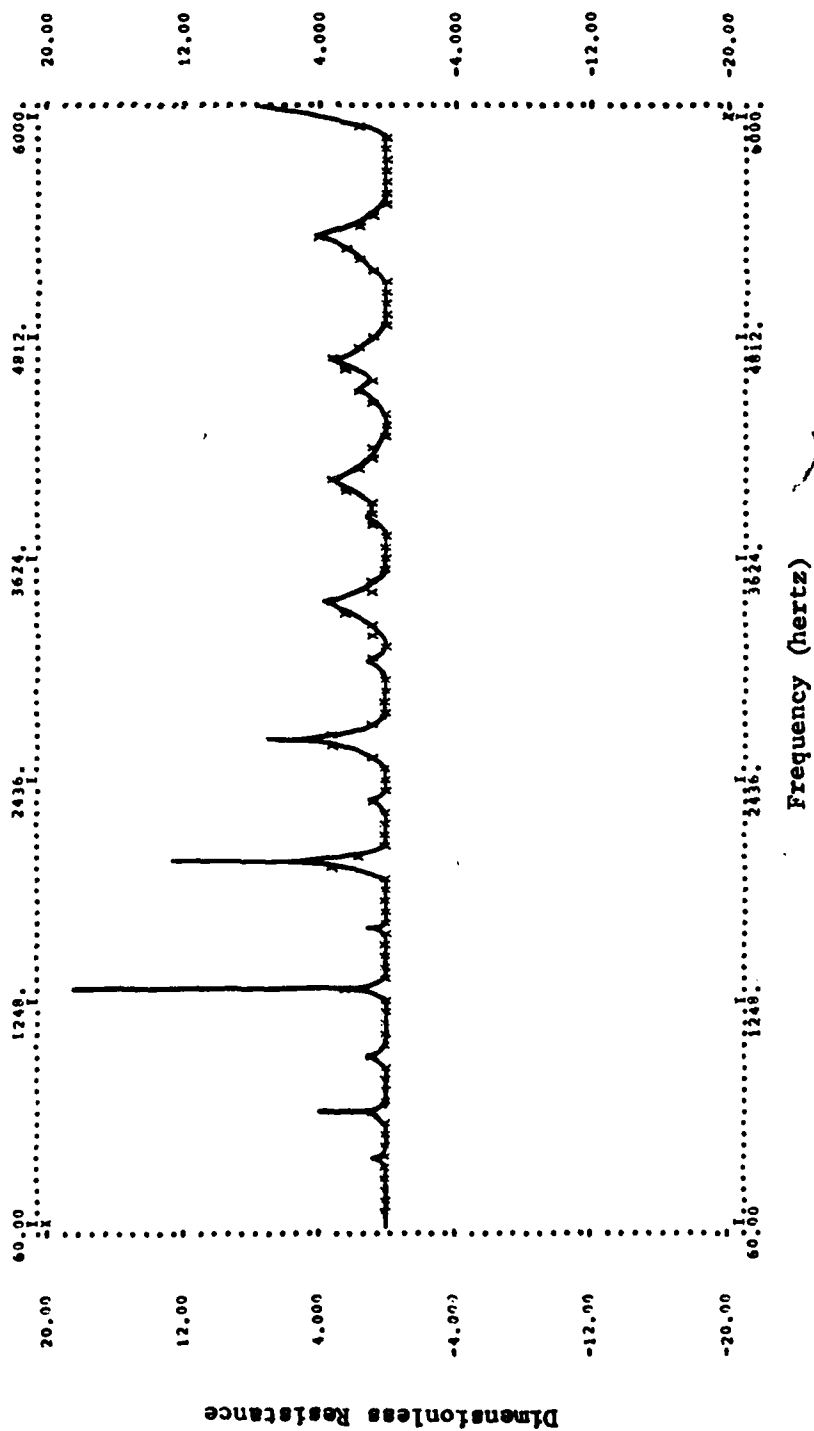


Figure 74. Simulated Engine Dimensionless Resistive Impedance
Using a 5% Volume Resonator Effect and a 95% Close
Ended Tube Effect

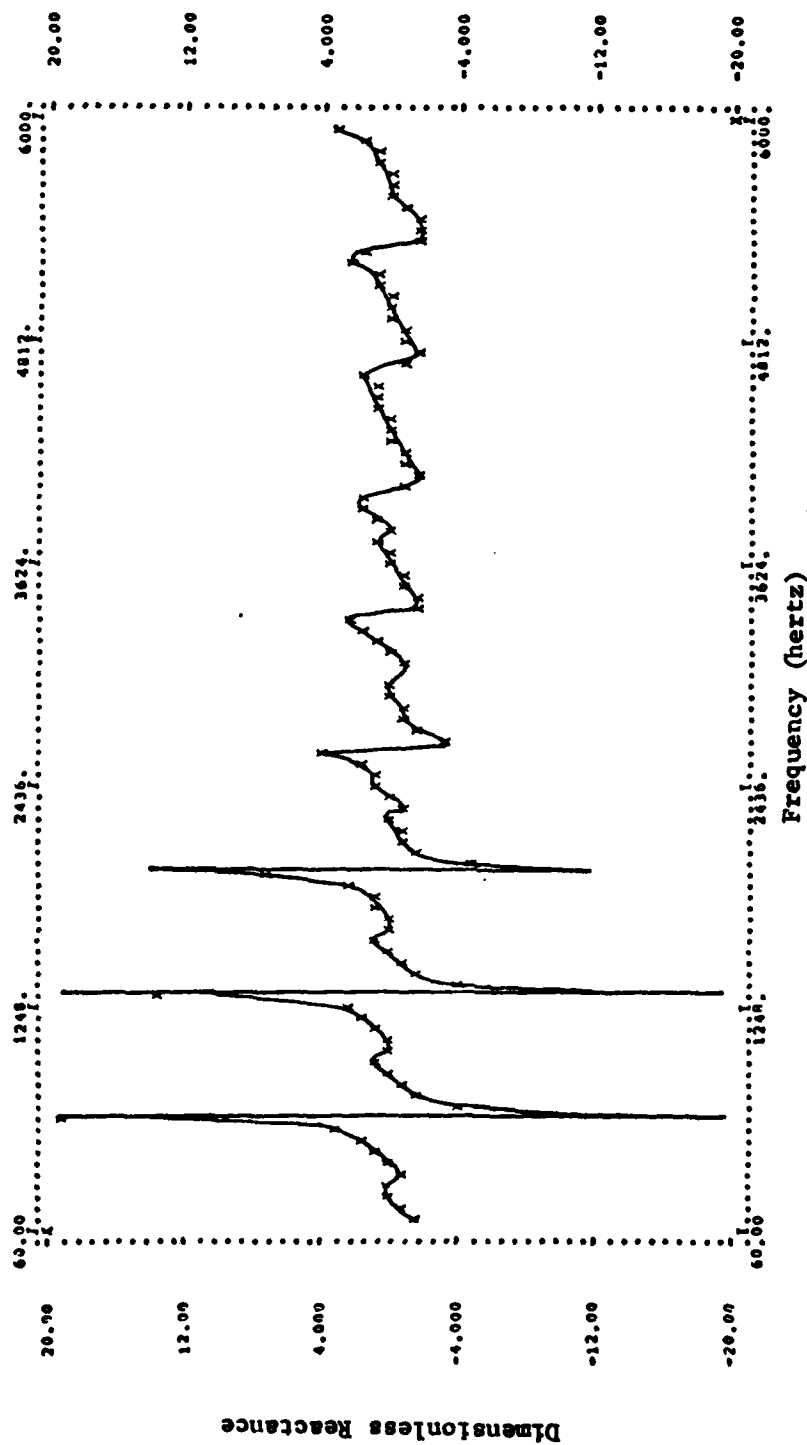


Figure 75. Simulated Engine Dimensionless Reactive Impedance
Using a 5% Volume Resonator Effect and a 95% Close
Ended Tube Effect

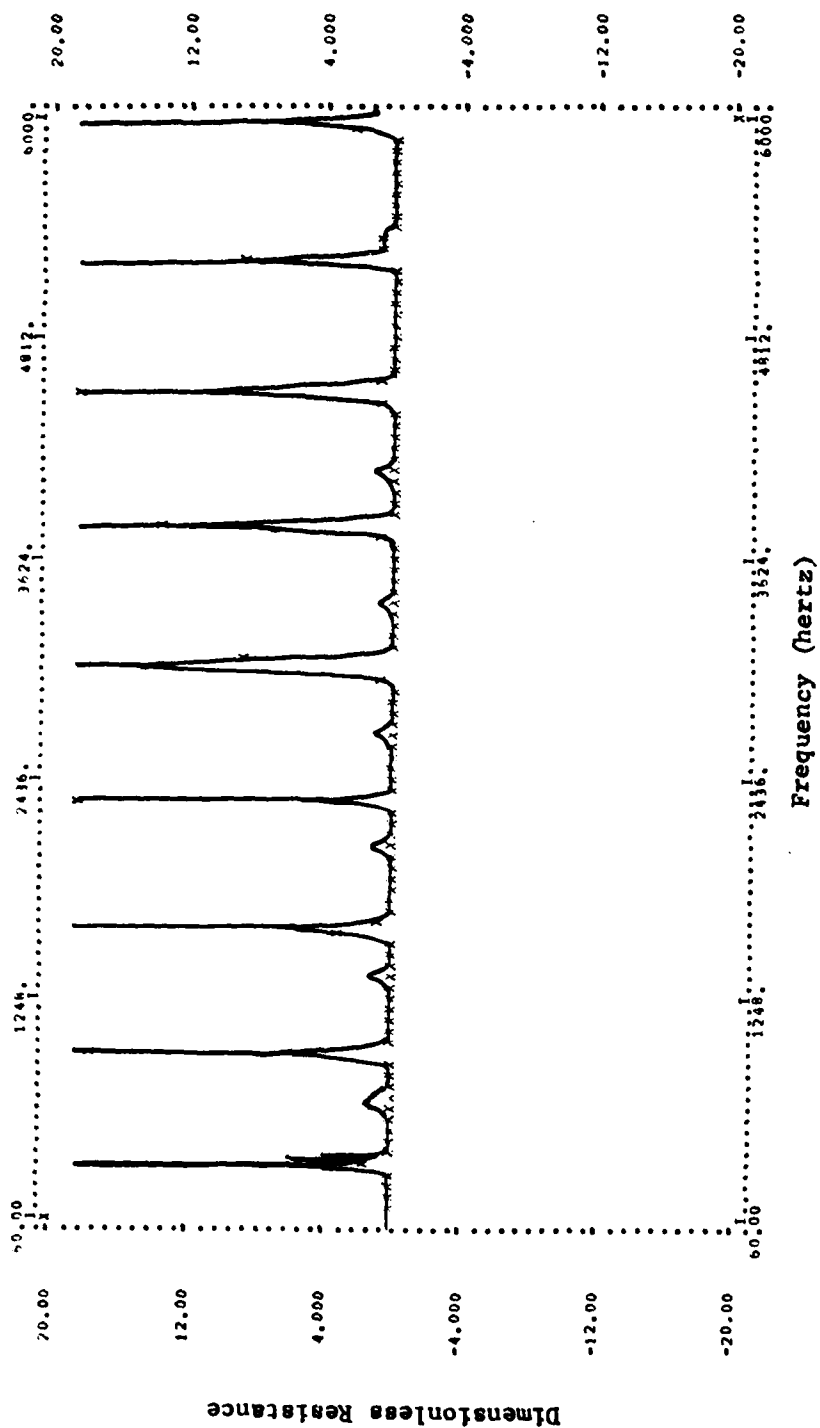


Figure 76. Simulated Engine Dimensionless Resistive Impedance Using a 90% Volume Resonator Effect and a 10% Close Ended Tube Effect

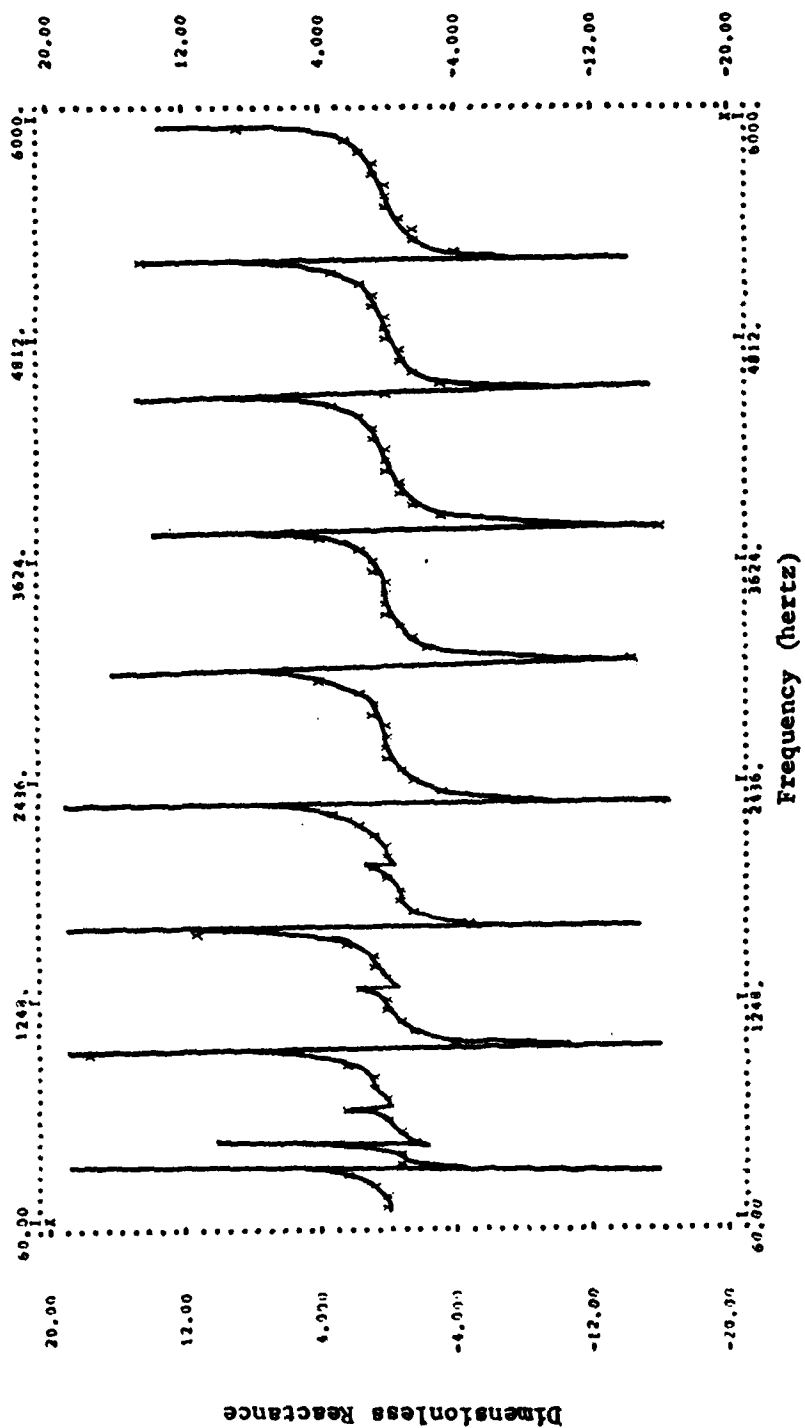


Figure 77. Simulated Engine Dimensionless Reactive Impedance
Using a 90% Volume Resonator Effect and a 10% Close
Ended Tube Effect

SECTION V

EVALUATION OF ANALYTICAL AND EXPERIMENTAL RESULTS

1. PASSIVE SYSTEM IMPEDANCE EVALUATION

a. Evaluation of Computer Modeling Efforts for Passive Systems

Upon examination of the computer analysis results, definite trends in the predicted impedances caused by certain system geometries were observed to exist. Appreciation of the associated theoretical development indicated, for example, that the pipe-type impedance which occurred in the plotted results was a consequence of the incorporated length λ of the measurand tube between the acoustic pressure sensors and the termination impedance (Figure 14). The following five designated subsections provide some insights that have been appreciated from the study of the theoretical dimensionless acoustic impedances at $x = -\lambda$:

(1) The expected resistive and reactive component interrelation of impedances was confirmed, with the peak of the resistive impedance corresponding to a zero reactive impedance. A plot of resistive impedance against reactive impedance would be a varying amplitude ellipse with a minor axis positioned 90° from the resistive impedance axis.

(2) The predominant periodicity of both the resistive and reactive impedances was a result principally of the equivalent length of straight pipe between the acoustic pressure sensor port and engine chamber, and not of the terminating passive system impedance (Figure 65). Upon comparison of Figures 67 and 69, the periodicity of the impedances is observed to be not quite the same. The slight variation between periods was expected since the straight tube length (that distance between the acoustic sensor ports and the engine exhaust chamber) used in the computer program was different by .75 inch for the close ended tube than for the volume resonator. This incorporated length difference is inherent in actual engines.

The resonant conditions for the analytic close ended tube and volume resonator cases can be calculated using the previously defined lengths and checked against the period of impedance variation which appeared in the computer output. For the analytic closed tube reactive impedance case (Figure 67), the period was 670 Hz. The computer program computed a measured impedance as one which the pipe impedance interacted with the terminating impedance which is truly representative of the experimental case. The resonant condition shown in the computer output resulted because of the combined length of the straight pipe (9.25 inches) and the smaller length contributed by the exhaust manifold (estimated at one inch). The resonant frequency (f_n) defined by this equivalent pipe geometry can be calculated using the following equation:

$$f_n = \frac{c}{2 \left(l + \frac{8a}{3\pi} \right)} \quad (44)$$

where

a is the pipe radius

l is the total length of the pipe

c is the speed of sound

Upon substitution of experimental values,

$$f_n = 640 \text{ Hz}$$

This calculated resonant frequency is inherent in the computer indicated impedance variation with frequency.

The resonant frequency of the straight tube length for the terminating volume resonator case can be calculated in a similar manner. However, the effective pipe length is longer due to an additional pipe length beyond the exhaust port into the cylinder volume. The corresponding fundamental resonant frequency was calculated based on straight pipe resonant conditions, as 600 Hz, where an effective straight tube length of 11 inches was estimated.

The resonant condition indicated in the computer simulated volume resonator reactive impedance was dominated by this calculated pipe resonant condition. The above resonant frequency calculations for straight pipe impedance based on estimated equivalent lengths can be implicitly identified as the dominant contributor to both the computed and experimental impedance periodicity.

(3) The terminating impedance contribution to the measured impedance (Figure 14), had an effect on the magnitude of the measured impedance and was also responsible for a phase shift in the measured impedance relative to the straight pipe impedance. These magnitude and phase shift phenomena were clearly evident in the computer simulated close ended tube case of Figure 67. It is observed that the magnitude envelop of the computed impedance exhibits an amplitude proportional to the magnitude of the terminating reactive impedance. The cotangent function defined by the envelop of the peak amplitudes in Figure 67 has a period of approximately 9000 Hz. The period for the ideal $\cot(kx)$ function of the close ended tube case would be about 13,700 Hz. This represents a 30% difference, which would imply that an additional consideration is needed to completely explain the envelop tendency of the impedance.

This magnitude envelop tendency of the computer evaluated reactive impedance is also evident in the volume resonator case (Figure 69). For the volume resonator reactive impedance case, the magnitude of the terminating impedance is known to increase with increasing frequency, which would imply that the magnitude of the measured reactive impedance should decrease with increasing frequency, a behavior which does appear in the computer results.

The phase shift indicated between the close ended tube reactive impedance (Figure 67) and the volume resonator reactive impedance (Figure 69) is indicative of the interaction between the open pipe impedance and the terminating impedance. See paragraph 1 of Section V.1.a. If it is assumed that the open pipe impedance defines the phase information for

the measured impedance, it would be expected that the magnitude of the measured reactive impedance would be zero at zero frequency. Examination of Figures 67 and 69 indicated that this zero magnitude assumption is not correct. The terminating impedance interaction with the open pipe impedance must thus establish the locations for the resonant peaks of the measured impedance amplitudes. Hence, as the open pipe impedance was seen to influence the major periodicity of the measured impedance, this terminating impedance influences the resonant frequency locations of the measured impedance.

Referring to Figure 67, the magnitude of reactive impedance at zero frequency is noted to be of some negative value. It was projected that when the pipe impedances were added in parallel combination with the terminating impedance, the negative infinity magnitude of terminating reactive impedance dominated the pipe reactive impedance, thus causing the indicated measured impedance to approach a negative non-zero value. In Figure 69 the volume resonator reactive impedance was observed to be slightly negative at zero frequency. When considering the terminating reactive impedance to be a negative magnitude of some finite amount at zero frequency, it would be expected that when added to the zero magnitude of the pipe impedance at zero frequency, the indicated measured reactive impedance would be a non-zero negative value, which was the case.

(4) The peak-to-peak magnitude of the measured impedance was primarily defined by the magnitude of the resistive component of the terminating impedance. The magnitude dependency was studied by changing the resistive constant of the terminating impedance and noting the corresponding change in the measured impedance. An increasing of the terminating resistive impedance correlated to a decrease in both measured resistive and reactive impedance outputs. It was noted that the trends in magnitude variation over the range of frequencies evaluated would not change with terminating resistive impedance but only with a change in terminating reactive impedance, as indicated in paragraph (3) of Section V.1.a.

(5) In Figure 68, a noticeable effect due to the resonant condition of the volume termination is present. The first resonant condition is identified in the resistive impedance at 340 Hz. The first peak-to-peak period of 600 Hz bandwidth is thus smaller than those periods indicated at higher frequencies. If an average volume of 20 in^3 is used when determining the measured impedance, the resonant condition that would exist for this volume would be 326 Hz. The resonant frequency of 326 Hz had probably dominated and masked the nearby resonant condition indicative of the pipe impedance as previously discussed. Consequently, a slightly shorter period is evident in the lower frequency range.

b. Evaluation of Experimental Results of Standard Passive Acoustic Systems

Comparison of the theoretical results shown in Section IV.3 for the passive acoustic systems with the experimental results of Section IV.1.a indicated that the laboratory measurement technique employed for experimental study of similar passive acoustic systems was rather accurate. There were few inconsistencies, which denied an exact comparison of experimental to theoretical passive acoustic system results. The inconsistencies which did exist between experimental to theoretical results could essentially be explained by the slightly different geometrical considerations for each. For the experimentally attained passive system impedances, the acoustic pressure sensors were placed within six inches of the passive engine termination in agreement with initial laboratory studies. However, the computer program simulated the acoustic pressure sensors later as being 9.25 inches from the passive engine termination in agreement with engine impedance studies. This difference in the indicated lengths caused the period of the respective impedance results to differ correspondingly. Consequently, the period was 1500 Hz for the experimental close ended tube results and 610 Hz for the theoretical close ended tube results. The cause of the period variation can be analytically identified in the " $\tan k\ell$ " term incorporated in both the resistive and reactive definitions of measured impedance (Equations 25 and 26). The " ℓ " parameter defined the length between the acoustic pressure sensors and the engine

termination. Consequently, as the length term was increased, the period of both impedance components decreased, and thus the theoretical components cycled more often through the tangent function.

c. Evaluation of Experimental Engine Crankangle Studies

The engine crankangle study was performed to permit possible identification of measured impedance due to the engine's internal geometry in terms of certain passive system acoustic characteristics. For example, the 90° crankangle analysis (Figures 19 and 20), where the exhaust valve is closed, was the most easily definable case. The results of this aspect of the study resembled not only the results of the passive close ended tube analysis (Figures 15 and 16) but also the related computer modeling results for a close ended tube (Figures 66 and 67). The most essential characteristic identified in the results for the 90° crankangle study was the strongly developed inverse cotangent function (Figure 20) of the reactive impedance. A noticeable behavior pattern for the results of the 90° crankangle study was the decreasing period for this inverse cotangent function at higher frequencies. The shortening of the period for the experimental crankangle study was indicative of an increased distance between the acoustic pressure sensor port, and the reflective surface (the exhaust valve), which was attributed to the effective acoustic size of the engine's manifold. Geometry changes along the measurand tube to the exhaust manifold of the test engine, as well as geometry irregularities of the exhaust valve, resulted in the generation of additional acoustic phenomena such as secondary resonance and partial reflection of the acoustic pressure signal. At higher frequencies, there was an increased likelihood of the geometry changes to act as an acoustic discontinuity severe enough to cause reflection. (There is a high frequency plane wave limitation which restricts the wavelength of the frequency transmitted to the minimum about equal to the inside diameter of the measurand tube.) The resultant effective length between the acoustic sensors and the acoustic termination thus could potentially increase with increasing frequency and hence, the period of the acoustic impedance would decrease with increasing frequency.

When developing the computer model for this engine, the effective geometry changes within the measurand tube manifold system were not incorporated into the acoustic engine model. Thus, the computer model accurately defined only the more dominant characteristics of the resistive and reactive impedance for the experimental facility.

The credibility of the exhaust and intake valve position with crankangle can be shown through examination of experimental resistive impedance data at varying crankangle. At a frequency of 455 Hz, a peak in the resistive impedance originated and increased in magnitude from the 90° crankangle to 260° crankangle and then decreased from the 260° to 400° crankangle where the peak completely disappeared. If a passive helmholtz resonator is defined from the engine's cylinder dimensions, where the neck of the resonator is the combined length of the manifold and chamber length to the cylinder, then it would be possible to estimate the resonant helmholtz frequency of the actual system from the following relationship (Reference 9):

$$f_n = \frac{c}{2\pi} \frac{S}{\ell'V} \quad (45)$$

where

ℓ' is the effective neck length including end effects

V is the volume of the resonator

S is the cross-sectional area of the neck

The resonant frequency for the volume of the engine's cylinder was thus theoretically approximated to be 456 Hz. It is observed that this resonant peak corresponded to the resistive peak shown in the experimental data.

Attention is now directed to the crankangle studies between 130° and 260° (Figures 21 to 26) by comparing these crankangle studies to the computer model of a theoretical volume resonator (Figures 68 and 69).

Some evident relationships can be seen, particularly the inverse cotangent waveform which is developed in both experimental and theoretical data. Another observation of the project was that in experimental results, several waveforms resembling superimposed inverse cotangent waveforms existed in much of the results. This response can be identified as an extension of the phenomena of partial reflection and partial transmission of the acoustic signal. As noted previously, the geometric discontinuities, which are present in the manifold and through to the cylinder, cause partial reflection of the transmitted lower frequency due to a change of impedance. Additional reflections are caused by the exhaust valve itself. The exhaust valve has limited opening area when fully opened, and the gap allowed does inhibit transmission of white noise into the cylinder to the higher frequency content of the externally generated white noise signal. However, since the high frequency content is normally heavily damped, transmission inside the cylinder and the reflected high frequency signal is expected to be low. Assuming full transmission into the cylinder area by the acoustic signal, the crank-angle study at 340° shows most closely the expected active system acoustic impedance. The effects of geometry and attenuation really limit the applicability of passive systems toward active engine modeling, to the two selected, since other passive systems added would be too specialized and probably masked by the already considered and more dominant acoustic characteristics.

2. ACTIVE SYSTEM IMPEDANCE EVALUATION

a. Analysis of Computer Modeling Effort of an Active Engine Acoustic System

The results obtained from computer simulated active engine acoustics are useful in explaining some of the features observed from experimental data reduction. The idea that several superimposed passive acoustic systems can represent the actual engine acoustically is a justifiable statement when one compares the theoretical results to the slow speed engine experimental results. The experimentally obtained peaks shown in Figures 45 through 48, for example, are similar to the corresponding theoretical results shown in Figures 70 through 77.

The developed computer model for the engine was less effective towards a quantitative comparison for experimental hot engine than cold engine evaluation. However, the computer model was productive in defining qualitative trends in the active engine data. An example of where qualitative comparison is found is in the higher frequency range of the experimental motored engine studies wherein volume termination rather than close ended tube termination similarities apply. In Figure 48 several peaks which occur after 4000 Hz have attenuated to the degree that the reactive impedance was essentially zero. At 3300 Hz through 6000 Hz, the wavelength was small so that the geometric changes through the engine's manifold did not pose a significant impedance change to cause a great amount of acoustic reflection. This implied that much of the frequency content in the 3300 Hz to 6000 Hz bandwidth reacts with the volume in the vacated cylinder. This predominant volume type termination caused a strong cotangent waveform to develop with a reduced period. This phenomena is indicated somewhat within the 3300 Hz to 4000 Hz bandwidth due to less attenuation over this range. This conclusion is justifiable when related to the previously discussed theoretical results in the superimposed addition of close ended tube and volume resonator reactive impedances. The superimposing of these two passive system impedances indicated that it was possible to have a reactive impedance with several cotangent functions of differing periods to result as the measured impedance of an experimental active system. In the reaction impedance case of a motored engine (Figure 48), the 0 through 3000 Hz range indicated a closed tube reactive impedance effect while the 3000 Hz to 6000 Hz bandwidth showed primarily a volume resonator effect with partial close ended tube effect.

b. Analysis of Motored Engine Studies

First investigations of active engine impedances focused on slow motored engine speeds such as the 2 rpm and 24 rpm studies (Figures 33 through 36). The most obvious characteristic identified was the inverse cotangent function in the reactive impedances by overlaying

the 90° crankangle reactive impedance and the 2 rpm and 24 rpm motored engine reactive impedance, the resulting graph led to a definite indication that the motored engine at low speeds resembled a close ended tube (Figures 78-81).

Consideration of the method triggering by the digital signal analyzer to obtain proper sampling of the acoustic signal becomes an important criteria for determining operating engine impedance similarities. The sampling time specified for the FFT digital signal analyzer was 39.1 microseconds for the 0-6400 Hz frequency bandwidth selected. By establishing thermodynamic cycle completion time as a function of engine speed, and assuming the presence of a close ended tube 57% of the thermodynamic cycle, a 35% volume resonator presence and 8% expansion chamber presence, it was possible to determine how much time each of these passive systems would be present within one sample for the FFT analyzer. Figure 82 indicates graphically how much time each passive system is available as a function of engine speed. Approximately three thermodynamic cycles are shown by means of the crankangle positions on the graph. With the engine speed lower than 100 rpm, it was assumed that the close ended tube reactive impedance characteristics tend to mask most other reactive impedance behaviors of the engine, particularly considering the fact that the FFT sampling time of only 39 microseconds was quite small in comparison to the time that the exhaust valve remained closed.

As the motored engine speed is increased, the results became less pronounced. But, in certain instances such as the 450 rpm, 555 rpm, and 560 rpm impedance studies (Figures 41-42 and Figures 45-48), the results have indicated a resemblance to the 90° crankangle study. The sporadic peaks which occurred in both resistive impedances are not the contribution of one type of acoustic behavior but the combined resonant impedance effect of many internal geometry changes of the engine.

The engine speeds in the motored engine studies were below 600 rpm, which implied that harmonic resonances contributed by the engine's

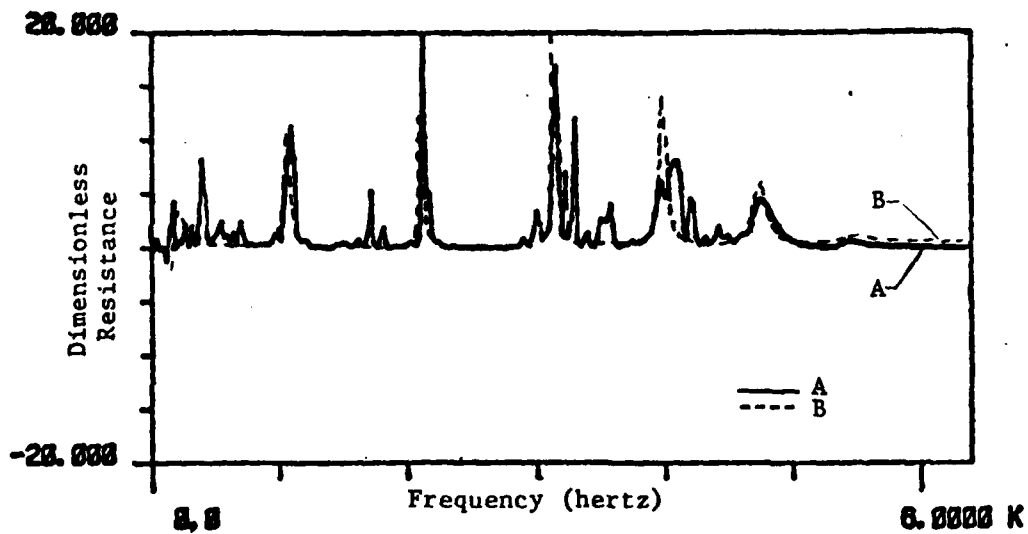


Figure 78. Dimensionless Resistive Impedance of 90° Crankangle Study (B) and 2 RPM Motored Engine Study (A)

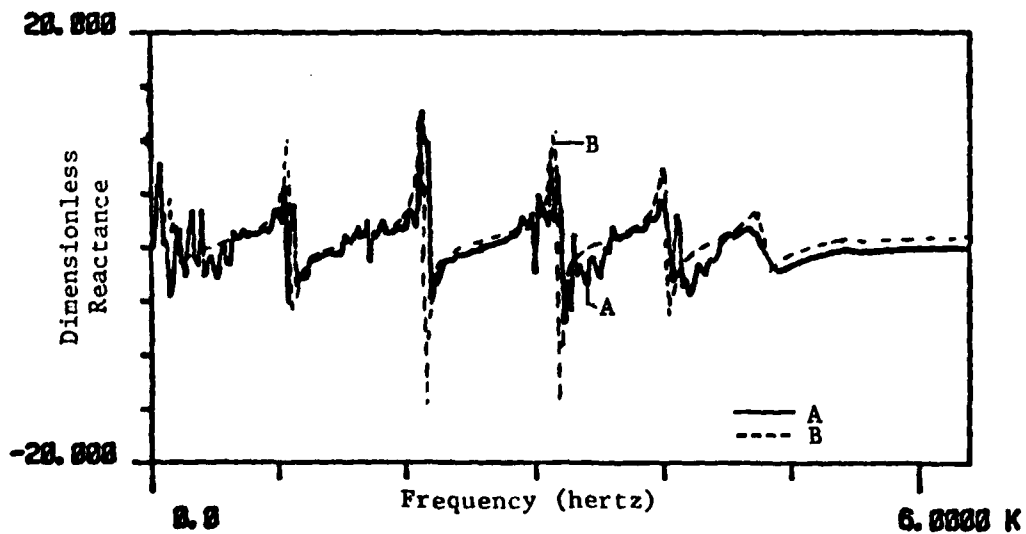


Figure 79. Dimensionless Reactive Impedance of 90° Crankangle Study (B) and 2 RPM Motored Engine Study (A)

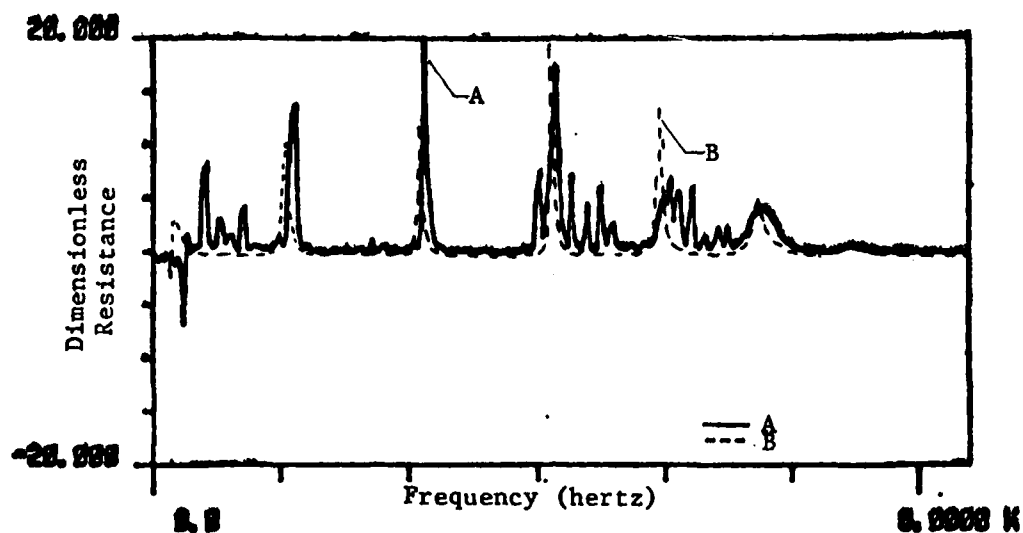


Figure 80. Dimensionless Resistive Impedance of 90° Crankangle Study (B) and 24 RPM Motored Engine Study (A)

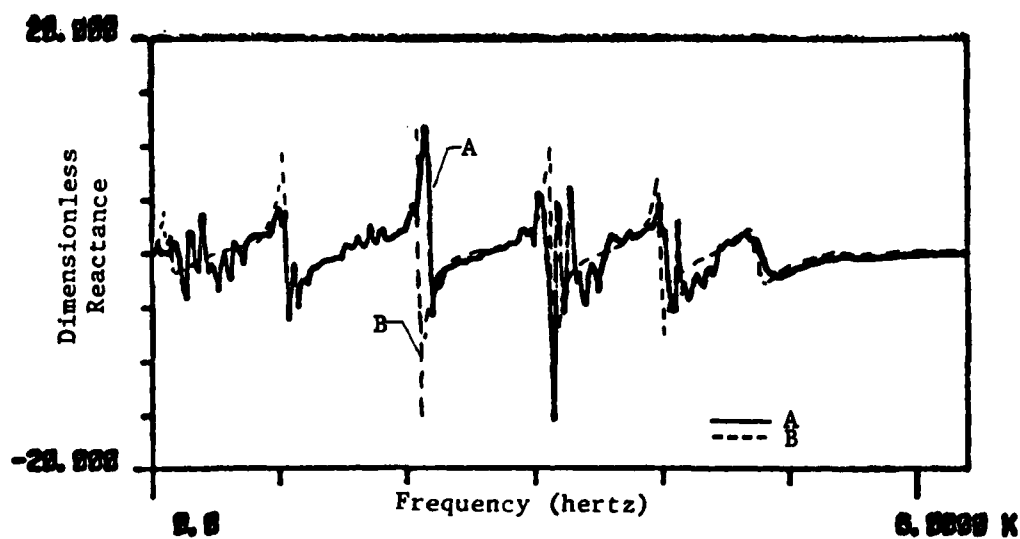


Figure 81. Dimensionless Reactive Impedance of 90° Crankangle Study (B) and 24 RPM Motored Engine Study (A)

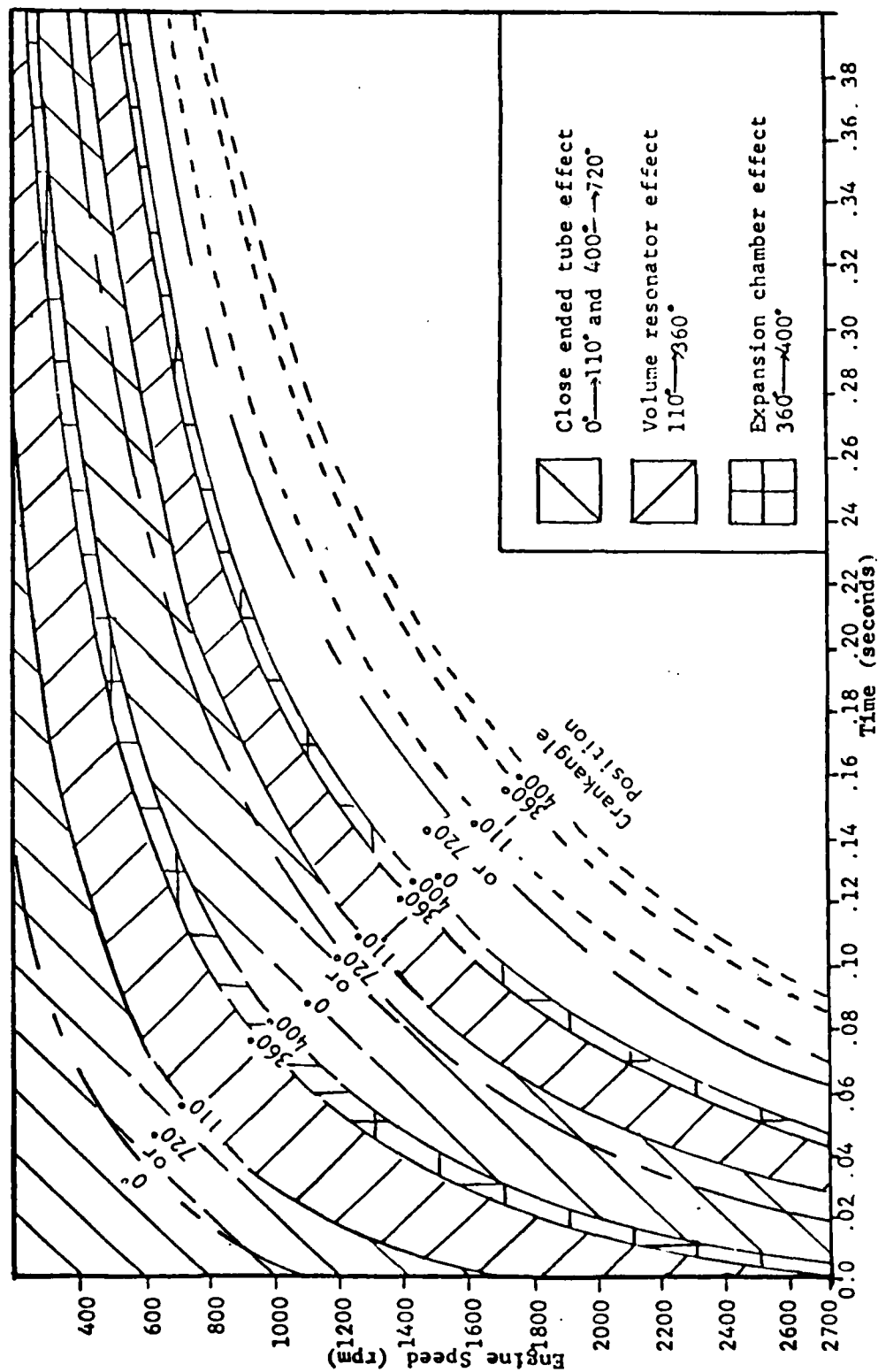


Figure 82. Thermodynamic Cycle Completion Time as a Function of the Engine Speed

pressure pulsations at the firing frequency had a negligible effect on these engine impedance measurements. The fundamental frequency at an engine speed of 600 rpm would be 10 Hz, well below the frequency analysis range considered by this project.

c. Analysis of Operating Engine Data

The results obtained from powered engine studies were less conclusive than the project's previous experimental results. The results are somewhat interrelated to other experimental results, particularly with regards to the development of an inverse cotangent behavior in the reactive impedance. The inverse cotangent behavior was only marginally evident in the 1600 rpm reactive impedance study (Figure 40) but became more fully developed in the 2100 rpm (Figure 52), 2200 rpm (Figure 54), and 3520 rpm (Figure 62) reactive impedances. However, for the remaining powered engine impedance results no dominant cotangent continuity feature existed. The variability in these results was believed to be largely direct consequence of the sampling technique used for digital signal analysis in this phase of experimentation, particularly, in regards to type of triggering operation utilized.

Assuming that the inverse cotangent relationship should have been a contributing influence on the impedance characteristic of power engine acoustics, the possibility that the actual impedance characteristics would be masked by other acoustic phenomena becomes a viable possibility and therefore, will be considered here. One of the more dominant disruptive effects on the acoustic environment within the measurand tube would be that of the hot exhaust gases. The temperature gradient along the measurand tube, caused by cooling hot exhaust gases, varies with the engine's cycle and speed. It becomes questionable if this temperature gradient ever stabilizes within the measurand tube to a mean temperature profile during any part of the powered engine thermodynamic cycle. With the temperature gradient dramatically changing with time, accurate time sampling of transfer functions to resolve the acoustic signal into the incident and reflected acoustic pressures, and thereby define the

engine acoustic characteristics, becomes exceedingly more difficult if not impossible. Another combustion process effect which had possible adverse contributions to accurate acoustic impedance assessment was the large velocity head produced each thermodynamic cycle. Associated with the velocity head was a dynamic pressure which raised the pressure within the measurand tube cyclically as a function of the firing frequency. The dynamic pressure could contribute to sporadic peaks within the experimental results of both motored and powered engine tests. The combination of a fluctuating temperature gradient and large cyclic dynamic pressure could cause severe changes in the acoustic transmission medium. Another disruptive by-product effect of the combustion process was the varying density gradients within the transmission (measurand) tube which would cause distortion in the acoustic plane waves that were propagated.

SECTION VI

DISCUSSION AND RECOMMENDATIONS

1. GENERAL REMARKS

Defining the engine system acoustically has been a long sought-after goal. Recently, significant advances have been made in several areas of engine acoustics. It had been made a goal of this project to identify the acoustic impedance of an internal combustion engine when viewed at the exhaust port.

The investigation presented in this work identifies a method of pursuit towards defining impedance characteristics of an engine. Table 3 shows the method of pursuit taken to evaluate engine impedance.

TABLE 3
EXPERIMENTAL APPROACH TAKEN TO EVALUATE
ENGINE SOURCE IMPEDANCE

A) Standard Passive Acoustic Impedance Evaluation	
Open Ended Tube	Close Ended Tube
B) Engine Passive Acoustic Impedance Evaluation	
Crankangle Variation	
C) Motored Engine Active Acoustic Impedance Evaluation	
Engine Speed Variation	
D) Powered Engine Active Acoustic Impedance Evaluation	
Load and Engine Speed Variation	

The acoustic source impedance of an engine has been experimentally defined quite accurately for the motored engine investigations. A moderate definition of powered engine acoustic source impedance has been achieved, although falling short of an accurate definition of acoustic source impedance of a powered engine. Significant advancement has been made by showing that acoustic pressure measurements can be taken in the hostile environment posed by the engine's hot exhaust gas. Also, information obtained from motored engine studies indicate the potential for acoustical modeling of the engine using the computer. The importance of this work is found not only in the success of defining acoustic source impedance but in the informational foundations developed towards future investigations.

2. SUCCESS OF PROJECT'S APPROACH

The primary contribution made by this work was the refinement of an experimental-cum-analytical method for evaluating acoustic impedance. Particular improvements can be seen in the adaptation of the acoustic sensors and external noise source to resist high temperature environment of an engine exhaust system. Corresponding analytical improvements are the identification of open pipe impedance and termination impedance interrelationships which exist within the experimental system.

Another important development is the conclusion, from motored engine experimental studies in comparison with computer modeling efforts, that the engine can be acoustically modeled as a changing volume. The volume during specific parts of the engine's thermodynamic cycle can be presented either as a closed tube of specified length and diameter or as a helmholtz resonator of fixed neck and varying enclosure dimensions.

3. RECOMMENDATIONS

The following list of recommendations, discussed in some detail in previous sections, are offered as suggestions toward more successful acoustic analysis of an engine for future studies:

- a) Digital signal analysis at higher engine speeds could be more successfully utilized if triggering had been incorporated into the combined experimental engine digital signal analyzer system. Triggering would be particularly useful with powered engine analysis, with triggering being set as a function of the firing frequency. If the triggering potential of the digital signal analyzer is limited, possible lengthening of the sampling time to any multiple of the thermodynamic cycle completion time would lead to a more exact measurement of the impedance for an engine. Proper readjustments would have to be considered for each engine speed since the firing frequency would also change.
- b) Left and right transfer functions could be more accurate in powered engine acoustic analysis if these transfer functions were established in a measurand tube with a temperature gradient approximated by expected exhaust gas temperatures. It is important to note that left and right transfer functions were adapted to the case of a high temperature acoustic transmission medium by adjusting one of the acoustic sensors to compensate for the increase in the speed of sound. However, this method was found experimentally cumbersome.
- c) Further investigation of motored engine studies, particularly at higher engine speeds, could accurately disclose contributive acoustic behavior caused by engine geometry effects.

- d) Additional loading of the test engine would possibly decrease the overall sound pressure level of the noise produced by the engine as much as 15 dB at lower frequencies (Reference 1). With a lower sound pressure level produced by the engine, the externally generated white noise signal would be more identifiable for digital signal analysis and for data reduction. This result is positively identified in the comparison of Figures 40 to 42 where a difference of approximately 10 dB between externally generated acoustic signals makes identifying engine acoustic characteristics much more difficult.
- e) A definite improvement in the data would be made if the sound source could produce a white noise signal with a broadband sound pressure level in excess of 145 dB. The effect of an increased sound pressure level would not only contribute to having more definable acoustic characteristics but can optionally be used to expand the frequency bandwidth of analysis. The increased bandwidth would be particularly useful in extending the acoustic analysis into the lower frequency range, i.e., below 500 Hz. The lower frequency range is important due to the fact that much of the noise content of a powered engine is located at the lower frequency end of the frequency spectrum. A suggested acoustic source might be a pneumatic horn device.

The work presented in this report is a beginning effort in the experimental analysis of acoustic source impedance using measurement techniques adapted to an actual powered engine. Defining the acoustic source impedance was successful in motored engine studies and moderately successful in powered engine studies. Much was learned from this report and the groundwork for further investigations has been established.

REFERENCES

1. R. J. Alfredson and P. O. A. L. Davies, "The Radiation of Sound from an Engine Exhaust," J. Sound Vib. 13, (4), 1970, pp. 389-408.
2. M. L. Munjal and M. L. Kathuriya, "Accurate Method for the Experimental Evaluation of the Acoustical Impedance of a Black Box," J.A.S.A., 58, 1975, pp. 451-54.
3. M. L. Kathuriya and M. L. Munjal, "A Method for the Experimental Evaluation of the Acoustic Characteristics of an Engine Exhaust System in the Presence of Mean Flow," J.A.S.A., 60, 1976, pp. 745-51.
4. M. L. Munjal and M. L. Kathuriya, "Method for Evaluation of the Acoustical Impedance of a Black Box, With or Without Mean Flow, Measuring Pressures at Fixed Positions," J.A.S., Vol. 62, No. 3, September 1977, pp. 755-759.
5. R. Singh and W. Soedel, "An Efficient Method of Measuring Impedances of Fluid Machinery Manifolds," J. Sound Vib. 56, (1), 1978, pp. 105-125.
6. A. F. Seybert and D. F. Ross, "Experimental Determination of Acoustic Properties Using a Two-Microphone Random-Excitation Technique," J.A.S.A., Vol. 61, (5), May 1977, pp. 1362-70.
7. H. Levine and J. Schwinger, "On the Radiation of Sound from an Unflanged Circular Pipe," Phys. Rev. 73, pp. 383-406, (1948).
8. P. M. Morse and K. U. Ingard, Theoretical Acoustics, McGraw-Hill Co., New York, 1968.
9. L. E. Kinsler and A. R. Frey, Fundamentals of Acoustics, Second Edition, New York, John Wiley and Sons, Inc., 1962.
10. B. A. Blaser and J. Y. Chung, "A Transfer Function Technique for Determining the Acoustic Characteristics of Duct Systems with Flow," Inter-Noise 78 Proceedings, 1978, pp. 901-908.
11. R. Singh and T. Katra, "On the Dynamic Analysis and Evaluation of Compressor Mufflers," Proceedings 1976 Purdue Compressor Technology Conference, July 6-9, 1976, Purdue University, West Lafayette, Indiana, 1976.
12. C. M. Harris, Handbook of Noise Control, McGraw-Hill Book Company, 1957.
13. W. S. Gatley and R. Cohen, "Methods for Evaluating the Performance of Small Acoustic Filters," J.A.S.A., 46, pp. 6-16, 1969.

REFERENCES (Concluded)

14. M. L. Munjal and P. T. Thawani, "The Effect of Mean Flow and the Exhaust System on the Performance of Exhaust Mufflers," Mechanical Engineering Bulletin, Central Mechanical Engineering Research Institute, Durgapur, India, Vol. 6, No. 3. September 1975, pp. 96-101/108.
15. L. L. Beranek, Noise Reduction, McGraw-Hill Book Company, 1960.
16. E. Meyer and E. G. Neumann, Physical and Applied Acoustics - An Introduction, Academic Press, 1972.
17. J. T. Broch, in cooperation with Bruel and Kjaer Measurement Systems, Acoustic Noise Measurements, K. Larsen and Sons A/S, Denmark, 1975.
18. M. L. Munjal, "Exhaust Noise and Its Control - A Review," Shock and Vibration Digest, August 1977, pp. 22-32.
19. American Society for Testing and Materials, "Standard Method of Testing for the Impedance and Absorption of Acoustical Materials by the Tube Method," Part 14, Reprinted from Copyrighted 1966 Book of ASTM Standards.
20. Briggs and Stratton, "Service and Repair Instructions," Briggs and Stratton Corp., Milwaukee, Wis. 53201, U.S.A., Litho in U.S.A., Part No. 270962.
21. H. D. Hogge and E. W. Ritzi, "Theoretical Studies of Sound Emission from Aircraft Ducts," Paper Number 73:1012, AIAA Aero-Acoustics Conference, Seattle, Wash., October 15-17, 1973.

APPENDIX A
ACOUSTIC PRESSURE SENSOR SPACING

The following pages provide justification for variable acoustic pressure sensor spacing, and includes the mathematics used to quantify proper sensor spacing. The results from this analysis are condensed and represented graphically in Figure A-1.

The relationship which relates temperature to the speed of sound in a gas is as follows:

$$c = c_0 \left(1 + \frac{T}{273} \right) \quad (A-1)$$

where

c_0 is the speed of sound at standard atmospheric temperature and pressure; equaling $336.1 \frac{\text{meters}}{\text{second}}$.

T is the temperature of the acoustic medium in degrees celsius.

The above equation is for air; but, this analysis was contingent on the premise that exhaust gases will resemble air as an acoustic medium at elevated temperatures.

For the experimental case where the temperature of the acoustic medium is 800°F the speed of sound is calculated to be 538 meters per second. The increase in speed of sound from standard atmospheric conditions is 60%. Since the speed of sound will vary significantly over the operating temperature range, the acoustic pressure sensor spacing must be correspondingly adjusted for correct usage of the internal time delay of the FFT digital signal analyzer system.

The time delay in the digital signal analyzer was used so that the acoustic signal received by acoustic pressure sensor number 2 and acoustic pressure sensor number 1 both are analyzed simultaneously to yield the transfer function (H_{12}). The transfer function contains magnitude and phase information, which when used mathematically with predetermined left- and right-transfer functions (H_{12_l} and H_{12_r}), will provide the acoustic characteristics of interest. Consequently, if the distance between the two acoustic pressure sensor access ports are mispositioned, the transfer function derived will contain wrong magnitude and phase information.

The relationship which exists between the time delay (Δt), speed of sound (c), and spacing between acoustic pressure sensors ($\Delta \ell$) is developed as:

$$\Delta t = \frac{\Delta \ell}{c} \quad (A-2)$$

Continuing with example of the acoustic medium at 800°F; the spacing between the two acoustic pressure sensors is 42 millimeters. A complete analysis of acoustic sensor spacing over a temperature range of 0°F to 1300°F yields the graphical result shown in Figure A-1.

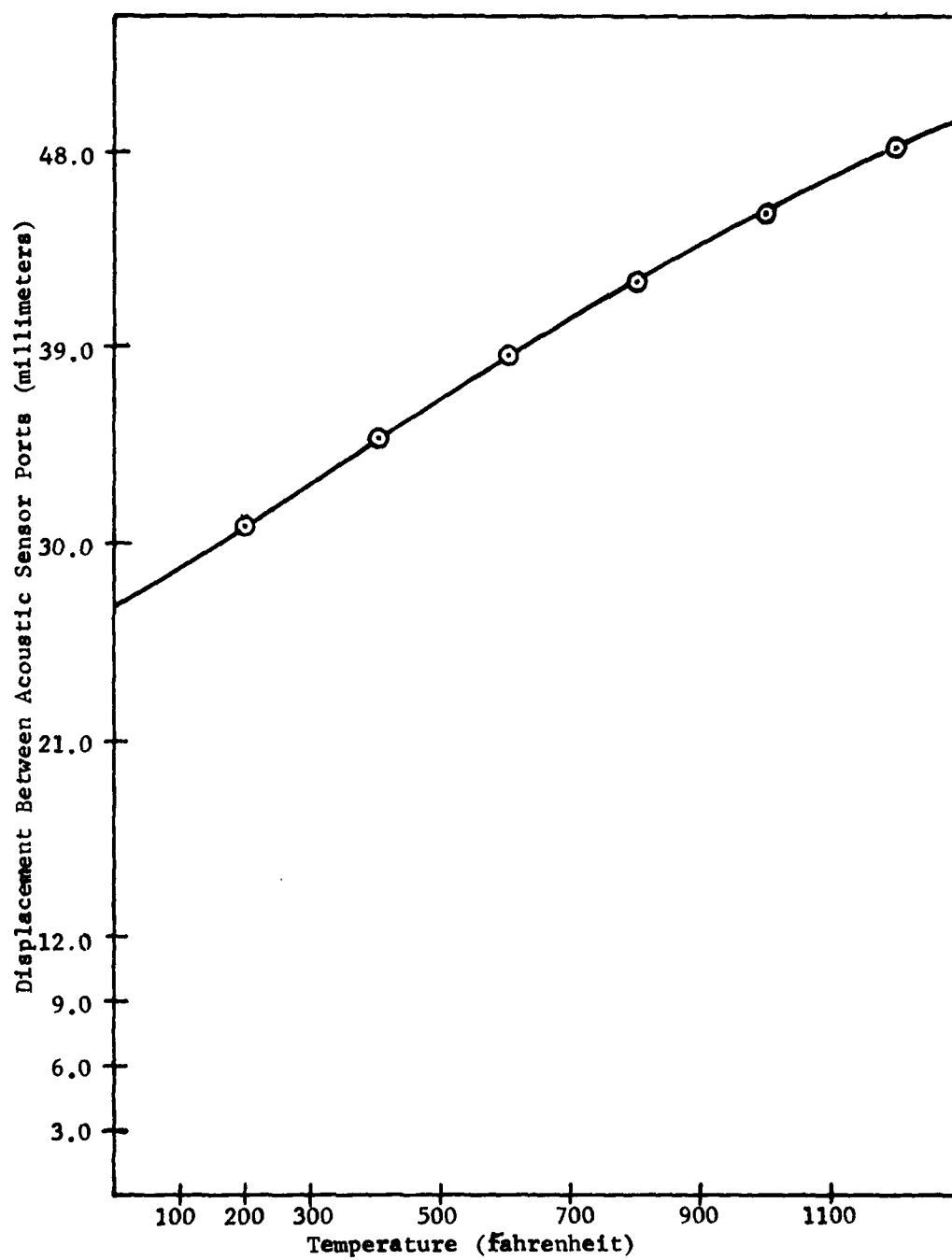


Figure A-1. Temperature Effects on Acoustic Sensor Position

APPENDIX B

COMPUTER ACOUSTIC MODELING EFFORT FOR AN INTERNAL COMBUSTION ENGINE

The development of digital computer acoustic simulation for an internal combustion engine was deemed necessary to reaffirm certain experimental results. Formulation of the computer program was developed about the concept of obtaining the engine acoustic impedance by adding the resistive and reactive acoustic impedances for several types of passive systems. The proportions in which these passive system impedances were added were specified by the proportions in which 100 samples of the acoustic signal were selected during actual experimentation by the digital signal analyzer. An example would be where experimental sampling of the acoustic signal was simulated by the computer as a closed tube termination for 60% of total samples and volume resonator termination for 40% of total samples.

An important extension was made in the volume resonator simulation since the volume resonator impedance has a pronounced effect on the total simulated impedance. Within the 40% sampling by the digital signal analyzer, the actual cylinder volume is constantly changing. Consequently, at each frequency, 40 computer calculations were completed using a cyclic series of volume dimensions for the resistive and reactive impedance simulations and then averaged to gain a net effect for the changing volume acoustic impedance contribution.

The following methodology was used to determine an appropriate cyclic volume magnitude and appropriate sequence.

The known information given with the 10 horsepower Briggs and Stratton engine of application was bore, stroke, and compression ratio. Knowing the bore and the stroke, it was possible to calculate the total displacement volume as 28 in³. To find the total available volume within the engine's combustion chamber, it was necessary to find the

volume when the piston was bottom dead center (V_{BDC}) and the volume when the piston was top dead center (V_{TDC}). It is known that:

$$\text{Compression Ratio} = \frac{V_{BDC}}{V_{TDC}} \quad (B-1)$$

$$= 6$$

and

$$\begin{aligned} \text{Displacement Volume} &= V_{BDC} - V_{TDC} \\ &= 28 \text{ in}^3 \end{aligned} \quad (B-2)$$

Knowing the compression ratio and the displacement volume, it is possible to solve both Equations B-1 and B-2, simultaneously yielding:

$$V_{BDC} = 33.6 \text{ in}^3$$

and

$$V_{TDC} = 5.6 \text{ in}^3$$

Assuming the reciprocating motion of the piston can be approximated as a sinusoidal motion with crankangle position, the graphical representation of Figure B-1 is obtained. By examining those crank-angles where the exhaust valve is open, the corresponding volumes are obtainable as shown in Table B-1.

Included in Figure B-2 is the computer program used to calculate the simulated engine acoustic impedance. The program is in a Fortran IV language and format.

TABLE B-1
CYLINDER VOLUME WITH ENGINE CRANKANGLE VARIATION

Crankangle with Respect to the Thermodynamic Cycle	Corresponding Volume (in ³)
0	5.6
30	6.5
60	11.25
90	18.00
120	25.00
150	30.00
180	33.60
210	30.00
240	25.00
270	18.00
300	11.25
330	6.5
360	5.6
390	6.5
420	11.25
450	18.00
480	25.00
510	30.00
540	33.60
570	30.00
600	25.00
630	18.00
660	11.25
690	6.5
720	5.6

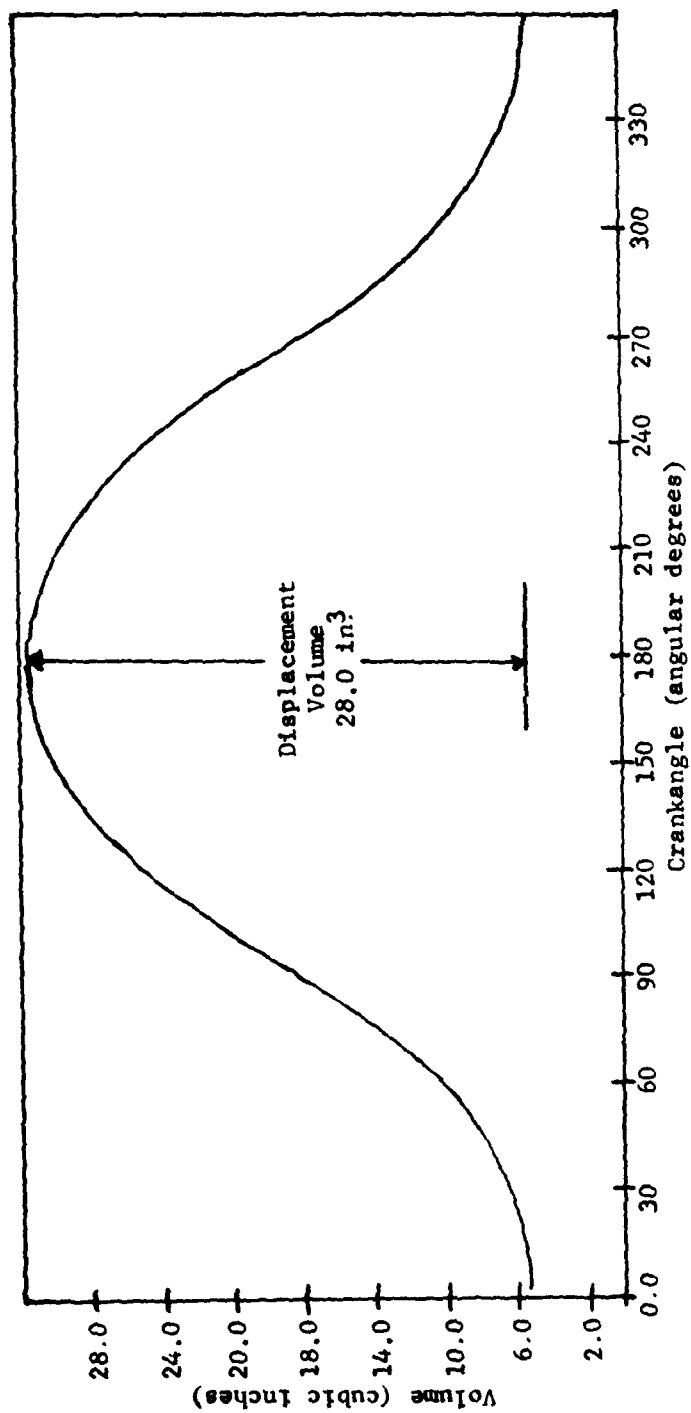


Figure B-1. Cyclic Volume Variation with the Engine Crankangle

```

REAL K, LB, LPV, LPH, LT, MFREQ, LPC, LPM
COMPLEX TOPZ, BOTZ, ZRLOW
DIMENSION HIMAG(100,1), VIMAG(100,1), CIMAG(100,1), OIMAG(100,1),
*IMAG(100,1), FREQ(100,1), ZIMAG(100,1), ICHAR(1), NPT(1)
DIMENSION FIMAG(100,1), CREAL(100,1), VREAL(100,1), ZREAL(100,1)
DATA NPT/100/, ICHAR/'XXXX'/
25 READ(5,100) LB, AB, VOL, LT, ALPHA, HETA, MFREQ, BR, RR, BI, VI, R
*1, CI, OI, EI, DO
100 FORMAT(8F10.4,/,8F10.4)
IF(MFREQ.EQ.0.0) GO TO 50
LT=LT/12.0
PI=3.141592654
C=1140.0
THE LENGTH TERM 'LPV' DEFINES THE LENGTH OF THE PASSIVE VOLUME RESONATOR
IMPEDANCE
THE LENGTH TERM 'LPC' DEFINES THE LENGTH OF THE CLOSED TUBE TERMINATION
IMPEDANCE
THE LENGTH TERM 'LPM' DEFINES THE LENGTH OF THE MEASURAND TUBE DISTANCE
FROM THE EXHAUST PORT INTERFACE TO THE SENSOR INPUT AREA, AND IS USED
AND IS USED TO TRANSFER AND MODIFY THE ACTUAL INPUT IMPEDANCE AT THE
SENSORS
LPV=1.75/12.0
LPC=1.0/12.0
LPM=9.25/12.0
X=MFREQ/100.0
FREQ(1,1)=X
DO 1 I=2,100
J=I-1
1 FREQ(I,1)=FREQ(J,1)+X
TOTAL=EI+VI+RI+CI+OI
DO 2 I=1,100
K=2.0*PI*FREQ(I,1)/C
S=.79/144.0
THE VALUE OF R IS THE RESISTIVE COMPONENT OF THE TERMINATING
IMPEDANCE AND IS ASSIGNED AN ARBITRARY MAGNITUDE BASED ON THE PREMISE
THAT THIS MAGNITUDE IS MUCH LESS THAN UNITY.
R=(2.0E-08)*((FREQ(I,1))**2)
THE QUANTITY 'CXIMAG' AND 'VXIMAG' DEFINE THE TERMINATING IMPEDANCE
FOR THE CLOSED TUBE AND VOLUME RESONATOR CASES.
CXIMAG=(-1.0/(TAN(K*LPC)))
CIMAG(I,1)=((-1.0*CXIMAG*(TAN(K*LPM))**2)-((CXIMAG)**2+R**2-1.0)*T
*AN(K*LPM)+CXIMAG)/((1.0-CXIMAG*TAN(K*LPM))**2+(R**2)*(TAN(K*LPM))**
**2)
IF(CIMAG(I,1).GT.0.2E+02) CIMAG(I,1)=20.0
IF(CIMAG(I,1).LT.-0.2E+02) CIMAG(I,1)=-20.0
CREAL(I,1)=(R*((1.0+(TAN(K*LPM))**2)/((1.0-CXIMAG*TAN(K*LPM))**2+(R
**2)*(TAN(K*LPM))**2))
IF(CREAL(I,1).GT.0.2E+02) CREAL(I,1)=20.0
VOLUME=25.0
VOL=VOLUME/1728.0
VREALT=0.0
VIMAGT=0.0
IV=VI
DO 3 J=1,IV
VOL=VOLUME/1728.0
VXIMAG=S*((K*LPV)/S)-((1.0/(K*VOL)))
VIMAG(I,1)=((-1.0*VXIMAG*(TAN(K*LPM))**2)-((VXIMAG)**2+R**2-1.0)*T
*AN(K*LPM)+VXIMAG)/((1.0-VXIMAG*TAN(K*LPM))**2+(R**2)*(TAN(K*LPM))**
**2)
VIMAGT=VIMAGT+VIMAG(I,1)
VREAL(I,1)=(R*((1.0+(TAN(K*LPM))**2)/((1.0-VXIMAG*TAN(K*LPM))**2+(R
**2)*(TAN(K*LPM))**2))
VREALT=VREALT+VREAL(I,1)
IF(VOLUME.EQ.25.0) GO TO 49
IF(VOLUME.EQ.30.0) GO TO 51
IF(VOLUME.EQ.33.6) GO TO 52
IF(VOLUME.EQ.30.01) GO TO 53
IF(VOLUME.EQ.25.01) GO TO 54
IF(VOLUME.EQ.18.0) GO TO 55
IF(VOLUME.EQ.11.25) GO TO 56
IF(VOLUME.EQ.6.5) GO TO 57
49 VOLUME=30.0
GO TO 3
51 VOLUME=33.6
GO TO 3
52 VOLUME=30.01
GO TO 3

```

Figure B-2. Computer Program which Simulates the Engine Acoustically


```

51 VOLUME=25.01
GO TO 3
54 VOLUME=18.0
GO TO 3
55 VOLUME=11.25
GO TO 3
56 VOLUME=6.5
GO TO 3
57 VOLUME=25.0
3 CONTINUE
VIMAG(I,1)=VIMAGT/VI
IF(VIMAG(I,1).GT.0.2E+02) VIMAG(I,1)=20.0
IF(VIMAG(I,1).LT.-0.2E+02) VIMAG(I,1)=-20.0
THE 'ZIMAG' TERM DEFINED WITHIN THIS PROGRAM EVALUATES THE EFFECTS OF
THE TWO TERMINATING IMPEDANCES TO IDENTIFY INPUT IMPEDANCE TRENDS
ZIMAG(I,1)=(VI*VIMAG(I,1))+(CI*CIMAG(I,1))
ZIMAG(I,1)=ZIMAG(I,1)/TOTAL
VREAL(I,1)=VREALT/VI
IF(VREAL(I,1).GT.0.2E+02) VREAL(I,1)=20.0
ZREAL(I,1)=(CI*CREAL(I,1))+(VI*VREAL(I,1))
ZREAL(I,1)=ZREAL(I,1)/TOTAL
CREAL(I,1)=20.0
VREAL(I,1)=20.0
ZREAL(I,1)=20.0
VREAL(100,1)=-20.0
CREAL(100,1)=-20.0
ZREAL(100,1)=-20.0
CIMAG(I,1)=20.0
VIMAG(I,1)=20.0
ZIMAG(I,1)=20.0
CIMAG(100,1)=-20.0
VIMAG(100,1)=-20.0
ZIMAG(100,1)=-20.0
2 CONTINUE
PRINT 500
500 FORMAT(1H1,////)
CALL FPLOT(FREQ, VIMAG, NPT, ICHAR, 1, 100)
PRINT 501
501 FORMAT(///,20X,'Z IMAGINARY',///,25X,'VS',///,21X,'FREQUENCY',///,20X
*,'FOR VOLUME')
PRINT 500
CALL FPLOT(FREQ, VREAL, NPT, ICHAR, 1, 100)
PRINT 401
401 FORMAT(///,20X,'Z RESISTIVE',///,25X,'VS',///,21X,'FREQUENCY',///,20X
*,'FOR VOLUME')
PRINT 500
CALL FPLOT(FREQ, CIMAG, NPT, ICHAR, 1, 100)
PRINT 502
502 FORMAT(///,20X,'Z IMAGINARY',///,25X,'VS',///,21X,'FREQUENCY',///,20X
*,'FOR CLOSED TUBE')
PRINT 500
CALL FPLOT(FREQ, CREAL, NPT, ICHAR, 1, 100)
PRINT 402
402 FORMAT(///,20X,'Z RESISTIVE',///,25X,'VS',///,21X,'FREQUENCY',///,20X
*,'FOR CLOSED TUBE')
PRINT 500
CALL FPLOT(FREQ, ZIMAG, NPT, ICHAR, 1, 100)
PRINT 504
504 FORMAT( /,20X,'Z IMAGINARY', /,25X,'VS', /,21X,'FREQUENCY', /,20X
*,'FOR COMBINED CONFIGURATIONS')
WRITE(6,505) LB, AB, LT, ALPHA, BETA, BI, VI, RI, CI, OI, EI, C
505 FORMAT( /,5X,'LENGTH OF BRANCH=',F10.2,/,5X,'DIAMETER OF BRANCH=',
*F10.2,/,5X,'LENGTH OF TUBE=',F10.2,/,5X,'ALPHA=',F5.2,/,5X,'BETA=',
*F5.2,/,5X,'BRANCH RATIO=',F5.1,/,5X,'VOLUME RATIO=',F5.1,/,5X,'BL
*OB RATIO=',F5.1,/,5X,'CLOSED RATIO=',F5.1,/,5X,'OPEN RATIO=',F5.1
* /,5X,'EXPANSION RATIO=',F5.1,/,5X,'SPEED OF SOUND=',F6.1)
CALL FPLOT(FREQ, ZREAL, NPT, ICHAR, 1, 100)
PRINT 404
404 FORMAT( /,20X,'Z RESISTIVE', /,25X,'VS', /,21X,'FREQUENCY', /,20X
*,'FOR COMBINED CONFIGURATIONS')
WRITE(6,505) LB, AB, LT, ALPHA, BETA, BI, VI, RI, CI, OI, EI, C
GO TO 306
305 NPT(1)=16
PRINT 500
CALL FPLOT(FREQ, ZIMAG, NPT, ICHAR, 1, 16)
PRINT 504
WRITE(6,505) LB, AB, LT, ALPHA, BETA, BI, VI, RI, CI, OI, EI, C
DO 300 I=1,16

```

Figure B-2. (Continued)

```

      FREQ(1,1)=FREQ(16+I,1)
300  ZIMAG(1,1)=ZIMAG(16+I,1)
      PRINT 500
      CALL FPLOT(FREQ, ZIMAG, NPT, ICHAR, 1, 16)
      PRINT 504
      WRITE(6,505) LB, AB, LT, ALPHA, BETA, BI, VI, RI, CI, OI, EI, C
      DO 301 I=1,16
      FREQ(1,1)=FREQ(32+I,1)
301  ZIMAG(1,1)=ZIMAG(32+I,1)
      PRINT 500
      CALL FPLOT(FREQ, ZIMAG, NPT, ICHAR, 1, 16)
      PRINT 504
      WRITE(6,505) LB, AB, LT, ALPHA, BETA, BI, VI, RI, CI, OI, EI, C
      DO 302 I=1,16
      FREQ(1,1)=FREQ(48+I,1)
302  ZIMAG(1,1)=ZIMAG(48+I,1)
      PRINT 500
      CALL FPLOT(FREQ, ZIMAG, NPT, ICHAR, 1, 16)
      PRINT 504
      WRITE(6,505) LB, AB, LT, ALPHA, BETA, BI, VI, RI, CI, OI, EI, C
      DO 303 I=1,16
      FREQ(1,1)=FREQ(64+I,1)
303  ZIMAG(1,1)=ZIMAG(64+I,1)
      PRINT 500
      CALL FPLOT(FREQ, ZIMAG, NPT, ICHAR, 1, 16)
      PRINT 504
      WRITE(6,505) LB, AB, LT, ALPHA, BETA, BI, VI, RI, CI, OI, EI, C
      DO 304 I=1,16
      FREQ(1,1)=FREQ(80+I,1)
304  ZIMAG(1,1)=ZIMAG(80+I,1)
      PRINT 500
      CALL FPLOT(FREQ, ZIMAG, NPT, ICHAR, 1, 16)
      PRINT 504
      WRITE(6,505) LB, AB, LT, ALPHA, BETA, BI, VI, RI, CI, OI, EI, C
      NPT(1)=100
306  GO TO 25
50  STOP
      END

```

Figure B-2. (Continued)

DATE
FILMED
-8